INVESTIGATIONS ON WELDABILITY OF ALUMINIDE COATED 9Cr STEEL

By

ZALA ARUNSINH BAKULSINH

ENGG06201504007

Institute for Plasma Research, Gandhinagar

A thesis submitted to the

Board of Studies in Engineering Sciences

In partial fulfillment of requirements

for the Degree of

DOCTOR OF PHILOSOPHY

of

HOMI BHABHA NATIONAL INSTITUTE

February, 2021

Homi Bhabha National Institute[1]

Recommendations of the Viva Voce Committee

As members of the Viva Voce Committee, we certify that we have read the dissertation prepared by ZALA ARUNSINH BAKULSINH entitled "Investigations on Weldability of Aluminide Coated 9cr Steel" and recommend that it may be accepted as fulfilling the thesis requirement for the award of Degree of Doctor of Philosophy.

Chairman – Dr. Subroto Mukherjee	S Mukherjee 4/2/2021
Guide – Dr. Nirav I. Jamnapara	Jamnapara 4/2/21
Co-guide – Dr. Mukesh Ranjan	Mukesh Ranjan 4/2/21
Examiner – Prof. M. Kamaraj	M. Kamaraj
Member 1 – Dr. Samir S. Khirwadkar	Khirwadkar
Member 2 – Dr. Paritosh Chaudhuri	Chaudhuri
Member 3 – Dr. G. Ravi	Ravi 04/02/2021

Final approval and acceptance of this thesis is contingent upon the candidate's submission of the final copies of the thesis to HBNI.

I/We hereby certify that I/we have read this thesis prepared under my/our direction and recommend that it may be accepted as fulfilling the thesis requirement.

Date: 4th February, 2020

Place: IPR, Gandhinagar

Mukesh Ranjan 4/2/21
Signature
Co-guide

Jamnapara 4/2/21
Signature
Guide

[1] This page is to be included only for final submission after successful completion of viva voce.

STATEMENT BY AUTHOR

This dissertation has been submitted in partial fulfillment of requirements for an advanced degree at Homi Bhabha National Institute (HBNI) and is deposited in the Library to be made available to borrowers under rules of the HBNI.

Brief quotations from this dissertation are allowable without special permission, provided that accurate acknowledgement of source is made. Requests for permission for extended quotation from or reproduction of this manuscript in whole or in part may be granted by the Competent Authority of HBNI when in his or her judgment the proposed use of the material is in the interests of scholarship. In all other instances, however, permission must be obtained from the author.

Arunsinh Zala

Zala Arunsinh Bakulsinh

DECLARATION

I, hereby declare that the investigation presented in the thesis has been carried out by me. The work is original and has not been submitted earlier as a whole or in part for a degree / diploma at this or any other Institution / University.

Arunsinh Zala

Zala Arunsinh Bakulsinh

CERTIFICATION ON ACADEMIC INTEGRITY

1. I, Zala Arunsinh Bakulsinh, HBNI Enrolment No. ENGG06201504007 hereby undertake that, the Thesis titled ***"Investigations on Weldability of Aluminide Coated 9Cr Steel"*** is prepared by me and is the original work undertaken by me and free of any plagiarism. That the document has been duly checked through a plagiarism detection tool and the document is plagiarism free.

2. I am aware and undertake that if plagiarism is detected in my thesis at any stage in future, suitable penatlty will be imposed as per the applicable guidelines of the Institute/UGC.

Signature of Student

Endorsed by the thesis Supervisor:

(I certify that the work done by the Researcher is plagiarism free)

Signature:

Name: Dr. Nirav I. Jamnapara

Designation: Associate Professor

Department/Centre:

Name of CI/OCC: Institute for Plasma Research, Gandhinagar

List of Publications arising from the thesis

Journal

a. <u>Published</u>

1. **Zala, A. B.**, N. I. Jamnapara, V. J. Badheka, S. Sam, and M. Ranjan **(2019):** "Effect of aluminide coatings on penetration and microstructure of TIG welded 9Cr-1Mo steel for fusion blanket applications." **Fusion Engineering and Design** 144 : 172-179.
2. **Zala, A. B.**, N. I. Jamnapara, V. J. Badheka, C. Sasmal, S. Sam, and M. Ranjan **(2019):** "Delta (δ) Ferrite Formation in the Welds of Aluminized 9Cr-1Mo Steels." **Metallography, Microstructure, and Analysis** 8, no. 2 256-262.
3. **Zala, A. B.**, N. I. Jamnapara, C. S. Sasmal, P. Chaudhuri, and M. Ranjan **(2019):** "Investigation of alumina film formed over aluminized RAFM steel by plasma assisted heat treatment." **Fusion Engineering and Design** 146 :2002-2006.

b. <u>Communicated:</u>

1. **Zala, A. B.**, N. I. Jamnapara, V. J. Badheka, C. S. Sasmal, S. Sam, and M. Ranjan. " Effect of Activating Fluxes on Microstructure and Hardness Properties of A-TIG welded Aluminized Coated 9Cr-1Mo Steels." *Manuscript #MPC-2020-0168,* **Materials characterization and performance (ASTM).** (Under Review)
2. **Zala, A. B.**, N. I. Jamnapara, C. S. Sasmal, S. Sam, and M. Ranjan. " Study of Microstructures and Mechanical Properties of TIG Welded Aluminized 9Cr-1Mo Steel." to be submitted to **Materials & Design** (Under review (IPR library))
3. **Zala, A. B.**, N. I. Jamnapara, C. S. Sasmal, S. Sam, and M. Ranjan. " Study on Weldability of Aluminized Indian RAFM steels." to be submitted to **Material Science & Engineering-A** (Under preparation)

Conferences/Symposium

<u>Oral Presentation:</u>

1. "Effects of Activated Fluxes on Microstructure and Hardness Properties of A-TIG welded Aluminized coated 9Cr-1Mo steels" - 71st IIW Annual Assembly and International Conference (15-20 July 2018, Bali, Indonesia).

<u>Poster Presentation:</u>

2. Effect of Heat Inputs on Alumina Coated RAFM Steel by GTAW Process SOFE2019: 28th IEEE Symposium on Fusion Engineering, 2–6 June, 2019, Florida, USA
3. Investigation of Plasma assisted heat treatments on Aluminized RAFM steels, SOFT 2018: Symposium on Fusion Technology, 16^{th} to 21^{st}September 2018, Giardini Naxos, Italy
4. Investigations on Weldability of Aluminide Coated 9Cr-1Mo Steels, Plasma 2017: 32nd National Symposium on Plasma Science & Technology, 07^{th} to 10^{th} November, 2017, Gandhinagar, India.

Others

1. Patel, Payank, N. I. Jamnapara, Arunsinh Zala, and S. D. Kahar. "Investigation of hot-dip aluminized Ti6Al4V alloy processed by different thermal treatments in an oxidizing atmosphere." Surface and Coatings Technology (2020): 125323.

~ ***<u>Dedicated to</u>*** ~

My beloved parents and my loving brother.

ACKNOWLEDGEMENTS

Foremost, I would like to show my gratitude to my thesis supervisor **Dr. N. I. Jamnapara**, IPR, Gandhinagar without whose guidance, vision and encouragement at crucial times my research experience would have been unfulfilling. His most important contribution to my life however; will always be the lesson to remain humble to learn more.

I am also very much grateful to my co-guide advisor Dr. Mukesh Ranjan whose ever helpful nature with indomitable spirit will always motivate me. I would also like to acknowledge my doctoral committee members Dr. Subroto Mukherjee, Dr. Samir Khirwadkar, Dr. Paritosh Chaudhuri and Dr. G. Ravi for their timely insightful comments and suggestions on the progress and direction of the research.

This acknowledgement would be incomplete without the mention of my Lab mates Hiren, Jainik, Vaibhav, Vyom, Ankit, Pooja, Anjuman, Payank, Rakesh, Karan, Vikas, Jeet, Janki and Bharavi all of whom have broadened my horizons with perpetually interesting discussions about physics, engineering and life. I consider myself fortunate, to have all of you as my Lab mates. A special mention to my friend Subrat Kumar Das (APD division, FCIPT); as he always stood with me as I grappled with research and personal problems over the past 3 years.

Mr. Gautam Vadolia of FCIPT (workshop); Mr. Chirayu Patil (APD division) Section, Dr. Balasubramanian (APD Division, FCIPT), Computer Section, IPR stores too many people to mention here; all have played their role in this work and deserves a worthy mention in this acknowledgement. My Batch mates Bhumi, Jay, Montu, Mayank, Arnab, Yogesh, Priti, Chinmoy, Neeraj, Garima, Deepshikha, Srimanta all have made my time at IPR full of happy memories. My interactions with Mr. Hardik Tailor, Mr.

Mitul Abhangi have been brief but still worthy of a mention here. A shout out to all my teachers who have made me the person, I am today. My final acknowledgement must go to my family; my parents, my brother Krushnapalsinh and my all friends for their unconditional love, support and moments of sheer joy. I ask for compassion, if I forgot to mention anyone who have contributed in any way to this work.

Table of Contents

List of Figures

List of Table

CHAPTER 6

CONCLUSIONS

The objective of this research work was to investigate the weldability of aluminide coated P91 steels. The aluminide coated 9Cr steel has many applications such as petrochemical plants, turbine-driven systems, automobile industry, and especially for test blanket module of fusion reactors. However, work related to the weldability of aluminide coated structures are scarcely reported and many issues are still unaddressed leading to lacunae. Issues such as the effect of al dissolution from coating into the weld, its effect on delta ferrite formation, grain size of weld metal and dissolution of inclusions were needed to be addressed as observed from literature review. Thus, this doctoral thesis work was an attempt to investigate the weldability as a primary step to applicability of such coated steels. Effect of Al contamination of weld on the microstructural properties and the weld profile was investigated using an autogenous TIG welding (bead-on-plate trials). This study revealed how the Al-rich coating would dissolve in the weld pool during welding and lead to detrimental effects. Consequently, a weld procedure considering a v-groove (edge preparation) was deduced to minimize the effect of Al on the resultant weld. Such a solution was assessed by mechanical tests to evaluate the acceptability of the resultant weld joint. The main conclusions are summarized below:

6.1 Conclusions

- The bead-on-plate trials using autogenous TIG welding revealed that the presence of alumina (Al_2O_3) on the top of coated samples resulted in an improved depth of penetration (DOP) due to arc constriction.

Presence of Al-rich coating in bead-on-plate experiments resulted in Al concentration of ~0.19% distributed across the weld zone. This Al content supports the formation of δ-ferrite (δ-Fe) in weld pool, which ultimately deteriorates mechanical properties of the weld joint. Results with bead-on-plate trials show that the δ-Fe had an average volume fraction of ~5.09% in the weld metal against a maximum permissible value of ~15-17% [161]. The δ-Fe showed a microhardness of 192–198$HV_{0.05}$. This microhardness is approximately half of the reported microhardness for martensitic laths (396–410 $HV_{0.05}$).

- Kaltenhauser equation used for predicting the δ-Fe content was validated in this study against various other equations such as Schaffler, Schneider and New house. As per the equation, if an average Al content exceeds ~0.13 wt% then it would lead to possibility of delta ferrite formation.
- The Al content in the weld metal was also observed to reduce the grain size. The prior austenite grain size in Al contaminated weld was found to be ~58 μm, whereas that of uncoated weld metal was ~38 μm. Al has been reported to be a grain reformer leading to finer grain sizes [194] results of this study are in accordance with the above observation.
- Conventional TIG welding process has been attempted with V-groove design as per ASME standards to restrict the δ-Fe formation within the permissible limit of 10 ferrite factor. The microscopic studies indicated the presence of alumina inclusion at the weld fusion line. Despite such inclusions, the observed tensile strength of the weld joint for coated steel is 648±16MPa,

which is in line with the weld joint of un-coated steel (667±14MPa) and substrate (643±18MPa).

- The impact toughness tests of welds of coated and uncoated steels were carried out at 0°C,-25°C, and room temperature. Observed toughness values were 55 J and 52 J at room temperature for welds of coated and uncoated P91 steels respectively. These impact toughness values are found acceptable in comparison to the reported impact toughness of 45 J at room temperature [125].

6.2 Future scope

The effect of Al contamination has been minimized. However, the resultant weld pool stands unprotected after the welding and the protection of such areas from high temperature corrosion would need to be addressed by an overlay deposition coating technique such as electro spark, laser based surface alloying and so on. An orbital TIG welding technique for coated tubes can be attempted to address the blanket specific applications for fusion reactors. The investigation of weldability of coated steels with different welding techniques such as, electron beam welding, friction stirs processing, laser welding and so on is yet unexplored. In addition, inclusions (Al_2O_3 and AlN) observed in a weld microstructure may affect the mechanical properties. Hence, a study on the effect of inclusions on creep rupture behaviour would be taken up in the future.

Thus, the Aluminium contamination of the weld metal can be mitigated through the V-groove weld joint. It is suggested that the Al content of the weld metal should be < 0.13-0.15 % for a sound and acceptable weld quality. The optimized weld process parameters in this study give an indication of the acceptability of the aluminide coated P91 steels.

Abstract

Name of the Student: Zala Arunsinh Bakulsinh
Name of the CI/OCC: Institute for Plasma Research, Gandhinagar
Enrolment No.: ENGG06201504007
Thesis Title: Investigations on weldability of aluminide coated 9Cr steel
Discipline: Engineering Sciences **Sub-Area of Discipline:** Metallurgy and Material Science
Date of viva voce: 4th February, 2021

9Cr-1Mo steels are structural steels extensively developed for power plant applications demanding higher creep resistance. Aluminide coating on 9Cr-1Mo steels is widely reported for enhancing service life conditions in numerous applications such as petrochemical plant, turbine-driven systems, automobile industry and especially for test blanket module of fusion reactors. One of the critical issues associated with such aluminide coatings (α-Al_2O_3 + FeAl) is the fabrication sequence. Considering the candidate aluminide coatings for different applications, it appears that fabrication followed by coating may not be a good option as diffusion heat treatment after the coating may induce distortions. Alternatively, the second option involving coating process followed by fabrication poses uncertainties of weldability of coated steels. Further, the weldability of aluminide coated P91 steel is scarcely reported. Weldability of aluminide coated structures is thus an area with lacunae and has been attempted to be addressed in this doctoral thesis work.

In this study, effects of aluminide coatings have been investigated by autogenous TIG welding through bead-on-plate trials. The weld microstructures were investigated using X-ray diffraction (XRD), scanning electron microscopy with energy dispersive x-rays (SEM-EDX) and microhardness tests. It was observed that the presence of alumina (Al_2O_3) on the top of coated samples resulted in an improved depth of penetration (DOP) due to arc constriction. The concentration of Al in the weld zone contaminated the weld metal and it supports the δ-ferrite formation which would deteriorate mechanical properties. Results with bead-on-plate trials show that the δ-ferrite had an average volume fraction of ~5.09% in the weld metal with an average 192–198$HV_{0.05}$ microhardness. This is approximately half of the reported microhardness martensitic laths (396–410$HV_{0.05}$). To restrict the delta ferrite formation within the permissible limit, conventional TIG welding process had been attempted with V-groove design in accordance to ASME standards. The resultant weld microstructure has been analyzed with respect to defects in microstructures (inclusions, delta ferrite) presence of δ-ferrite. The microscopic studies indicated the presence of alumina inclusion at the weld fusion line. Despite such inclusions, the observed tensile strength of the weld joint for coated steel is 648 MPa±16MPa which is in line with weld joint of un-coated steel (667±14 MPa) and substrate (643 MPa±18MPa). The impact toughness tests were carried out at 0°C,-25°C and room temperature indicate that there is no drastic effect of coating on weld joint and the observed toughness values are acceptable as per the reported data (45J). The present investigation would be helpful to understand the effect of aluminized coating on weldability for 9Cr-1Mo steels. Subsequently, the welding parameters deduced from this study can be utilized for the welding of aluminized 9Cr-1Mo steels for power plant, chemical processing industries and nuclear applications.

CHAPTER 1
INTRODUCTION

1.1 Background

The continual quest for higher efficiency and productivity across the full band of manufacturing and engineering industries has ensured that the majority of modern-day components are subjected to increasingly harsh environments during the routine process. Because of this, the critical industrial components become prone to rapid degradation as the components fail to resist the rigorous operating conditions. This has taken a heavy toll on the industry's economy. In an overwhelmingly large number of cases, some of the potential causes for accelerated damage of components and their eventual failure are due to aggressive environments, high relative motion between conjugation surfaces, extreme temperatures, and cyclic stresses. High-temperature processing is gaining importance in different sectors of industry, such as manufacturing, power generation, transportation, space, defense, environment (waste remediation) and so on. Particularly, high-temperature operation is of vital importance in the energy sector where the difference in temperature (ΔT) decides the efficiency of the power system. In other words, higher the operating temperature of power plants, better the efficiency of the power plant. The thermal efficiency of fossil-fired thermal power plants can be raised by reducing exhaust heat and heat-transfer losses. The limit has virtually been reached for reducing exhaust heat losses, which are mainly through the condensers for cooling turbine exhaust and boiler exhaust. Heat transfer losses, however, can be reduced by raising the pressure and temperature of the steam, but the extent to which this can be done is greatly influenced by the materials used.

The operating temperature and pressure of power plants are major factors for the consideration of a suitable material. The components operating at such high temperatures undergo microstructural changes over time and possible degradation such as creep, fatigue, hydrogen induced cracking, embrittlement, corrosion, and oxidation. Therefore, to improve the efficiency numerous studies on heat resistant steels, for instance, Chromium (Cr) and austenitic steels actively conducted since the early 1970. This allowed a significant progress to 9–12% Cr steels and austenitic steels [1-4]. The thermal efficiency of a steam-power plant can be improved significantly by increasing the temperature and pressure of the steam entering the turbine, an increase from 580 to 620 °C providing a thermal efficiency increase from 38% to 42% [5]. 9% Chromium heat resistant steel with an alloying element Molybdenum is designed for use at elevated temperature because of its higher creep strength as well as better resistance to oxidation [4, 6-9]. Therefore, in recent years, the microstructure of the alloy and optimization of the compositions for the 9Cr steels have improved their creep strength so that increased service temperatures are now taken into consideration [10-13]. Owing to this, the 9Cr-1Mo steels also (referred as P91 steels) are widely adopted in power plants, incinerators and in the petrochemical industry as the boiler or heat-exchange material for use in high temperature environments [14-21].

1.2 Performance issues of 9Cr-1Mo Steels

The Cr-Mo steels have been in application for over forty years. It has been extensively used in energy sector for high temperature use, where Cr-Mo steels are subjected to different environments (water, air, steam, helium, liquid sodium and so on.) depending on the application. The oxidation behaviour of 9-12%Cr steels has also been widely studied [22-27]. The bulk material strength and mechanical property degrades due to high temperature exposure. This also accelerates the reaction of the surface with the environment. Depending on the type of environment and the service conditions, a number of issues are generated which are undesirable for the reliable operation of the machines or systems. As a result, the mechanical properties of the material get modified with change in the environment. Some of the common issues associated with the surface are mentioned below.

- High temperature oxidation [28-30]
- Metal dusting [31-33]
- Liquid metal corrosion [34-38]

1.2.1 High temperature oxidation

It is now widely acknowledged that the high temperature oxidation resistance of the 9% Cr steels could well be the factor that limits their maximum service temperature. Due to the limited amount of Cr present in the alloy, oxidation resistance may become the significant life-limiting factor in this case in particular if lifetimes of up to 100000 h are desired [18, 20, 28-30, 39, 40]. Fig. 1.1 showcases the oxidation behavior of 2.5Cr-1Mo steels and 9Cr-1Mo steels. The oxidation kinetics indicates parabolic rate law until 5000h, at which the rate becomes more linear [18]. Vossen et *al.* [28] also studied the mass change measurement as a function of oxidation time for different Chromium steels at 650 ^{o}C and reported similar observations.

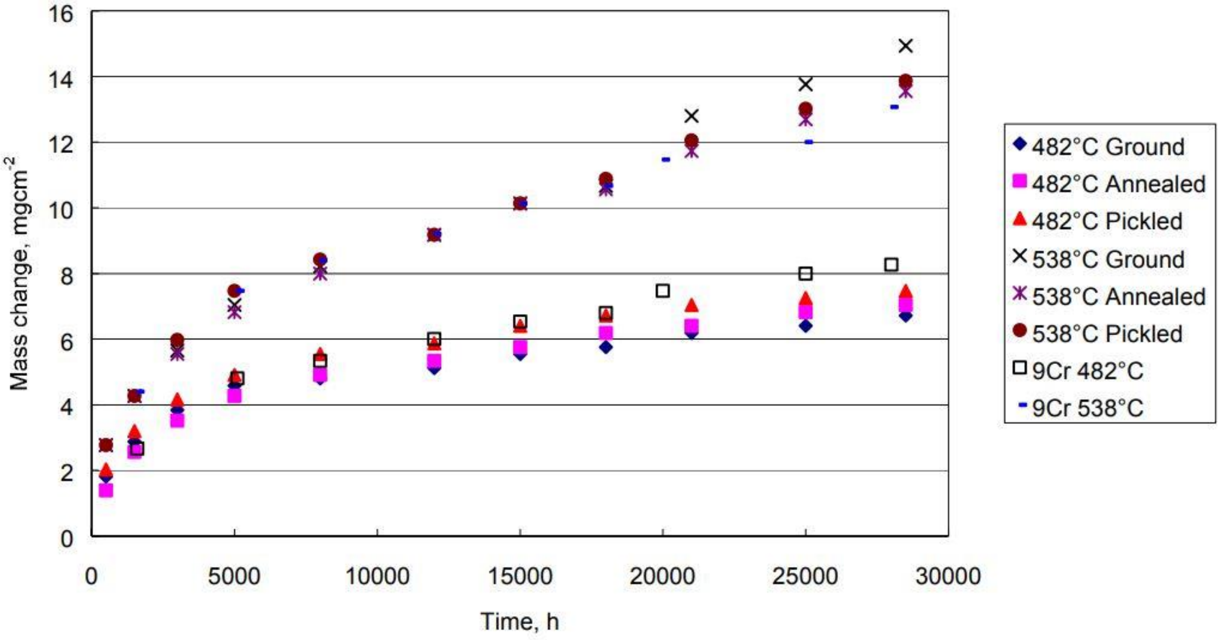

Figure 1.01 2.5Cr-1Mo and 9Cr-1Mo steels exposed to superheated plant steam [18]

1.2.2 Metal dusting

Metal dusting is a crucial issue related to high temperature processing under carbon rich environments having high carbon potentials (ac > 1). It is a form of catastrophic carburization that occurs in steels and iron (Fe), nickel (Ni), and cobalt (Co)-based alloys when exposed to process gas atmosphere of carbon monoxide (CO), Hydrogen (H_2), and carbon dioxide (CO_2) with some hydrocarbons at 400–800 ºC temperature. At such high temperatures, CO and H_2 tend to dissociate on metal surfaces and form carbon. Many authors [31-33, 41] have reported the issue of metal dusting for 9Cr-1Mo steel. Rosado et *al.* [41] explained this phenomenon at different operational temperature as shown in Fig. 1.2. It should be noted that to address this issue, he also investigated different coatings as a solution on P91 steels where Al-diffusion coating was protective at all temperatures.

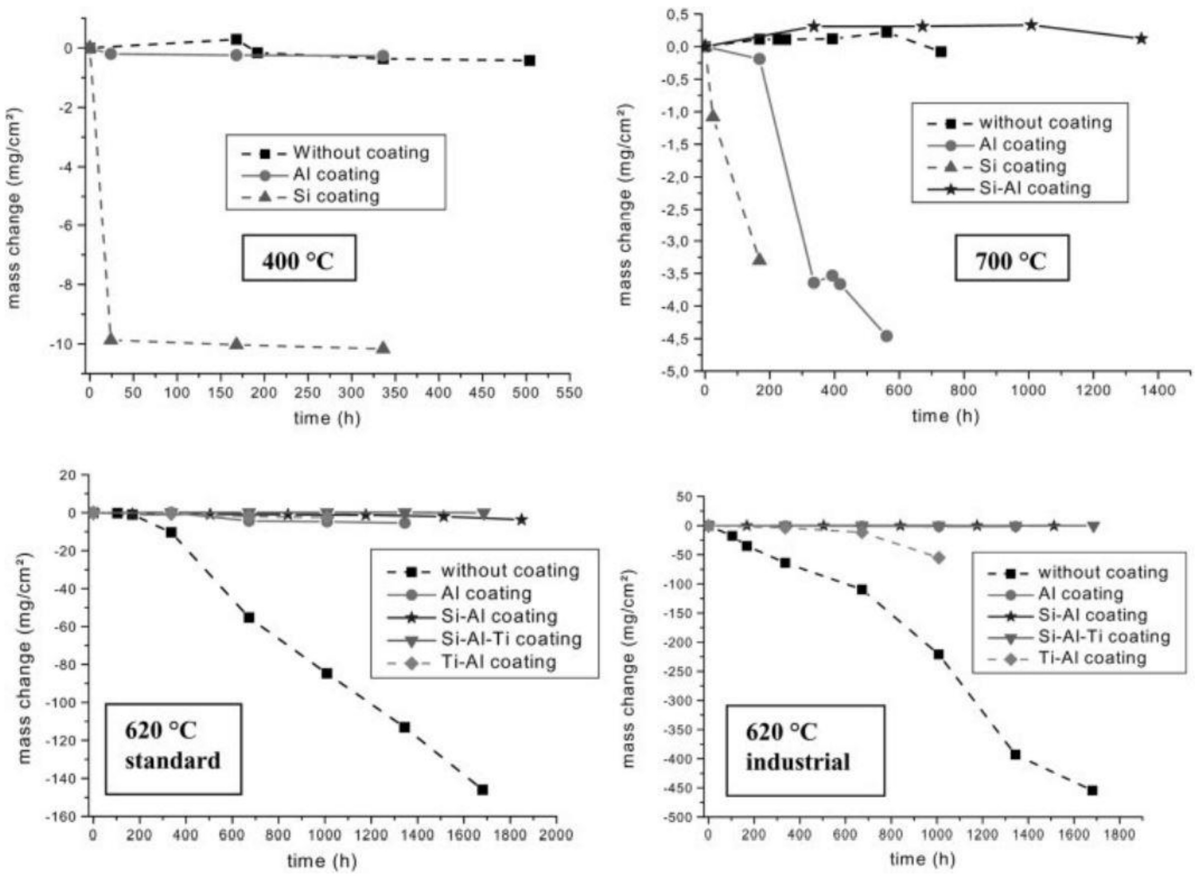

Figure 1.02 Mass change measurements of coated and uncoated alloy P91 tested under metal dusting conditions at 400 °C, 620 °C and 700 °C [41]

1.2.3 Liquid metal corrosion

Producing clean energy from thermonuclear fusion and hydrogen fuel-driven power generating systems has been the main focus of research in recent times. One of the critical challenges in the march toward a demonstration of an engineered nuclear fusion reactor concerns the compatibility of materials with the potential coolants [42]. Liquid metals like lead (Pb) and its alloys, e.g., lead–bismuth eutectic (Pb-Bi) and lead–lithium eutectic (Pb–Li), have been proposed as potential coolants for advanced nuclear energy systems [43-51]. However, liquid metal corrosion is one of the main issues studied a lot recently in the development of liquid metal technology with a P91 substrate [45, 52-56]. For instance, the corrosion rate reported for modified 9Cr steel is 80µm/year at a flow velocity of 0.22 m/s in Pb-15.7 Li at medium temperature (480 °C)[57]. Wulf et *al.* [58] studied the corrosion rates of Eurofer steel in flowing Pb-Li at 550 ºC with a velocity of 0.1 m/s for 10000 h. It has also been reported that aluminide coating through ECX process addresses the issues related to corrosion. The corrosion rate is reduced compared to bare Eurofer steel by a factor of up to 20. The same has been shown in Fig. 1.3. Under such conditions many corrosion studies revealed high corrosion rates for a variety of 9Cr steels e.g. RAFM, Eurofer, MANET, CLAM, and F82H-mod. in the past [59-61].

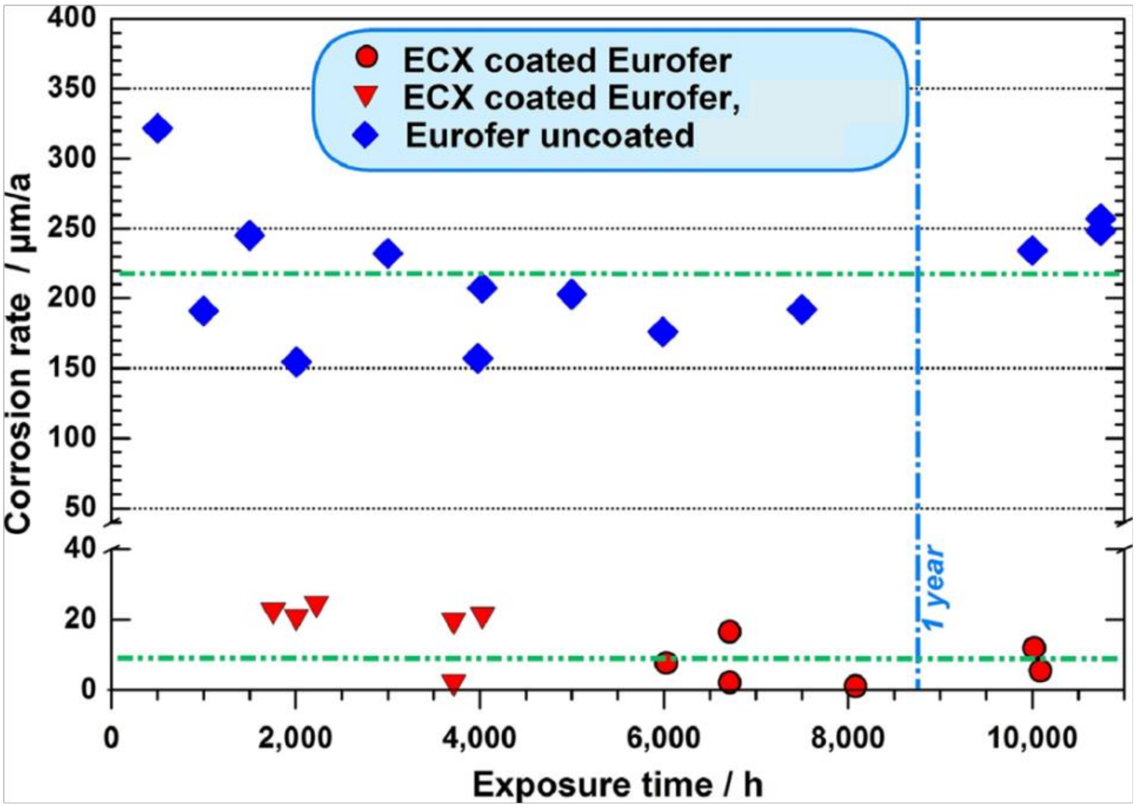

Figure 1.03 Comparison of the evaluated corrosion rates of ECX coated and bare Eurofer steel tested under similar conditions in flowing Pb–15.7Li (550 °C, 0.1 m/s) [58]

The corrosion rates were observed between 80 µm per year and 400 µm per year depending upon the flow velocity and testing temperatures which is very critical. [59, 62, 63]. So it is very essential to address liquid metal corrosion with a protective layer/coating over a substrate that can perform well against the discussed problem.

1.3 Coatings: a decent solution

The need for coating generates from the compatibility and functional requirements of the environmental and service conditions. With the above listed surface related issues for high temperature applications, it becomes inevitable to develop coatings that can combat the environmental conditions while being intact with the substrate. Coatings are not just important to protect the substrate, but to enhance the service life of components and thereby improve the reliability of the entire engineering assembly. The most widely used processes for generating coatings for high temperature applications are thermal spray, laser surface alloying, diffusion coating processes (e.g. aluminizing, chormizing, siliconizing and so on.) and vapor deposition techniques (e.g. CVD and PVD). Among which chromia (Cr_2O_3) and alumina (Al_2O_3) with Iron aluminides (FeAl) are the most common corrosion resistant coatings which have the potential to meet the requirements for high-temperature applications. Cr_2O_3 films have excellent resistance to hot corrosion, but their use beyond 850 °C is not preferred as it transforms to a volatile CrO_2 phase above 900°C thus rendering the substrate unprotected. Therefore, Aluminide coating is more promising compared to other existing coatings. Additionally, alumina with iron aluminide offers excellent high temperature oxidation resistance, corrosion resistance in a liquid metal environment, protection against metal dusting, and so on which attracted the researchers in the last few decades.

1.4 Aluminide (Al_2O_3+FeAl) coating and its applications

The aluminide coating consists of an alumina layer along with iron aluminides to avoid the thermal mismatch between the substrate and alumina. Alone alumina layer can lead to failure due to the large difference in the coefficient of thermal expansion between the substrate and oxide ceramic. The commonly adopted solution method is to form a functional gradient transition layer between the substrate and the alumina coating. Generally, the technique of thermal treatment followed by high temperature oxidation is employed to create aluminide coatings typically Al_2O_3+FeAl after Al deposition. Such iron aluminide coatings have numerous applications in different sectors of industry mainly in automobile, aerospace, petrochemical plants and power generation. Fig. 1.4 summarizes different applications of aluminide coated materials.

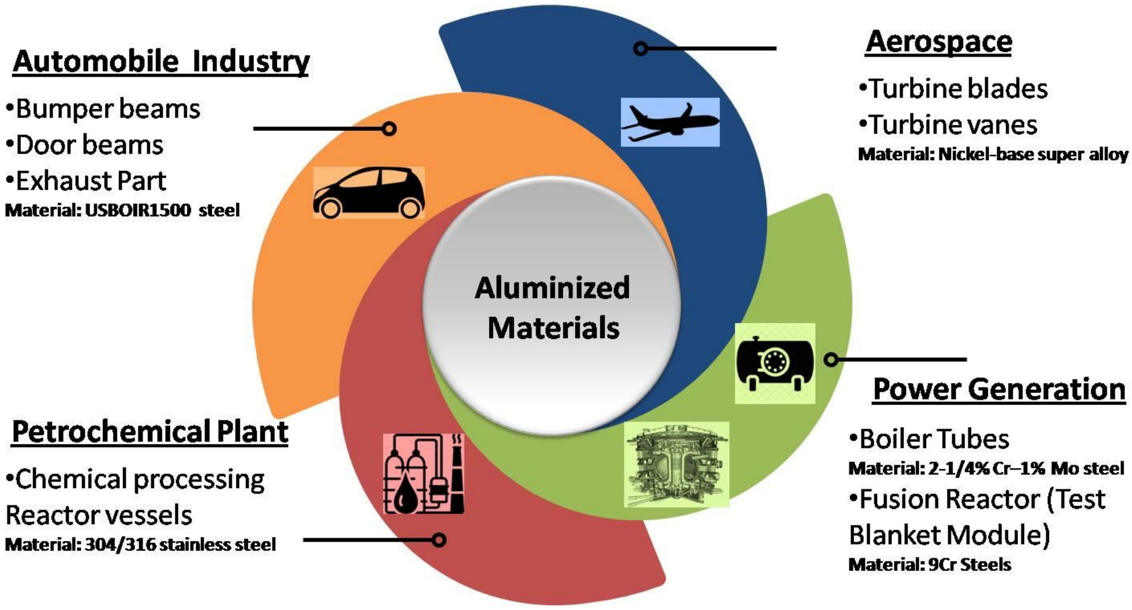

Figure 1.04 Applications of Aluminide coatings

In Europe, Arcelor has developed and commercially launched an aluminized steel sheet product called USIBOR 1500 steel which is used for different parts such as bumper beams, door beams, and exhaust parts in the automobile industry. Similarly, studies from Donaldson company product literature (2007) and AK steel corporation product data have mentioned the applications of aluminized steels. Aluminide Nickel base super alloys are also reported for aerospace applications in which aluminide coating has been developed on turbine blades and turbine vanes.

Aluminide coatings are explored as the potential to mitigate the different operational problems for the blanket module component for a nuclear fusion reactor device named ITER. A blanket module has different operational conditions and functions such as tritium generation, the flowing of Pb-17Li at ~350-460 °C which raises the issues tritium permeation into the structural material (RAFM steels), corrosion and magneto hydro-dynamic drag (MHD) [64, 65]. As explained earlier the flowing of Pb-Li at higher temperatures will cause the corrosion and can plug or choke the pipes of the component [57]. The tritium permeation is also one of the critical aspects as the structural materials such as Eurofer97, F82H ferritic-martensitic steels, and CLAM steels, 316L and 321 austenitic stainless steels are reported to have high permeabilities of hydrogen isotopes [66]. These issues lead the scientific community to come up with a solution to resist the Tritium permeation in to structural materials for fusion reactors. The development of tritium permeation barrier (TPB) can mainly be classified into oxides coatings as reported by different such as oxides Al_2O_3, Cr_2O_3 , Y_2O_3, SiO_2, Er_2O_3, ZrO_2 [67-82], non-oxide coatings (eg. TiC, TiN, SiC, Si_3N_4) [83-86], and their composites (eg. Cr_2O_3/SiO_2, Al_2O_3/SiO_2, TiC/TiN, $FeAl/Al_2O_3$, Al_2O_3/SiC, Er_2O_3/Fe) [87] have been reported for fusion blanket applications. Since the last decade, alumina coatings have been used extensively due to its excellent comprehensive properties such as high melting point, chemical stability, low hydrogen solubility and permeability.

1.5 Weldability issues of Aluminide coated steels

Aluminide coatings (Al_2O_3 + FeAl) have been reported as candidates from performance perspective; however, one of the major issues associated with such coating is the joining process. Conventional fabrication processes would be a very important aspect in the development of new coating processes which can be implemented for the structural components. In fusion blanket module, there is an uncertainty like the module will be fabricated first and then coated, or coated first and then fabricated. Considering the candidate aluminide coatings for blanket applications, it appears that fabrication followed by coating may not be a good option as diffusion heat treatment after the coating may induce distortions.

Alternatively, the second option involving the coating process followed by fabrication poses uncertainties of weldability of coated steels. Further, the weldability of aluminide coated 9Cr-1Mo steel is scarcely reported. There is a high possibility that the coating at the top along with iron aluminides (FeAl) will affect the weld metallurgy and consequently, the mechanical properties. The effects of coating on the weld microstructure will be also an important aspect as far as weldability is concerned. Some of the critical issues are listed below and all are elucidated further with respect to the weldability of coated steels.

- Aluminium contamination in weld
- Effect of coating on weld bead (size and shape)
- Delta ferrite formation in the weld metal
- Aluminium segregation at the weld fusion line
- Mechanical properties of weld joints

1.5.1 Aluminium contamination in weld

The Aluminium concentration in the substrate or weld zone is very crucial as it is susceptible to cracking. The cracking susceptibility as a function of Al concentration has been investigated for FeCrAl alloys by Field et *al*. [88]. He reported that during conventional welding processes such as Gas Tungsten Arc Welding (GTAW) and Gas Metal Arc Welding (GMAW) of FeCrAl alloys, the phenomenon of cracking occurs when the Aluminum concentration in the weld metal is greater than 8-11% approximately. Fig. 1.5 exhibits the results of cracking susceptibility as a function of Aluminium and Chromium concentration. Hence, Aluminium concentration plays a pivotal role in the weldability of aluminized coated steel.

The coating contains iron aluminides as diffusion layer which is very sensitive to the welding speed and alloy content conditions [89]. These iron aluminides (intermetallics) are brittle and susceptible to cracking when welded [90, 91]. Heinz et *al*. reported that iron aluminides are difficult to weld as it has low plasticity and high spatial values which causes cracks during welding process [92]. One of the possible reasons behind such cracking is hydrogen embrittlement. The iron aluminides have been reported to experience low room temperature ductility due to their sensitivity to environment embrittlement [93, 94]. This embrittlement has been attributed to the release of free Hydrogen (H_2) from a reaction between aluminium and water vapor which is reported as under.

$$2Al + 3H_2O \rightarrow Al_2O_3 + 6H^+ + 6e^- \qquad (1.1)\ [95]$$

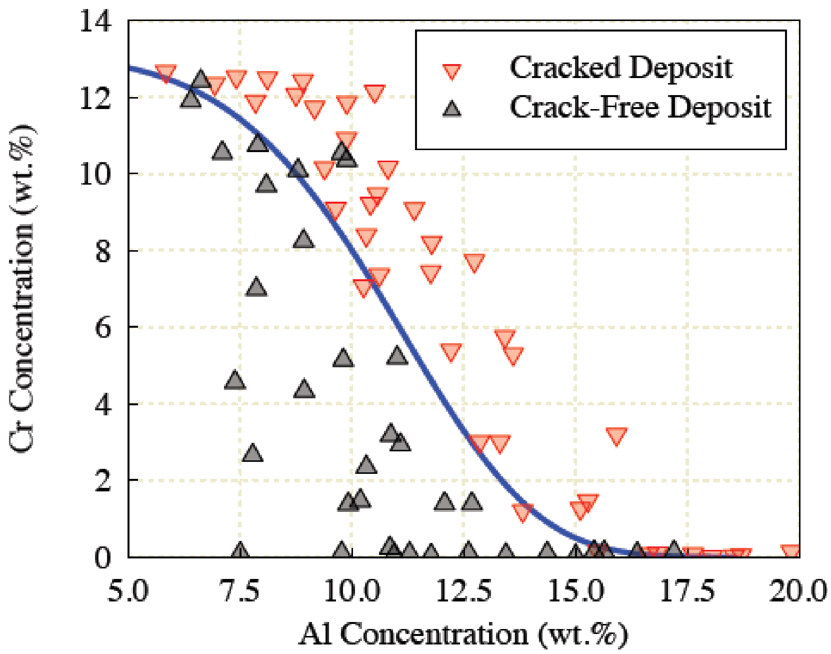

Figure 1.05 Composition effect on the weldability of FeCrAl alloys after gas tungsten arc welding (GTAW) [88]

The studies of Zacharia et *al*. reported the weld cracking at the centerline as shown in Fig. 1.6 due to the presence of Aluminium [96]. The detailed study and scientific explanation have been reported by Regina et *al*. [97].

Figure 1.06 Optical micrograph of FA-41 weldment showing a centerline [96]

1.5.2 Effect of Coating on weld bead (Size and Shape)

The weld geometry which includes the depth of penetration (DOP) and weld bead width are crucial aspects of weldability. The DOP and weld bead's width are functions of weld current and travel speed. However, the coating at the top might influence the weld geometry as reported by many researchers. Author Park et *al.* [98] explained the effect of coatings on weld bead for ferrite stainless steels. They demonstrated the effect coating with respect to different heat-inputs for coated steels and uncoated steels. In their study, the welds have been prepared at different weld speeds with a constant current 90A. As shown in Fig. 1.7 1a, 1b, 1c, 1d and 1e shows the cross sections weld bead at different weld speed respectively, (a) 0.32 m/min,(b) 0.42 m/min, (c) 0.52 m/min, (d) 0.60 m/min, (e) 0.64 m/min for uncoated steel. On the contrary, Fig. 1.7 2a, 2b, 2c, 2d, 2e show the depth of penetration and width of the weld bead is different at the same heat input (weld current and weld speed) are higher and more constricted. The study concludes that due to the Al-Si coating at the top different mechanism such as reverse marangoni conviction is responsible for higher depth of penetration in case of coated steels. Similar observations have been reported elsewhere [99] in which authors have investigated the effect of coating on the depth of penetration for Al-10%Si coated ferritic stainless steel with laser beam welding process. The comparison of cross sections for coated and uncoated steels has been shown in Fig. 1.8. Hence, it is essential to examine the effect of the coating on the depth of penetration and as well as weld bead width.

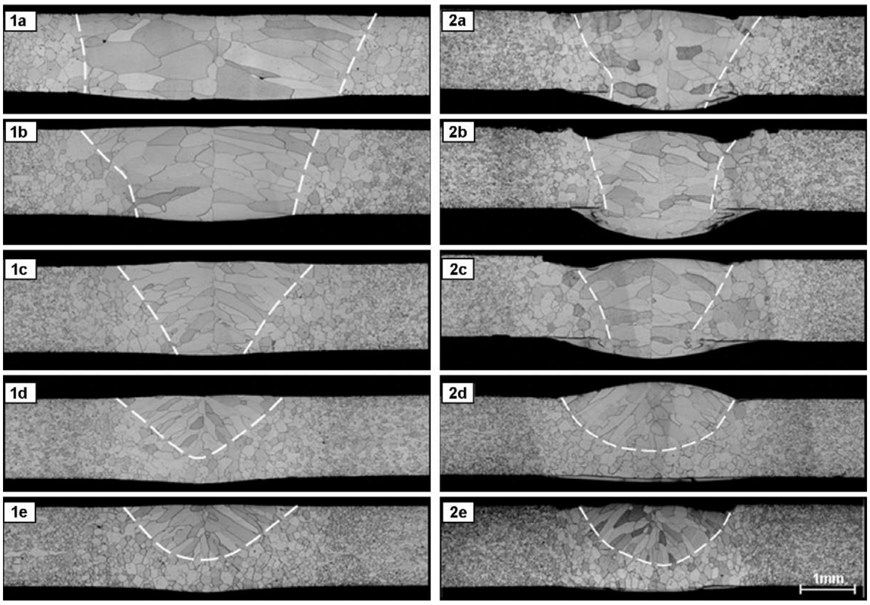

Figure 1.07 Cross-sections bead of the ferritic stainless steel 409L (1) and Al coated 409L (2) joints welded by various welding speed at welding current of 90 A: (a) 0.32 m/min,(b) 0.42 m/min, (c) 0.52 m/min, (d) 0.60 m/min, (e) 0.64 m/min[98]

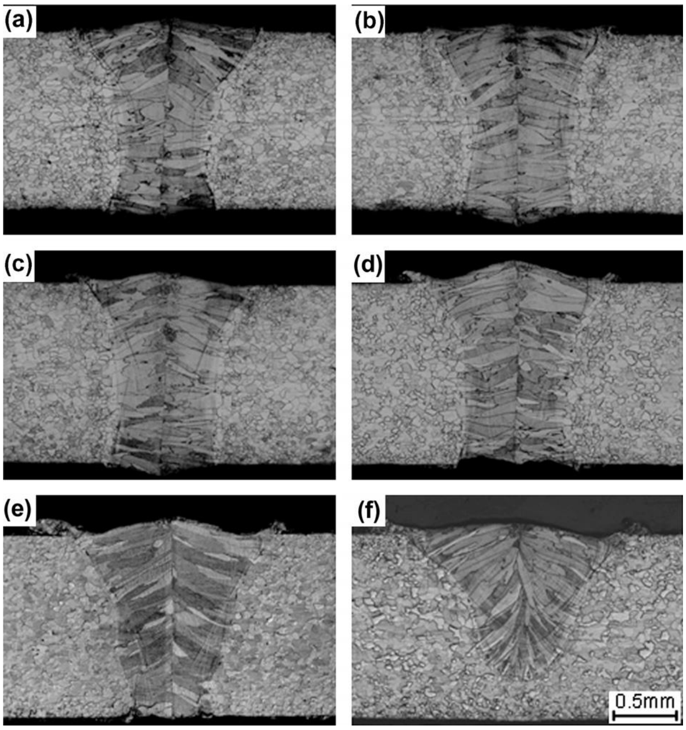

Figure 1.08 Cross-sections of welds with various welding speeds at laser power of 5 kW: (a) 5 m/min, (b) 6 m/min, (c) 7 m/min, (d) 8 m/min, (e) 9 m/min and (f) 10 m/min[99]

1.5.3 Delta (δ) ferrite formation

Another major concern is the delta ferrite formation in the weld metal during the welding of 9Cr steels. 9–12% Cr steels have one of the several sub-liquids phases depending on the temperature. During the process, the liquid metal solidifies as delta-ferrite and transforms into austenite crystals. This process starts at around 1300 °C and ends at 1200 °C under equilibrium condition. However, this equilibrium transformation is not possible during weld cooling cycle due to the high cooling rates. Hence, it is possible that some amount of delta-ferrite is retained in the weld metal even at ambient temperatures and up to some extent in the heat affected zone [100]. Fig. 1.9 indicates the presence of delta ferrite formation for 9 Cr steels.

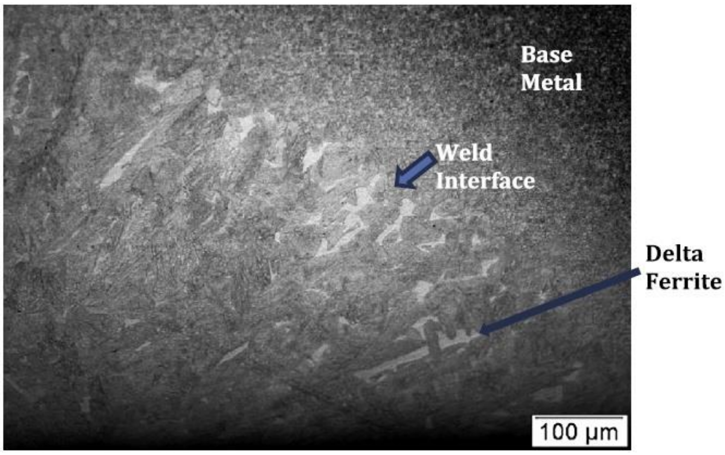

Figure 1.09 Delta ferrite formation at weld interface of 9Cr Steel[101]

The presence of delta-ferrite has been found to have detrimental effects on the toughness of base metal as well as welds [102]. With an increase in delta-ferrite in the matrix, a steep increase in the ductile brittle transition temperature (DBTT) has been observed and hence delta-ferrite is not preferable in the weld as it leads to a reduction in the notch toughness, creep ductility at high temperatures [103].

Delta ferrite formation has been reported for the weldments of coated steel too. Bertin et *al.* [104, 105] noticed that after the arc-welding of Aluminium coated steel, a phase consist of delta ferrite formed in the welded joint and inferior the tensile strength. Literature suggests that the concentration of Aluminium is also a major concern as it supports the formation of delta ferrite. Briand et *al.* [106] determined the presence of Aluminium (>2%) in the weld pool, which gives rise to the form of delta ferrite and resulted in lower hardness in the weld zone. Delta ferrite formation may enhance solidification cracking, impair toughness due to notch sensitivity of the delta ferrite phase, and reduce the creep ductility at high temperature and so on in 9-12% Cr metals and welds [107]. Wang, P. et *al*. and Anderko, K. et *al*. reported that the presence of delta ferrite deteriorates the impact properties and raises the DBTT of the martensitic stainless steel [102, 108].

1.5.4 Al_2O_3/FeAl segregation at the weld fusion line

The possibilities of segregation or accumulation of coating layer (Al_2O_3+FeAl) in weld metal are high. The alumina at the top will not get dissolved during the welding as it has a higher melting point (2200 °C). Consequently, the alumina or iron aluminides may get dissolve in weld metal or it may remain present at the weld interface. Author Kong et *al.* [99] have done analysis with reference to the distribution of an Aluminium through electron probe micro analysis (EPMA). Fig. 1.10 shows the distribution of Al and Si concentration after the welding of Al-10% Si coated ferritic steel. The content of both Si and Al were high at the surface and in the fusion zone. Therefore, the consequences of dissolved Al and Si on the microstructure of the fusion zone was investigated using an optical microscope and SEM in the fully penetrated joint by Kim et *al.* [109]. The small amount of Al and Si was observed in the weld zone, which was dissolved from the coating layer. The plate interface was enriched with Al and resulted in the formation of intermetallic compounds FeAl, $FeAl_3$, and Fe_2Al_5. Therefore, it is very important to investigate the segregation of alumina or iron aluminide in the weld microstructure as it may alter the mechanical properties.

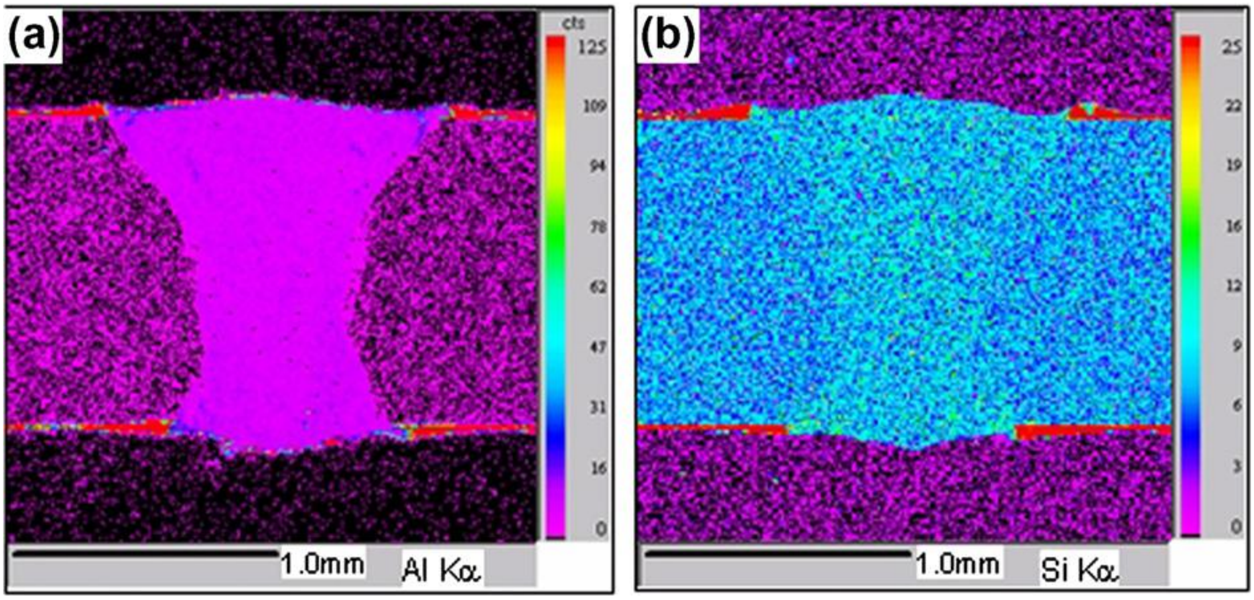

Figure 1.10 EPMA mapping results showing (a) Al and (b) Si in weldments of [99]

1.5.5 Mechanical properties of aluminide coated steels

The most important aspect of weldability is mechanical properties such as tensile strength and impact strength. It is a common understanding that the tensile strength and impact strength should be in-line with the base metal. Therefore, mechanical testing is a crucial aspect of any weld joint. In addition, the issues discuss prior might have detrimental effects on microstructure and consequently the mechanical properties may get alter. Hence, the mechanical properties of the weld joint of coated steels need detail investigations. The fractography study of tensile sample and impact samples will also be very crucial as it will enhance the understanding of the effect of coating on microstructure.

1.6 Aim and Objectives

The aluminide coating for different materials has been optimized microstructurally, however, the fabrications sequence is scarcely reported. Based on aforementioned issues, the aim is to address these lacunae with several sub-tasks and their objectives. One of the objectives is to investigate the effect of aluminide coating on weld bead dimensions. This is addressed by autogenous TIG welding bead-on-plate trials. Another important objective of this work is to examine the effect of Aluminium on weld microstructure. Bead-on-plate trials would thus reveal adequate information related to the effect of coating and Al concentration in the weld metal. Further, such an exercise would also provide data on possible optimization to achieve an acceptable weld microstructure and the same can be implemented with v-groove weld joint. Subsequently, the assessment of mechanical properties such as tensile strength and impact toughness of weld joint would be essential to demonstrate its engineering feasibility.

The present study emphasizes the need to study weldability of aluminide coated steels. The study elucidates the following objectives

<u>Objectives</u>

- ❖ Investigations on the effect of coating on weld bead dimensions (Size and Shape)
- ❖ Examine the effect the of Aluminium on weld microstructure
- ❖ Assessment of mechanical properties of the weld joint with V-groove

CHAPTER 2

EXPERIMENTAL WORK

2.1 Materials and Methods

The 9Cr-1Mo or P91 or Grade 91 steels were used in the experimental work as substrate material. The chemical composition of P91 alloy as confirmed by spark emission spectrometry (ASTM E415) is as given in table 3.01. The P91 steel confirming to ASTM A381 Grade 91 used in this study was manufactured by Arcellor Mittal, Belgium and were supplied in normalized and tempered heat treatment condition.

Table 2.00.1 Chemical composition of ASTM A 387 GRADE 91 steel (P91) in wt%

Elements													
C	**Cr**	**Mo**	**Si**	**Mn**	**Nb**	**V**	**Al**	**S**	**P**	**Cu**	**Ni**	**N**	**Fe**
0.09	9.30	0.88	0.20	0.45	0.088	0.20	0.04	0.01	0.02	0.10	0.20	0.07	Balance

The experimental work comprises of three different parts as follows. First part (Part I) covers aluminide coating processes with different steps such as hot-dipping followed by different heat treatments. Second part (Part II) focuses on welding process related to investigation of weldability of coated P91 steel in comparison with bare (uncoated) substrates. The third part (Part III) comprises of Characterization and assessment of mechanical properties of welded coated and uncoated samples..

2.2 Part I - Aluminide coating process

The aluminide coating process involves hot dip aluminizing followed by heat treatments such as normalizing and plasma tempering. The process flow chart is shown in Fig. 2.01. Hot dip aluminizing of P91 steels was carried out as per the steps specified in IS:8508-2006. Commercial grade Al-Si alloy were manufactured locally and supplied by a foundry in Ahmadabad, India. Chemicals such as K_2ZrF_6 powder, COVERAL flux (Fosesco make) for Al drossing, acetone for ultrasonic cleaning, H_2SO_4 for pickling were used during hot dip aluminizing process. The coating process has been explained below in detail and later the heat treatments are also discussed.

2.2.1 Hot-dip aluminizing (HDA)

The hot dip aluminizing (HDA) process involves dipping of P91 steel substrates in molten Al-7%Si bath and slow withdrawal after a fixed dwell time of few seconds. The hot dip aluminizing was conducted following the standard IS: 8508-2006. The sample preparation of P91 steel includes machining and polishing of the surface up to 2 delta surface finish. The P91 steel samples were wire cut in to different sizes. 75 x 25 x 5 mm samples were prepared for bead-on-plate TIG welding experiments and 150 x 100 x 5 mm samples were for conventional TIG welding experiments. The samples were suspended with a SS304 rod and subjected to ultrasonic cleaning in acetone for a period of 10 minutes. The ultrasonically cleaned samples were then subjected to pickling in 10% H_2SO_4 solution at 70-80 ºC for 20 seconds.

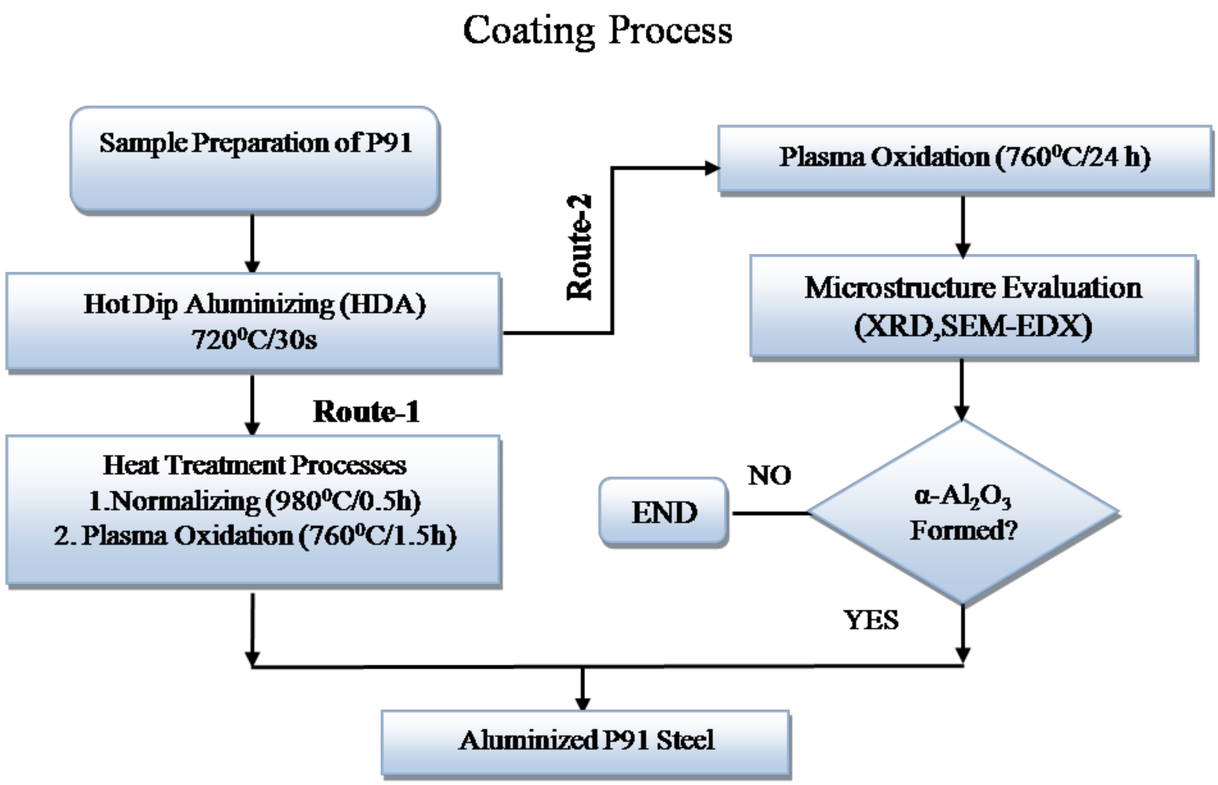

Figure 2.01 Process flow chart of Aluminide coating

This pickling was done to remove oxides from the surface. To avoid further contamination and improve the wettability with liquid Al, the P91 samples were treated with aqueous flux K_2ZrF_6 . The wettability of samples was increased with the help of 5% K_2ZrF_6 for a period of 5 minutes at 60-80 ºC and subsequently air dried prior to hot-dipping process.

The hot dip aluminizing (HDA) involves dipping of P91 steel samples in molten Al bath and slowly withdrawing to form an Al coating on P91 steel substrates. The equipment used for this HDA process include a Roop Telsonic make 1.5 litre ultrasonic cleaner, Sartorius make weigh balance with an accuracy of 0.01 mg, a hot plate for heating the flux solution for sample preparation; and 2kW top loading box type resistance furnace (Fig. 2.01). . The equipment and process details are explained below.

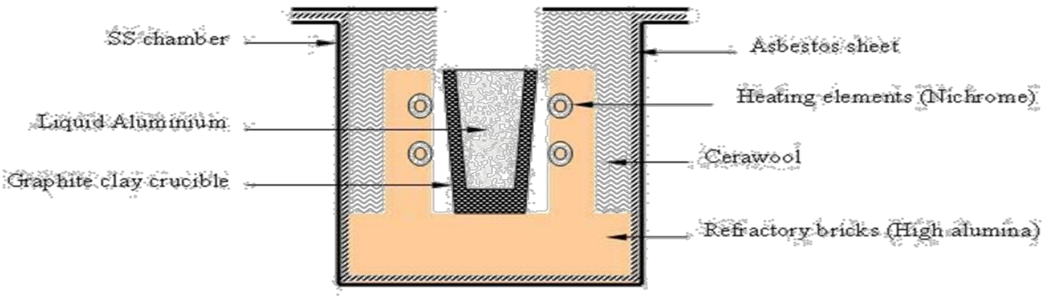

Figure 2.02 Conceptual drawing of box type top loading hot dipping aluminizing (HDA) furnace

The molten bath of Al-7%Si alloy was prepared by melting the Al-Si ingot bars in a graphite crucible in the top loading resistance furnace as shown in Fig. 2.02. Once the charge was melted, the molten Al-Si bath was held at 720 ºC as measured using the immersion type 'K' type thermocouple. The fluxed samples were then dipped in the Al-Si bath for a period of 30 seconds and slowly withdrawn and air cooled. This process is explained with schematic in Fig. 2.03. The as-coated HDA samples were then subjected to further heat treatment.

2.2.2 Heat-treatment processes

The samples after hot-dip aluminizing were weighed using a Sartorius make microbalance with an accuracy of 0.01 mg. The weighed samples were acetone cleaned and subjected to different heat treatments of normalizing (980 ºC/30 min) + plasma tempering (760 ºC/1.5 h) for facilitating diffusion as well as alumina formation. These heat treatments are denoted as route 1 (see Table: 2.02). Whereas in the Route 2, plasma oxidation heat treatment was conducted directly without normalizing up to 24hrs for 760 ºC. This was done to explore whether the required coating can be achieved without going to very high temperatures (980 °C).

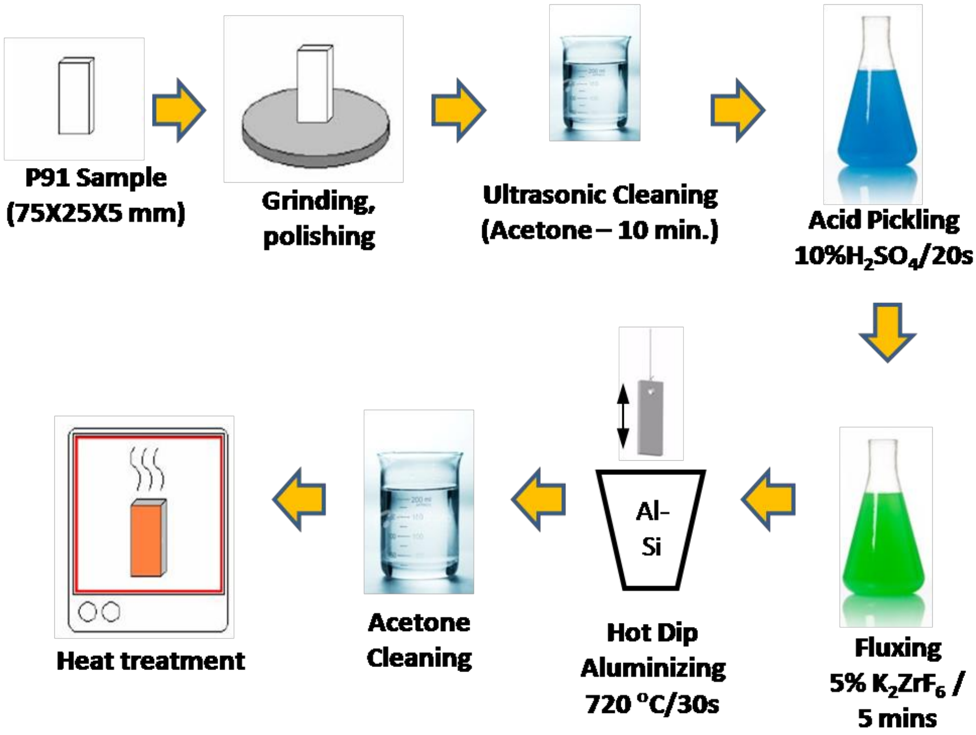

Figure 2.03 Schematic of different steps of hot-dipping process

The heat treatment equipment utilized for the normalizing of aluminized samples is a tube type muffle furnace (See Fig. 2.04 (a)). The tube type muffle furnace had a recrystallized alumina tube of dimensions Ø60 mm x 200 mm length wound with a nichrome resistance heater of 1 kW. The entire tube was enclosed in an SS enclosure and controlled using a variac and a controller linked to K type thermocouple. The muffle furnace as used in experiments is shown in Fig. 2.04 (a). The plasma oxidation system was modified and altered as per required heating configuration (Fig. 2.04 (b)). As shown in Fig. 2.04 (b), the system has vacuum chamber Ø250 mm x 250 mm ht with heating arrangement, rotary vane type vacuum pump (21 m^3/hr), vacuum gauges, precision gas dozing valve and 3A, -800V, 10kHz DC pulsed power supply for substrate biasing and plasma production [110]. Kanthal A1 (FeCrAl) heaters have been used under electrical isolation to avoid the glow discharge on the heating elements. The chamber was cooled externally using cooling channels. The process parameters of both the routes are summarized in the table 2.01.

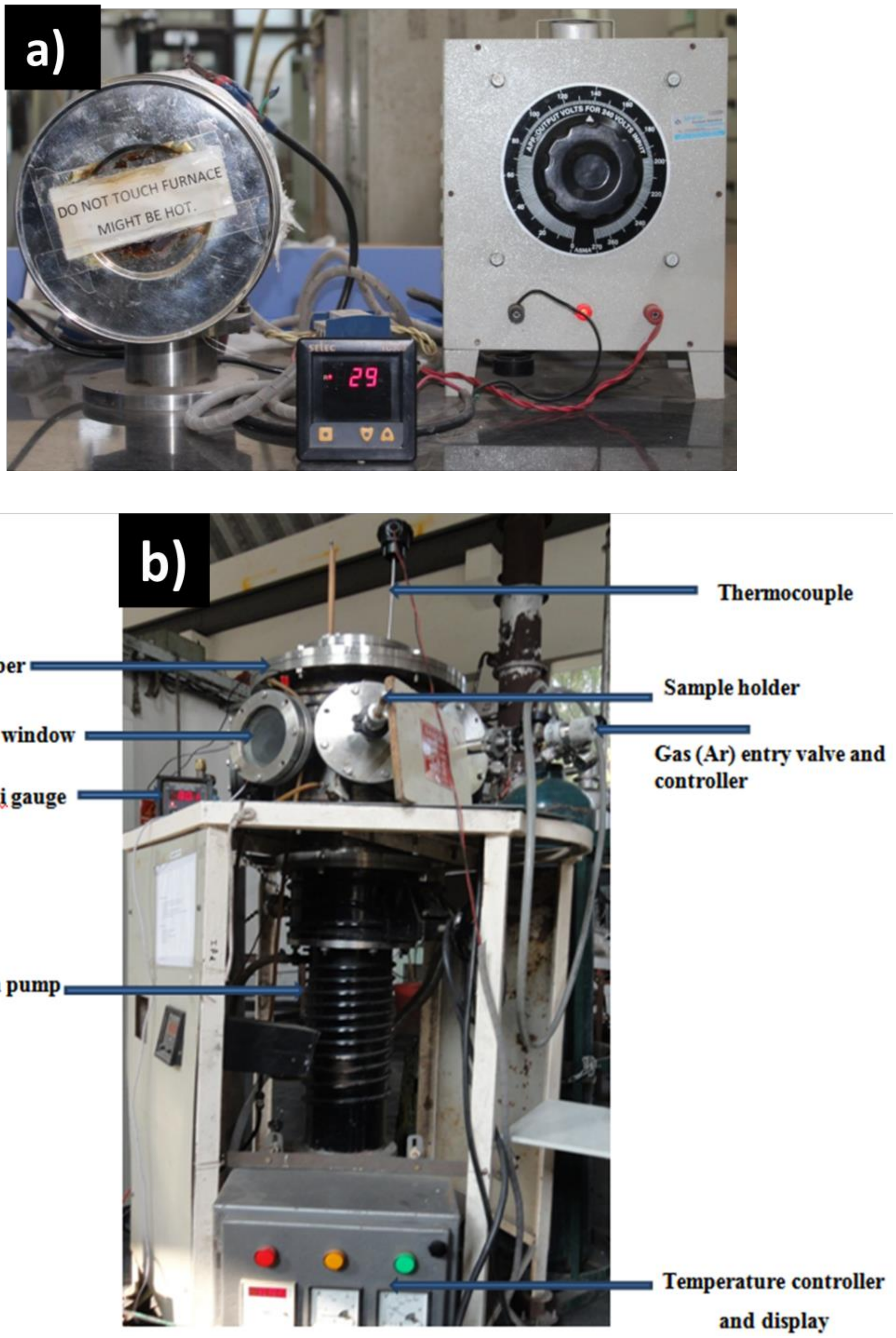

Figure 2.04 a) Tube type muffle furnace b) Plasma oxidation system

Table 2.00.2 Heat treatment parameters after hot dipping process

	Normalizing Parameters	Plasma oxidation parameters
Route-1	980 °C/ 0.5 hours muffle furnace	760 °C/ 1.5 h in vacuum furnace with pulsed DC- O_2 Plasma @ 5mbar pressure
Route-2	----	760 °C/ 24 h in vacuum furnace with pulsed DC- O_2 Plasma @ 5mbar pressure

Two types of heat treatments were studied to analyse the phase formation of α-alumina. The purpose of route 2 was to evaluate the effect of oxygen plasma environment on formation of α-Al_2O_3 as it was carried out for 24h. The normalizing process was eliminated in second route to achieve desired alumina layer without significant distortion. Another probable benefit on a larger scale is that the coating process can be completed with single heat treatment. The samples with effective route meeting required coating characteristics were then subjected to the welding processes.

2.3 Part II – Welding processes

There are several welding techniques reported for 9Cr-1Mo like manual metal arc welding, gas tungsten arc welding (GTAW) or TIG welding, submerged arc welding and so on [111-114]. Among these, TIG welding technique was selected for the present study as it is most widely used technique to weld the materials such as steels, aluminium and copper alloys. This welding technique delivers high quality welds with high purity. In TIG welding, an arc is formed between a non consumable tungsten electrode and the work (base metal), to create coalescence between two or more metals. Non consumable electrodes come in various sizes and lengths, and are typically made of pure tungsten or an alloy of tungsten. TIG welding process has been adopted as standard welding practice for high quality engineering jobs related to precision fabrication jobs including space components, nuclear fission and fusion power plants and so on. As a result of its weld quality and wide spread applicability, the welding experiments were conducted with TIG welding process. The TIG power source (Panasonic) having a capacity of 200A with 25% duty cycle was customized with an additional attachment for torch movement was used for these welding experiments. These equipments were assembled and used for autogenous TIG welding process available at Pandit Deendayal Petroleum University, Gandhinagar. This machine was developed under the sponsored research project from BRFST (Board of Research in Fusion Science and Technology) and have been used extensively for the TIG welding application by different authors [115, 116]. The set-up is shown in Fig. 2.05 with special purpose machine, argon cylinder for shielding the arc, fixture and welding torch. Welding experiments with various types of TIG welding processes were carried out, i.e. (a) Autogenous TIG welding (b) Autogenous Activated TIG welding and (c) conventional TIG welding processes. The welding technique with the most acceptable weld profile was chosen for further testing and assessment.

2.3.1 Autogenous TIG welding process

With the necessary expertise and/or appropriate equipment, TIG welding can be performed manually, automatically, or by using a hybrid approach. Extensive welding trials for this research were conducted with autogenous TIG machine as well as conventional method. The coated and bare 9Cr-1Mo samples were welded to optimize the weld parameters by preparing bead-on-plate welds (see Fig. 2.06). The bead-on-plate trials were conducted to investigate the effect of coating on weld microstructure as well as to analyze the depth and width of weld metal. The process parameters for bead-on-plate trials for both coated and uncoated P91 steels are mentioned in table 2.03.

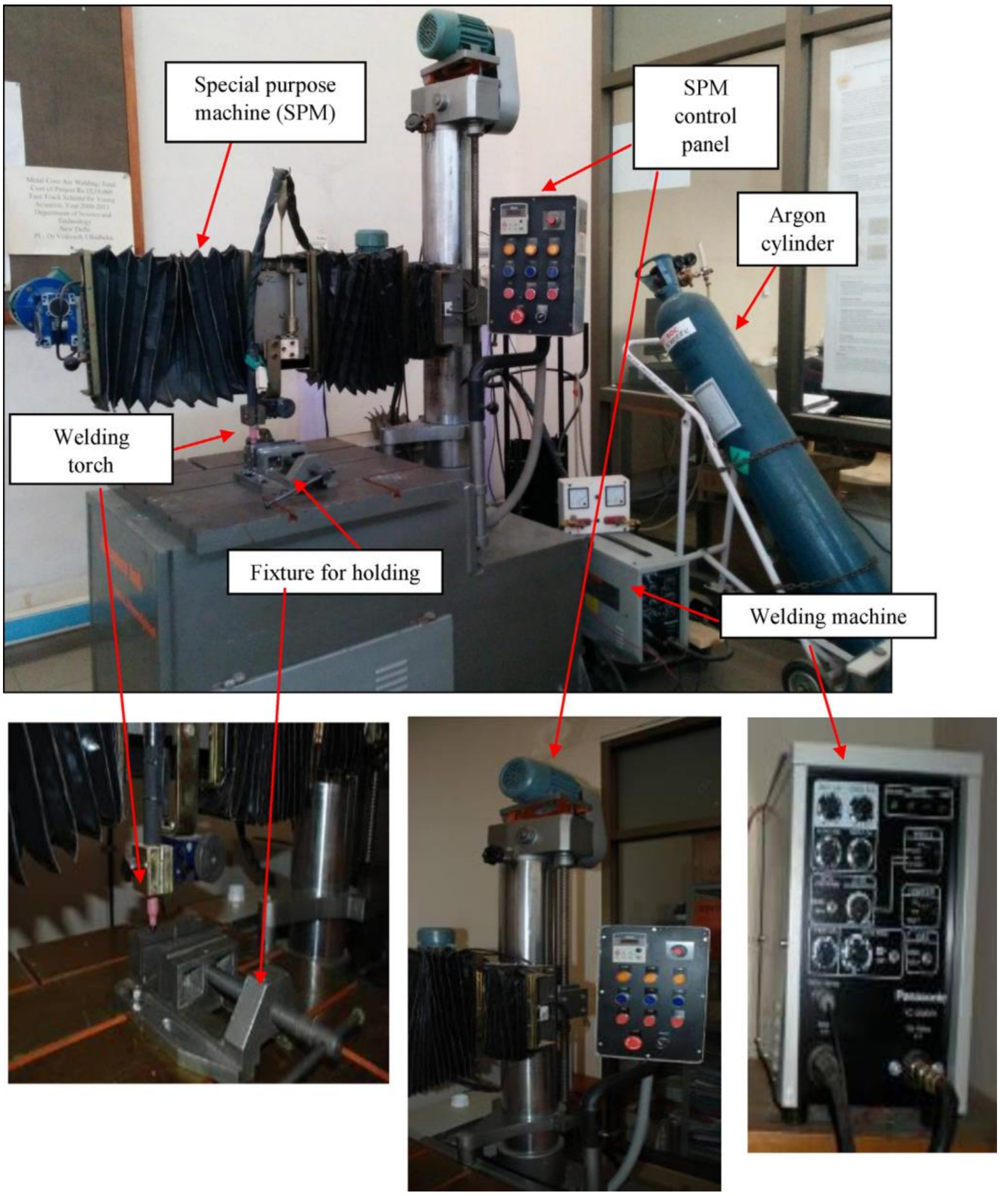

Figure 2.05 Autogenous TIG welding set-up [117, 118]

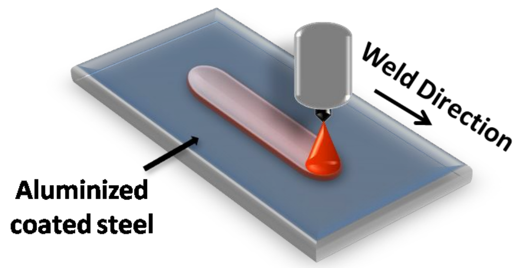

Figure 2.06 Schematic of bead-on-plate welding for aluminized coated steel

The bead-on-plate welds were prepared by keeping the current constant and varying the travel speed for both coated and bare 9Cr-1Mo steels. All other conditions, like the electrode diameter, electrode tip angle, arc gap, gas flow rate and so on. were kept constant for both coated and bare samples. The trials were conducted four times to ensure the repeatability for the same and average values have been reported in this study. These process parameters were set to investigate the effect of coating on weld metal dimension and microstructure. By varying the weld speed at same welding current for both coated and bare P91 steel, the heat input was varied. Subsequently, the effect of interaction of arc with coated layers was briefly studied.

Table 2.00.3 TIG welding parameters for coated P91 and bare P91 steel samples

Welding current	:	200A
Creator current	:	160A
Travel speed	:	100, 125, 150 mm/min
Electrode type	:	Tungsten (2% thoriated)
Electrode diameter	:	2.9 mm
Electrode angle	:	18–20° (blunt ground at tip)
Arc gap	:	2–3 mm
Gas flow rate	:	10–12 l/min
Welding position	:	1 G (flat)
Electrode extension	:	5–6 mm
Nozzle diameter	:	8 mm

2.3.2 Autogenous A-TIG welding process

Many advances have surfaced pertaining to TIG welding making the process more efficient and productive. The maximum weld penetration reported for the process ranges from 3.0 - 3.5 mm which makes the process incapable of welding plates of thickness 6 mm and higher in singles pass and autogenous mode [119]. The only option available to weld higher thickness was either double sided joint or addition of filler metal. However, both of these methods involved design considerations, escalation of cost and increased time for welding thereby reducing the productivity. A partial answer to the challenge was formulated by development of Activated TIG (A-TIG) welding process at Paton institute of electric welding in 1960 at Ukraine[117, 120]. A-TIG welding is a variant of TIG welding process which employs a single component or mixture of chemical powder/s (termed as flux) in TIG welding process. The flux is converted to paste form by adding solvents (such as acetone, methanol and so on.) and applied on the upper surface of the plate [118, 121]. Standard autogenous TIG welding process is then carried out with the flux layer being in between welding arc and plate. An increase of about 300% in the weld penetration has been reported by researchers [122]. The schematic of A-TIG process is explained in Fig. 2.07 (a) [118, 123]. It contains three different steps. As mentioned the first step is weighing of flux which is calculated according to the area applied and density of flux. The second step is mixing of that flux with a solvent such as acetone. The solvent acts as a carrier when the flux is applied with the help of brush. Once the acetone evaporates, the TIG welding has been performed. Fig. 2.07 (b) shows an image of A-TIG process after the application of flux on weld coupon. Once the welding was done, the cross-sections of samples were investigated to examine weld metal microstructure as well as the weld's bead width and depth.

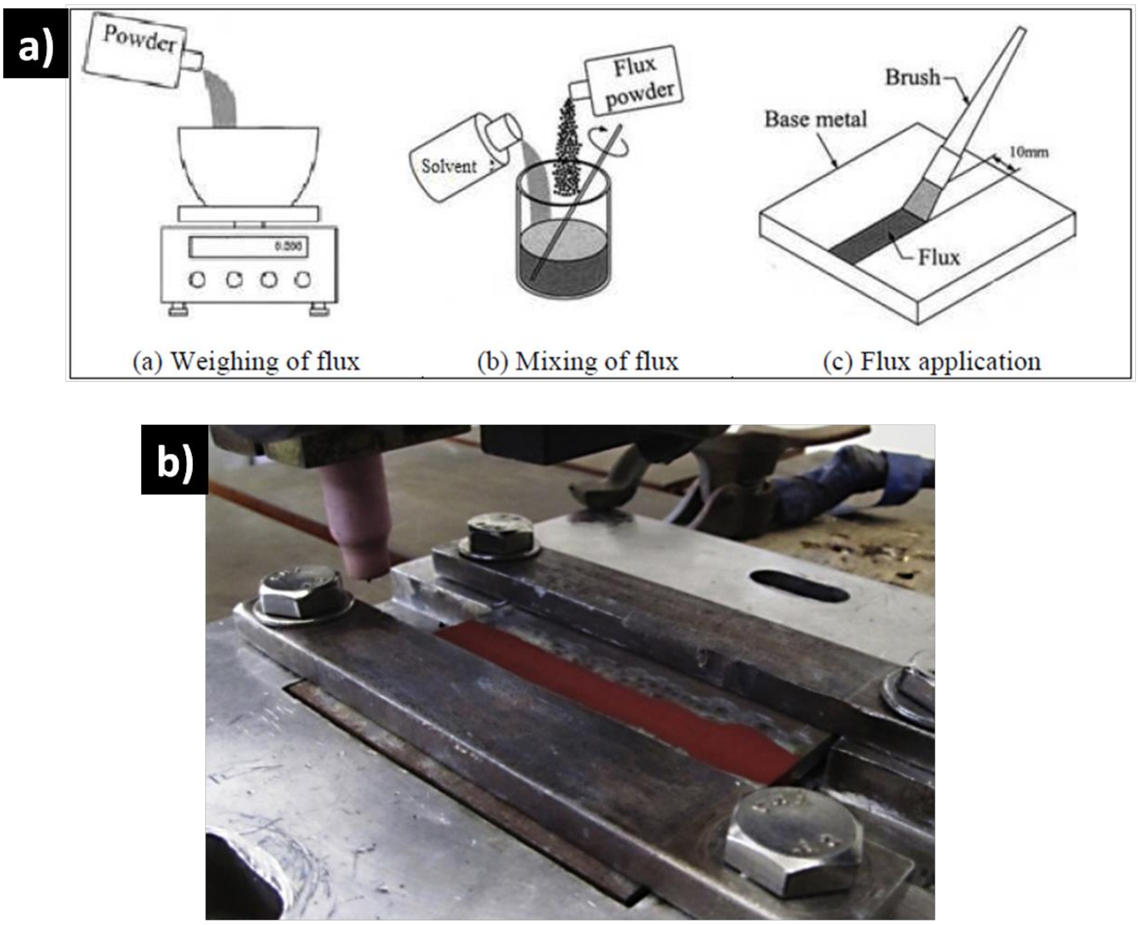

Figure 2.07 a) Schematic of different steps in Activated TIG welding process b) Weld coupon with Activated flux before welding

2.3.3 Conventional TIG welding process

The major process parameters such as weld current and weld travel speed was optimized through bead-on-plate trials with the help of autogenous TIG welding process as mentioned earlier. The coating at the top lead to the formation of oxide inclusions and other deteriorating phases which further affects the mechanical properties. In addition, to investigate the mechanical properties ASTM (American Society for Testing and Materials) standards were followed. Hence, the size of the P91 samples was modified and the coated P91 steel as well as the un-coated P91 steels were welded through conventional TIG welding process. The process parameters were utilized from the autogenous bead-on-plate trials.

In conventional TIG welding, the accuracy is highly dependent on the qualified welder. Different parameters such as current and weld current, weld speed, intermediate temperature during multi passes, heat input were very critical to achieve defect free and sound weld. Consequently, the welding was carried out by the WPS-PQR qualified welder for P91 steels. The coated and bare samples are having dimensions of 150mm x 100mm x 5mm as mentioned earlier. The v-groove design or edge preparation was made as per the ASME Section-IX, QW 200. The schematic is shown in Fig. 2.08.

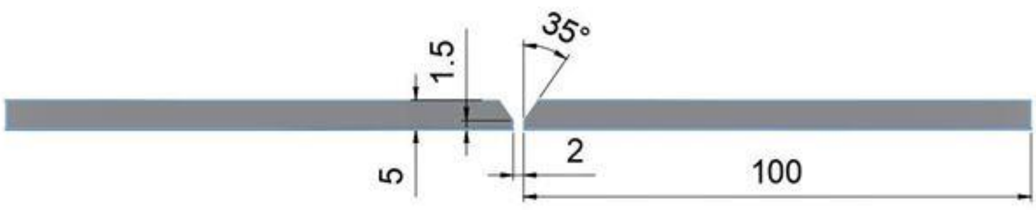

Figure 2.08 Schematic of V-grove design before welding

The details of V-groove design is as under.

- Bevel angle - 30-35º
- Root face – 1.5 mm
- Root gap – 2-3 mm
- Filler – ER 90S-B9
- Pre-heat temp.-200º-250º C
- Inter-pass temp.-250º-300ºC

The samples after edge preparation were utilized for the conventional TIG welding. The welding parameters are mentioned in the table 2.04 which includes weld current, travel speed, voltage and average heat input for root pass and subsequent multi passes of TIG welding process.

Table 2.04 Conventional TIG welding process paramters

Process (TIG)	No. of Pass	Current (I) Amp	Voltage (V) volts	Travel speed (T) mm/min	Heat input
root pass	01	115-120	11-12 V	~80	~1.1 kJ/mm
passes	1st	125-130	10-11 V	~70	~1.4 kJ/mm
	2nd	125	12V	~75	~1.3 kJ/mm
	3rd	130	12V	~70	~1.4 kJ/mm

Once the welding was done, the joints were subjected for radiography testing as per ASME section V article 2 procedures in as welded condition to ensure the weld is defect free. The weld joint for coated steel and weld for uncoated steel were defect free as per the acceptance standard ASME section IX QW 191.2.2. The welded plates were then subjected to post weld heat treatment (PWHT). The PWHT was carried at 760°C ± 5°C for 2h which also supports the literature for 9Cr-1Mo steel weld joints [111, 113, 124]. The PWHT is required to eliminate the residual stresses because during the welding cooling rate was not controlled. This usually leads to residual stress formation and distortion consequently it can deter the mechanical properties.

2.4 Part III - Characterization and assessment of mechanical properties

The samples prepared with coating processes and welded samples with different techniques were subjected to different characterization techniques. The phases formed after the coating and welding process were analyzed with the help of X-ray diffraction method. Similarly the macro and micro-structure analysis was attempted by Optical microscopy and scanning electron microscopy (SEM). The different phases and micro- structural studies were then correlated with micro-hardness. Finally, the examination of the mechanical properties such as tensile strength and impact toughness of the welded samples (both coated and uncoated) were carried out. These different analyses along with machine's details and testing parameters are explained one by one and analyzed in comparison with the bare P91 (uncoated) weld properties.

2.4.1 X-ray diffraction (XRD)

The Phase analyses of 9Cr-1Mo steels were conducted by using X-Ray Diffraction (XRD) for different samples such as bare P91 steels (uncoated), after HDA coating and after heat treatment. The XRD machine is manufactured by Bruker, Germany (Model: D8 Discover) with Cu$K\alpha$ radiation (λ = 1.5406 Å). The 2θ scanning range was maintained from 20º to 100º at a scan speed of 0.5 seconds/step with an increment of (step size) of 0.01º. The resultant scan data was analyzed from the ICDD database reconfirmed using Bruker Diffract.eva software provided with the XRD system.

2.4.2 Scanning electron microscopy (SEM) and Elemental analysis

The surface morphological studies and cross-sectional microscopy was conducted using a scanning electron microscope (HR-SEM Model: Carl Zeiss, Supplier: VP Merlin, Germany). All the samples for morphological studies were gold coated using a thermal evaporation method to avoid charging effects. The samples for cross-sectional studies were hot mounted on a Cu base conducting mount and in a mirror polished condition. Elemental analysis was conducted on the samples using energy dispersive spectroscopy (EDS). EDS analysis was conducted using Bruker make Energy Dispersive spectroscopy attachment, with SEM.

2.4.3 Micro-hardness measurement

Vicker's microhardness test is an indication of local hardening effects in various parts of the weldzone. It also helps in corroborating the presence of a particular phase. The Vickers micro-hardness (Model: Mitutoyo, JAPAN) tests were performed at the cross-section of all the coated and heat treated samples. Micro-hardness was measured in the molded specimens for both coated samples as well as the bare sample after welding in various regions such as base metal, heat affected zone and the weld metal across the cross-section. in the coated specimen. The hardness tests were performed at a load of 50gms with a dwell time of 10 sec. Measurements of multiple specimens and at multiple locations were taken and the average values are presented.

2.4.4 Tensile Tests and Impact Strength

Tensile strength and impact toughness of the weld joint were crucial properties for this study as they enable the applicability of the coated steels in selective sectors such as space, nuclear fission and fusion systems. Therefore, the effect of coating on microstructure and consequently on the tensile and impact properties needs to be investigated. The test samples were extracted transversely from the centre of the weld joint for both, tensile and impact testing (see Fig. 2.10). ASTM E8M-04 standard was followed for the tensile tests and dimensions are shown in the schematic (Fig. 2.09). The strain rate was $3 \times 10^{-3}\ s^{-1}$ maintained for all the tests for both coated and uncoated samples. The cross-head speed was 1.97 mm/min and the tests were conducted on vertical tensile test machine (INSTRON 5980). 3 sets of samples were tested at room temperature to ensure the consistency of results. Similarly, Charpy V-notched method was used on sub-sized samples (55mm x 10mm x 5 mm) for impact toughness of weld joint. The schematic of impact samples is shown in Fig. 2.10 which is in line with the dimensions specified in ASTM: E23-12c standard. V-notch has been made at the centre of the weld so that the fracture will occur within the weld zone. The tests were carried out at room temperature, 0°C, -25°C with two sets where each sets has 3 samples for each condition. The average values were considered for analysis for both and tensile and impact tests. These conditions for tensile and impact testing have been already reported elsewhere [120, 125, 126]. The fractured surfaces have been analyzed and correlated with weld microstructure along with reasonable arguments and supporting literature.

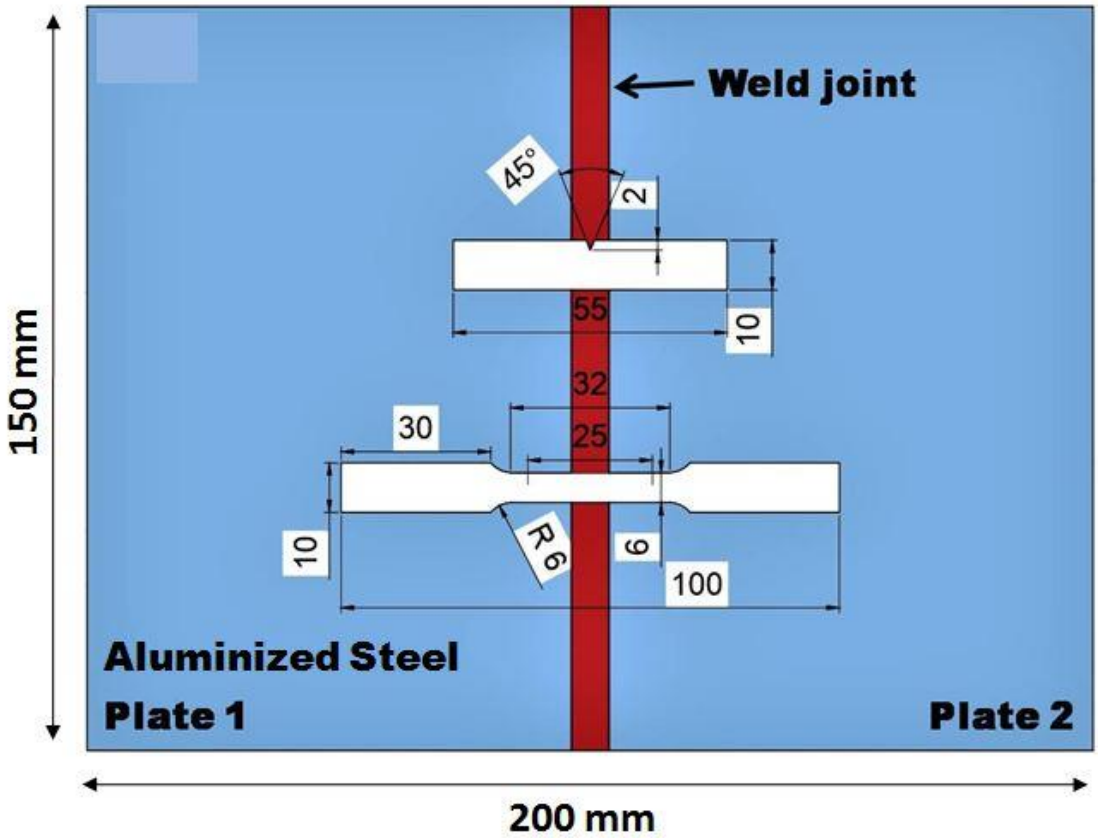

Figure 2.09 Schematic of welded plates with a) V-grove design b) Design of tensile and impact specimens

2.4.5 Fractrogaphy

To investigate the effect of coating on mechanical properties the fractured surface were investigated on macro and micro level. The mode of fracture and scientific explanation has been discussed in Chapter 5. This information was very helpful and it supported our scientific understanding. SEM was extensively utilized to analyze the fracture behavior of specimens. The details of fractrography along with different types of fractures and its photographs is illustrated in detail in results and discussion chapter 5.

2.5 Complete flow chart of experimental work

The flow chart of experimental work is illustrated on following page.

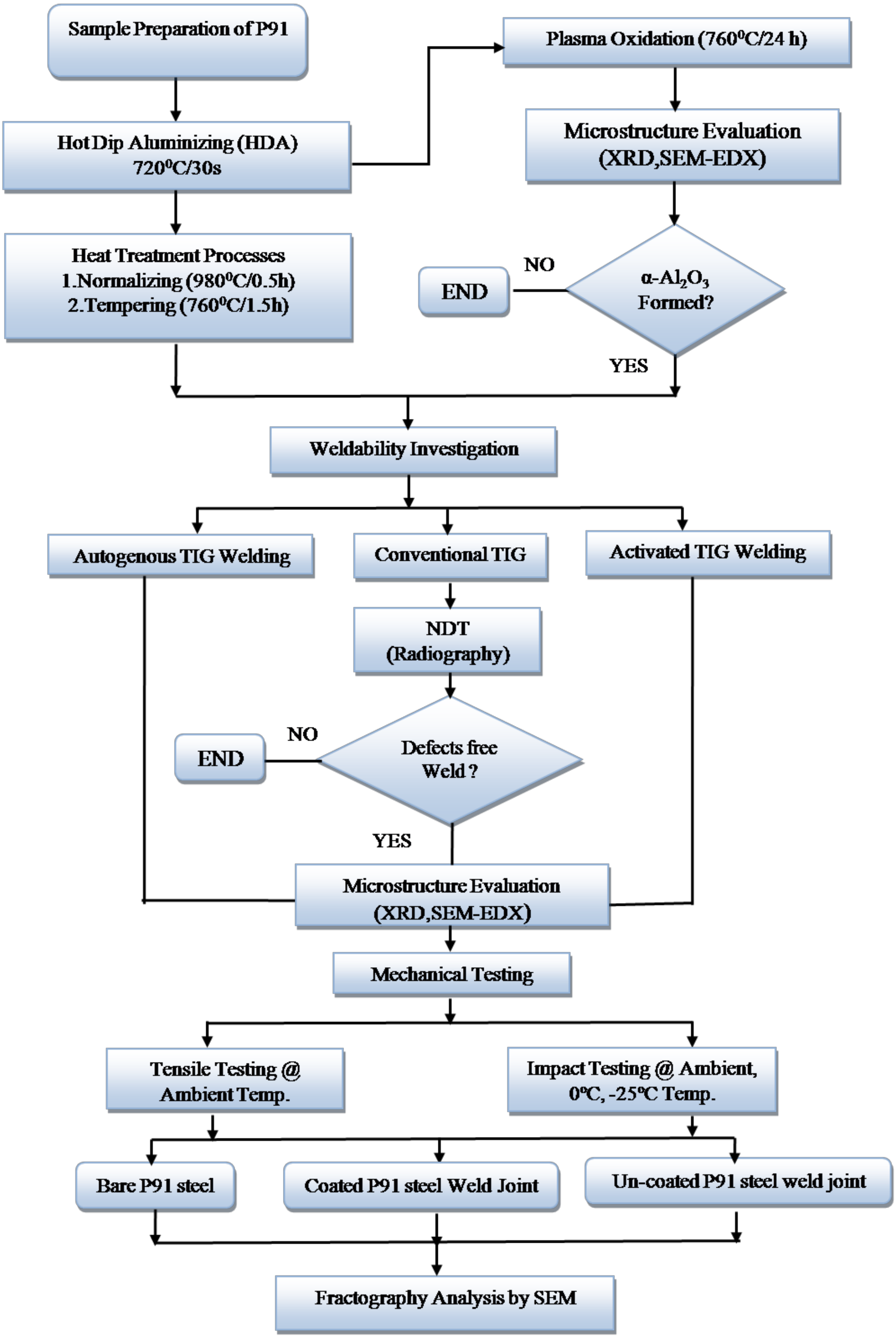

Figure 2.10 Flow chart of experimental work

CHAPTER 3
EFFECT OF COATING ON WELD METALLURGY

3.1 Introduction

The aluminide coating process explained in the previous chapter generates an alumina (Al_2O_3) film followed by iron aluminides (FeAl) layer on the surface of P91 steel substrates. These aluminide coatings have an Al reservoir of ~60-80 micronsin the diffusion coating. In order to understand the microstructure of the resultant diffused aluminide coating, the cross-section of coated samples was polished and and so on and followed by electron microscopy studies. Layers of Al_2O_3 and FeAl could be distinctly identified in the SE image (see Fig. 3.01). The phases such as α-Al_2O_3 and FeAl were confirmed through X-ray diffraction (XRD). The diffractrogaph of bare P91 steel and coated P91 steel is shown in Fig. 3.02. The Al_2O_3 oxide layer was confirmed by XRD in the heat treated samples. As shown in Fig. 3.02, the XRD spectra of bare GRADE 91 steel (substrate) revealed (110), (200), (211) peaks confirming the Fe-Cr alloy as per JCPDS the file no. 65-4607, while the XRD spectra of coated GRADE 91 steel indicates α- Al_2O_3 peaks from (012), (104), (110), (113), as per the JCPDS file no. 43-1484.

Though these coatings have been reported as candidates from performance perspective, especially in high temperature applications for oxidation and corrosion resistance; one of the major issues associated with such coating is the joining process. It is not very clear whether the components should get fabricated first and then coated or coated first and then fabricated. It appears that fabrication followed by coating may not be a good option as diffusion heat treatment after the coating may induce heavy distortions. Alternatively, the second option involving coating process followed by fabrication poses uncertainties of weldability of coated steels as the wedability of coated steel is scarcely reported. Hence, it is a primary step to investigate the weldability of aluminized P91 steels.

Published literature [98, 127] reveals that the Al present in the diffusion coating may alter the metallurgy of the weld metal upon welding and might subsequently deteriorate the mechanical properties. In order to do a preliminary assessment of the effect of Al on the resultant weld, a ‘bead-on-plate’ trial was required. This would reveal adequate information related to the Al concentration in weld pool, its effect on depth of penetration and microstructure of resultant weld pool. Further, such an exercise would also provide initial data on possible process optimization to achieve an acceptable weld microstructure.

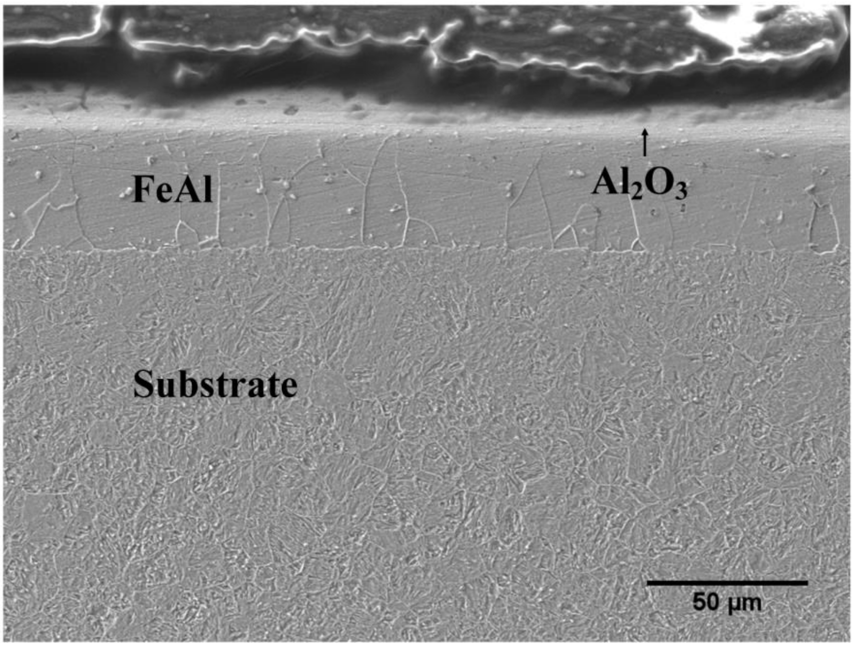

Figure 3.01 SEM image of cross-sectional microstructure of coated 9Cr-1Mo steel [128]

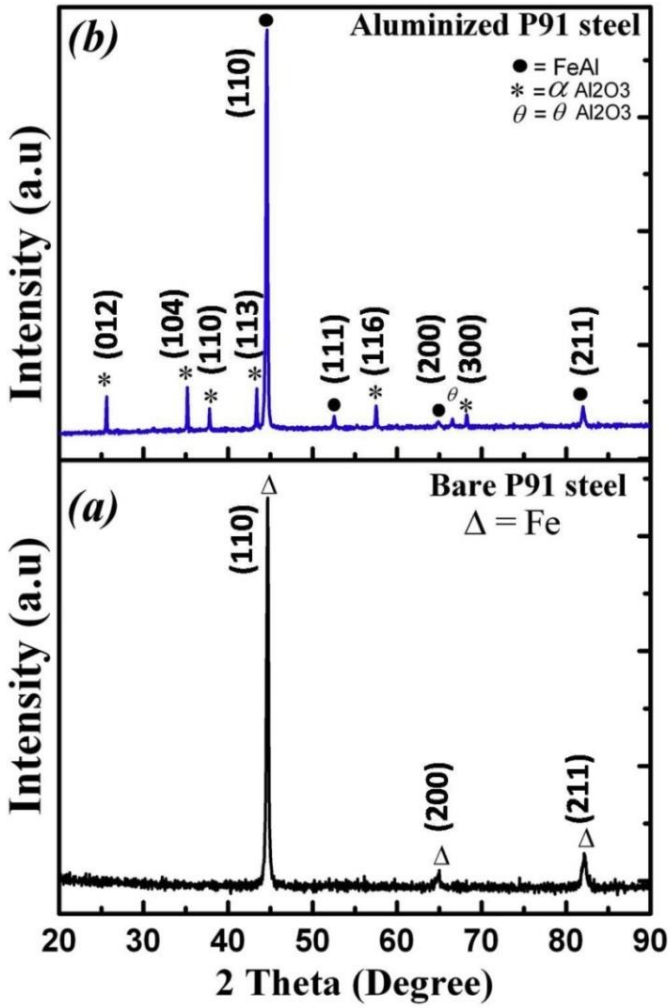

Figure 3.02 XRD spectra of bare and coated P91 steels [128]

The optimized parameters would be crucial to attempt conventional welding for the coated steel as it will also provide the important inputs regarding heat-input. This chapter includes the results obtained through bead-on-plate trials by autogenous TIG welding process, microstructural observation and data analysis using different characterization techniques and results from the experiments so conducted. . The data is published in fusion engineering and design [128].

3.2 Effect of coating on weld bead

The coated P91 steel contains an oxide layer of alumina at the top followed by a diffusion layer of FeAl. The oxide layer of alumina and iron aluminides has been confirmed through XRD results (see Fig. 3.02). These coated samples were then subjected to autogenous TIG welding process. The bead-on-plate trials were conducted with parameters mentioned in the Table 2.03 in chapter 2. The weld current was kept constant and the weld speed was varied to analyze the effect of heat input. These process parameters were chosen after rigorous feasibility trials.

3.2.1 Arc constriction in coated substrate

In TIG welding, the energy for melting the weld metal is obtained from the kinetic energy that is imparted to the charged species (electrons or positively charged ions). The coated and bare P91 samples acting as parent metal. The tungsten electrode was connected as cathode and the parent metal was connected as anode. The anode connection was grounded. Usually when a welding arc strikes between the tungsten electrode and the metal plate, it spreads in a limited exposed area owing to free electrons in metals showing a conducting path. In case of aluminized P91 samples, a thin insulating layer of alumina is present at the top surface exposed to the electrode. Hence, when the arc interacts with the top alumina layer, the electron does not get a free path to spread like in the bare material/uncoated steel. Due to this, constriction of arc takes place which increases the current density. Since more energy is dumped in a comparatively smaller area, the depth of penetration (DOP) increases and bead width of weld becomes narrower compared to that obtained in the bare P91 steel bead on plate. The schematic shown in Fig. 3.03 (a) illustrates the arc constriction mechanism. As visible in Fig. 3.03 (b) and (c), the width of arc bead (9 mm) in coated P91 steels is narrower compared to the weld bead of bare grade 91 steel (11.5 mm) at same heat input. This phenomenon of improved depth of penetration due to coating is known as insulation effect and reported by Vilarinho et *al.*[129]. Similar mechanism is also reported in Refs. [130, 131] where enhanced depth of penetration was achieved for P91 steels. For coated steels, similar observations on higher depth of penetration were reported by Park et *al*. [98] using Al-8Si% based aluminized based coatings on ferritic stainless steels. The effect of alumina layer can be clearly indentified from the visual inspection at the sample surface.

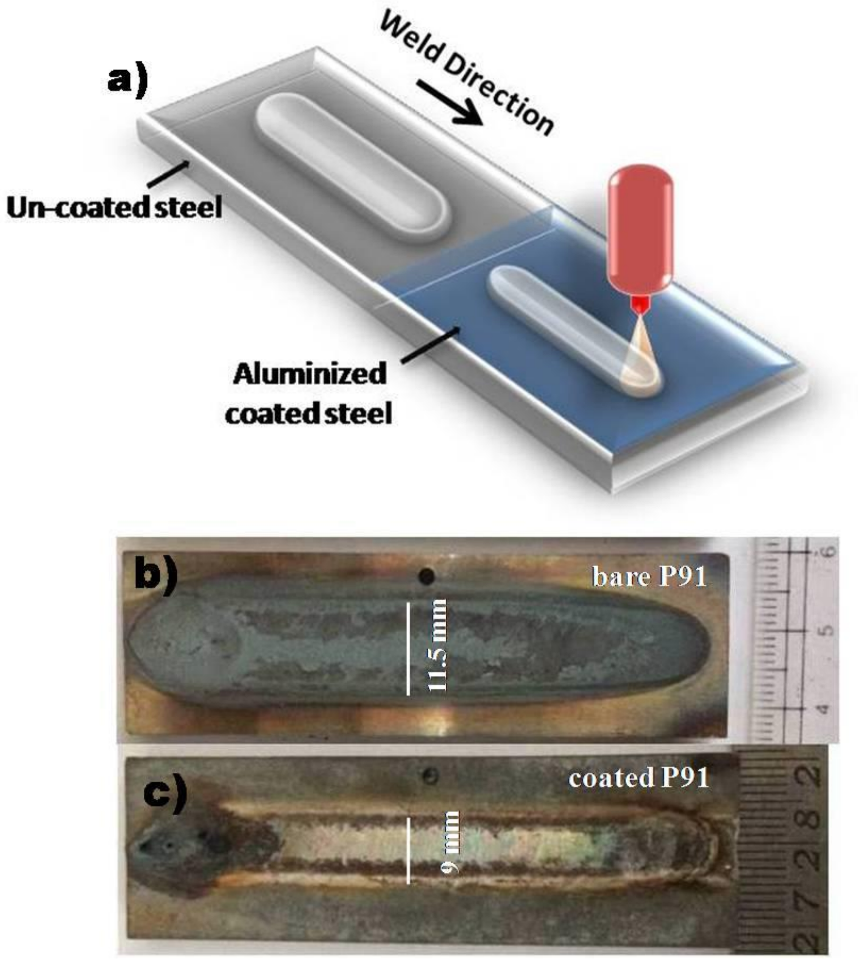

Figure 3.03 a) Schematic of arc constriction, Surface appearances b) weld bead of 9Cr-1Mo steel, c) weld bead of coated 9Cr-1Mo steel [128]

Esme et *al*. [132] conducted an analysis of variance (ANOVA) study on the most significant parameter affecting weld bead in TIG welding process and concluded that the welding speed was the most critical parameter. Based on this, the weld speed was varied i.e. 100 mm/min, 125mm/min, 150 mm/min and the weld current was kept constant at 200 A (see Table 3.01). Samples having weld bead for coated P91 steels were labeled as 1-a,b,c and, the bare P91 steel samples were labelled as 2-a,b,c. It should be noted that, the welding current (200A) and weld speed (100 mm/min) were kept same for both coated P91 steel (Sample 1a and 2a) as well as the uncoated (bare) P91 steel. Similarly, 1b and 2b are welded at 125 mm/min weld speed and 1c and 2c are welded at 125 mm/min. The nomenclature is summarized below.

Table 3.00.1 Weld parameter of samples with nomenclature

	Samples	**Weld speed**	**Weld current**
Coated P91 steel	1a	100 mm/min	
	1b	125 mm/min	
	1c	150 mm/min	200 A
Un-coated P91 steel	2a	100 mm/min	
	2b	125 mm/min	
	2c	150 mm/min	

3.2.2 Investigation of depth of penetration (DOP) through macrostructure

To investigate the weld pool and its metallurgy, the metallographic specimens were prepared by polishing on different grit size papers (400, 600, 800, 1000, 1200, and 2000) then and so onhed in Villella's solution (Picric acid 10 g + HCl 5ml +

Methanol 100 ml) as per ASTM E3-01 standard. The macro and microstructural examinations were conducted to check the weld bead shape and DOP by using an optical microscope (OM).

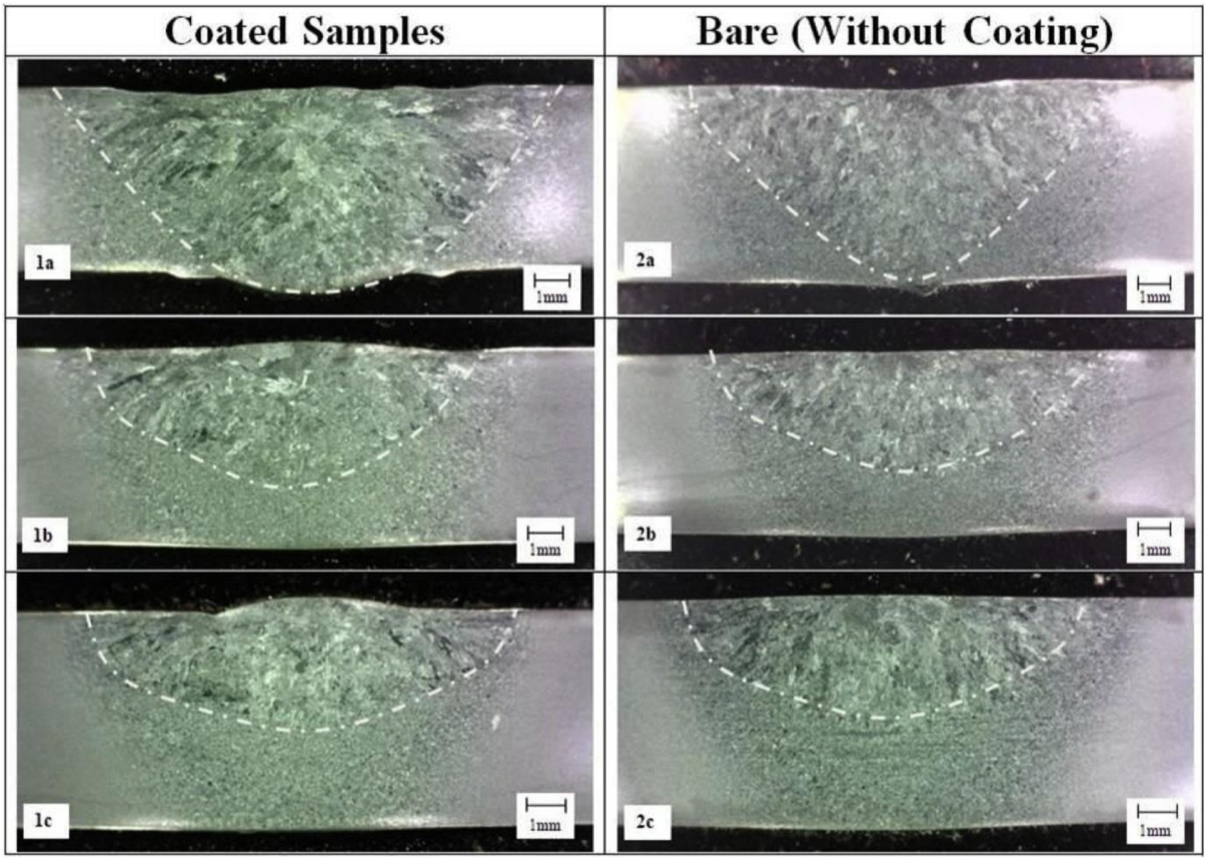

Figure 3.04 Cross-sections bead of the Aluminized coated 9Cr-1Mo Steel (1) and bare 9Cr-1Mo (2) joints welded by various welding speed at welding current of 200 A: (1a and 2a) 100 mm/min, (1b and 2b) 125 mm/min, (1c and 2c) 150 mm/min [128]

Fig. 3.04 represents the macrostructures of the weld bead for coated and bare samples, while the Fig. 3.05 shows the variation in bead width, depth of penetration; D/W (depth to width) ratios along with the heat input and weld speed. Samples having nomenclatures 1a, 1b, 1c are weld bead for coated P91 steels, whereas 2a, 2b, 2c represent bare steels. The depth of penetration is higher for the sample 1a (coated ones) compared to 2a which is un-coated. Both weld beads were prepared at the same current, i.e 200A and same weld speed 100 mm/min. The same trend has been observed for other samples namely 1b and 2b and 1c and 2c which were prepared by varying the weld speed 125mm/min and 150 mm/min and keeping the current constant, at 200A. In Fig. 3.05, the depth, width and D/W ratio has been shown graphically along with the heat input for both coated and bare P91 steel for better understanding.

It clearly indicates that, the coatings play a major role in arc constriction which subsequently results in higher depth of penetration (DOP) and good D/W ratio for the coated P91 steel. As the required DOP was observed in sample 1a and 2a, these two samples were considered for further characterization.

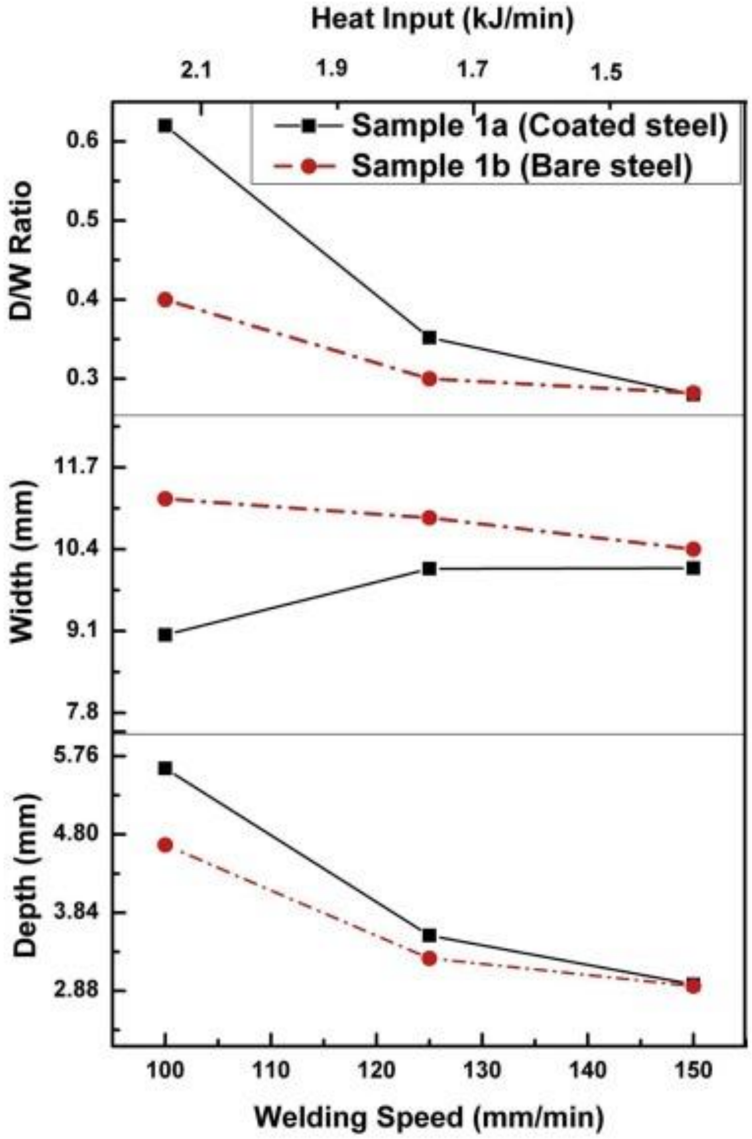

Figure 3.05 Variation of the penetration depth (D) and width of the bead (W) and the D/W ratio with heat input for sample 1a and 2a [128]

3.3 Microstructure of weld metal – AlN inclusion formation

The cross-sectional examination of coated samples before welding revealed the presence of AlN formation at the interface of FeAl and substrate. The nitrogen content in this steel was 0.07 wt% (max.). During diffusion coating process, Al diffuses into the base metal and reacts with the nitrogen at the interface and forms AlN [133, 134]. These precipitates were mainly formed during the coating process and they have subsequently been transferred into the weld bead during welding. The AlN precipitates were not dissolved and reformed during welding and cooling, due to their high melting point [135]. As shown in Fig. 3.06(a), the AlN precipitates were observed within the weld zone for sample 1a and it was confirmed through EDX mapping where red color represents the presence of Al (indicated with arrow in 3.06(c)), while the green is of Nitrogen (3.06(d)), blue and remaining one represents Fe (3.06(e)) and Oxygen (3.06(f)). The EDX spectra taken on the AlN inclusion is shown in Fig. 3.06(b) and the Al:N ratio confirms the composition of AlN. These AlN precipitates were absent in the weld zone of 2a sample as it was bare grade 91 steel.

To investigate the base (parent) metal, heat affected zone (HAZ) and the weld zone; the cross-section of 1A sample was examined and is shown in Fig. 3.07. The base metal of the welded sample is denoted as A and represents the base metal's grain in SEM image where the grain size was observed to be very small compared to the HAZ and weld zone. As we move from base metal to weld zone (from A to C) gradually, the grain size is observed to increase and in the weld zone, it is maximum compared to base metal and HAZ. However the HAZ revealed a combination of coarse grain (CGHAZ) near the fusion line of weld and fine grain (FGHAZ) near the base metal as the heat was dissipated during the cooling process towards the base metal (from C to A). Since the weld zone (part C) was the last to cool down, the grain size was in descending order from C to A.

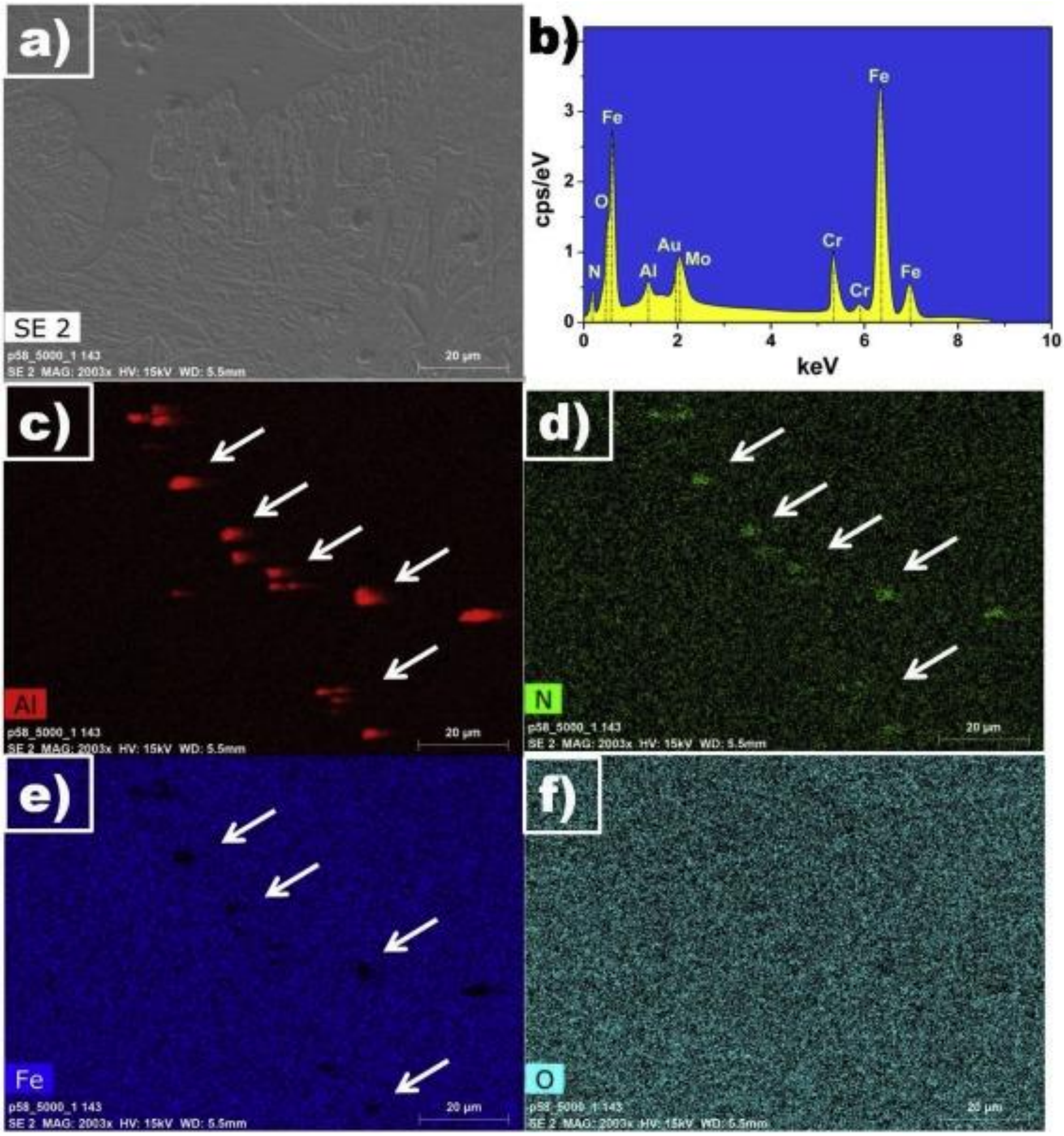

Figure 3.06 EDX mapping of AlN precipitates in the weld zone for sample 1a (Coated P91 steel). (a) SE image of weld zone used, (b) EDX spectra of the mapping data, (c) mapping of Al(aluminium) in red colour, (d) mapping of N (Nitrogen), (e) mapping of Fe, (f) mapping of O [128]

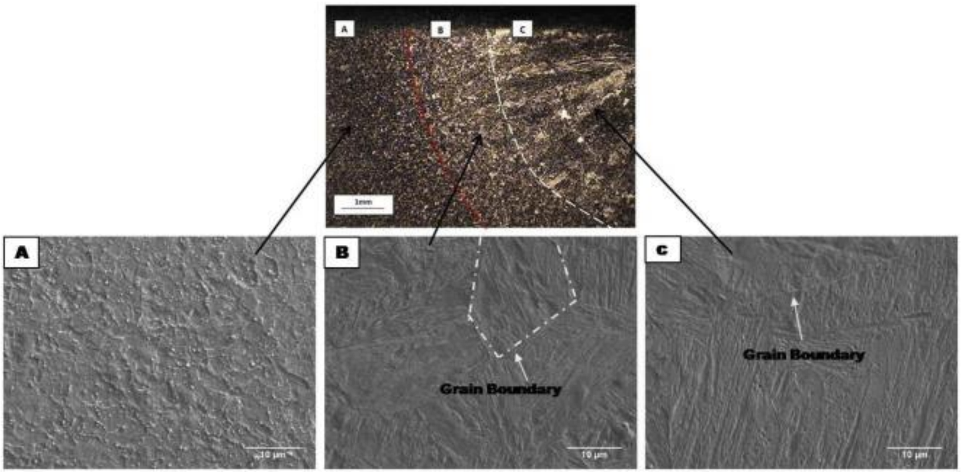

Figure 3.07 Optical and SEM image of cross-sections bead of the coated 9Cr-1Mo (sample 1 A) at welding current of 200 A and weld speed: 100 mm/min A) base Metal B) heat affected zone C) weld zone. [128]

Fig. 3.08 (A) shows the typical microstructure of weld zone for sample 1a. It revealed the prior austenite grain boundary (PAGB) along with the $M_{23}C_6$ precipitates (M: Cr, Fe, Mn and Mo) in a cluster form as it is in as weld condition. To confirm the presence of precipitates on PAGB, an EDX spot was taken for analysis which corroborated its presence.. The same trend was observed in the weld zone of 1b sample (bare P91 steel). It is also shown along with the EDX spot taken at PAGB in Fig. 8(c) and (d). Another observation was that the martensitic laths of sample 1b were larger in size (length and width) as compared to the weld zone of coated P91 steel (sample 1a).This could be linked with the average grain size being affected due to the presence of Al in the weld pool. More detail are discussed in section 3.4 of this chapter.

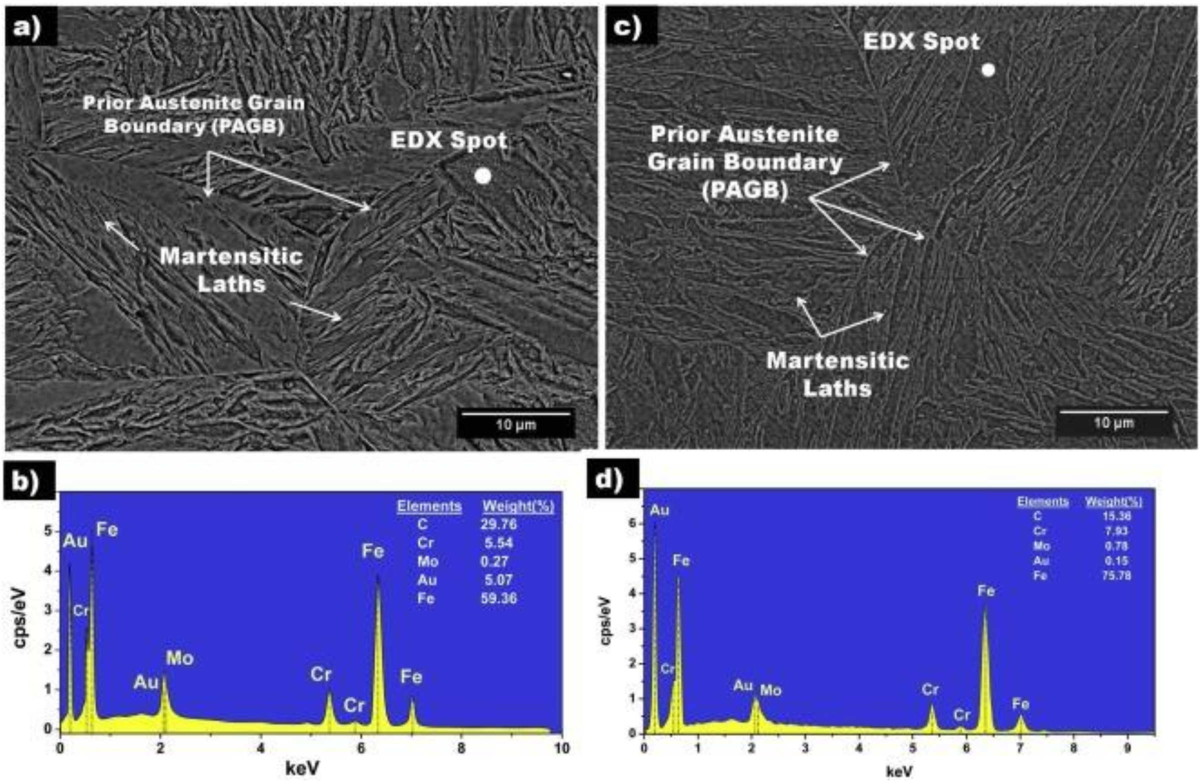

Figure 3.08 SE micrograph of weld zone (a) sample 1a (Coated 9Cr-1Mo), (b) EDX spectra of precipitates, (c) sample 1b (bare P91), (d) EDX spectra of precipitates. [128]

3.4 Al concentration in weld zone and its effect

To investigate the Al concentration from the surface to core in the coating region and weld metal, elemental depth profiling was done by EDS analysis. The profile of different elements is plotted along with the distance from surface to core at the parent metal (or base metal) side and at the weld metal side. Fig. 3.09 (a) illustrates the cross-section of sample 1a (coated 9Cr-1Mo steel) at the parent metal (also referred here as base metal) side and Fig. 3.09 (c) represents elemental depth profile of Al and other elements which are obtained with EDS. The base metal side of coated sample shows oxide layer (Al_2O_3) at the top up to ~3-5 microns followed by Fe-Al diffusion zone of ~80-100 microns. The concentration gradient of Al indicates the presence of FeAl and Fe(Al) according to the Fe-Al phase diagram. The FeAl phase in the coating was already confirmed through XRD (see Fig. 3.02). However, Aluminum in the weld zone (Fig. 3.09 b) and d)) was found almost same at different regions in the weld zone which indicates that Al is homogenously distributed in the weld metal region. It also confirms the absence of various phases such as FeAl, Al_2O_3 which were present in the coating prior to welding. The Al concentration in the weld zone was found to vary in to the range of ~1-2 wt%. In addition, across the weld the concentration of Al was investigated by area EDX and the same concentration was confirmed (~1-2 wt%).

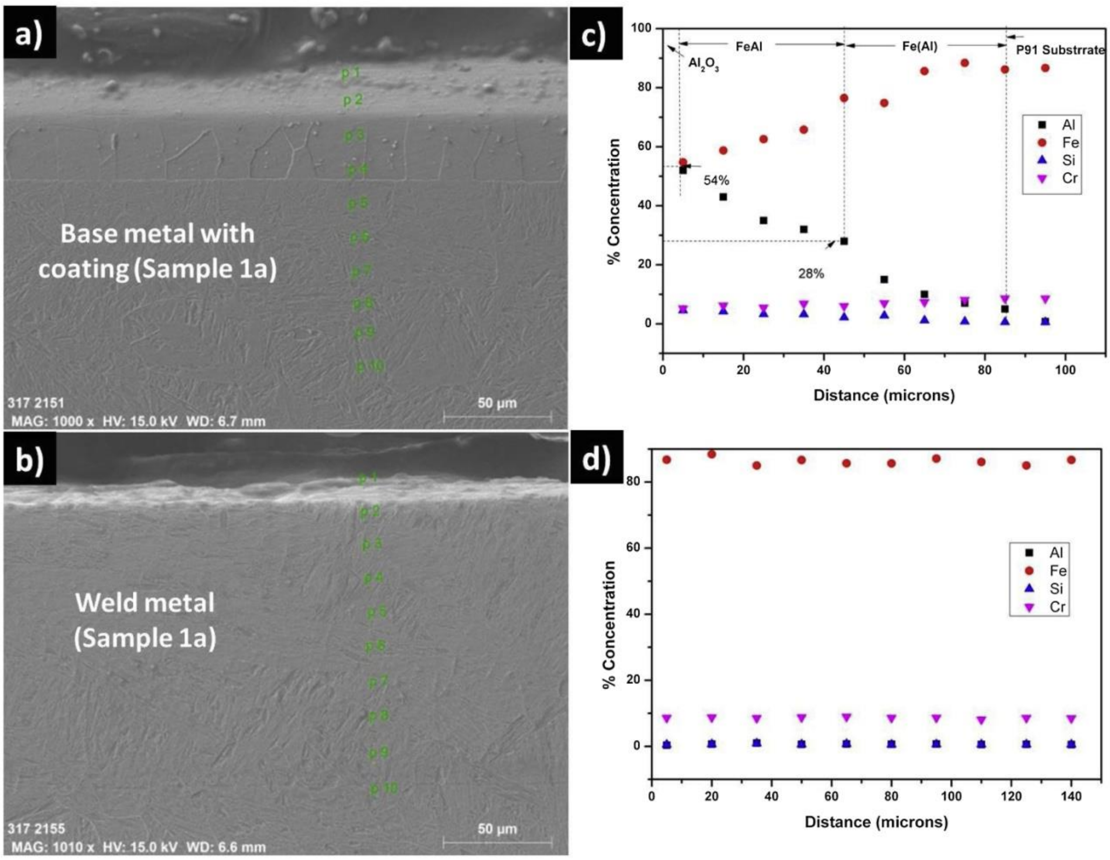

Figure 3.09 Elemental depth profiling of Cross-section bead of the sample 1a (coated 9Cr-1Mo) a) at base metal side b) at weld zone, plot of elemental depth profile c) at the base side d) at the weld zone. [128]

The presence of Al content in the weld metal seems to play an important role in the reduction of grain size as well. Hong et *al.*, [136] reported that the increase in Al content of the weld metal resulted in the reduction of grain size. This was because of the change in grain growth exponent n as a function of 't' (t=annealing time) where higher Al content steels revealed lower '*n*' values and thereby affects the grain size. As cited by Bruke et *al.* [137], the n values in grains with impurities are usually much less than the theoretical calculations (n=0.5) of system with no defects. An increase in defects would lead to a reduction in the value of 'n' (<0.5) [138]. A similar observation by authors [139-141] reported that the grain size could also be influenced by the presence of AlN precipitates in weld pool due to grain boundary pinning effect. This supports our hypothesis on the effect of Al on grain size of weld pool. A detailed investigation on the exact mechanism of Al distribution in weld metal and its effect on mechanical and microstructural properties are being pursued. Average grain sizes for both the samples 1a and 1b were measured according to ASTM E112-10 standard. The average grain size in the weld zone and HAZ of coated samples was lower compared to the uncoated P91 due to the presence of Al in the weld bead and the same has been plotted in Fig. 3.10.

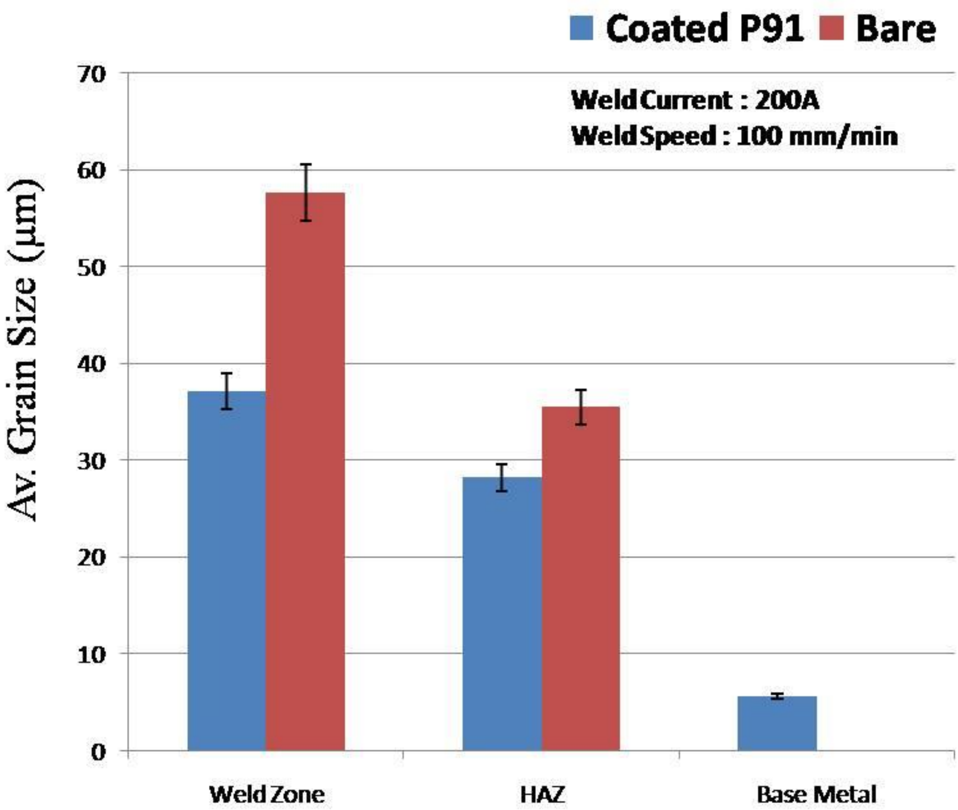

Figure 3.10 Effect of Al concentration on grain size on sample 1a and 2a [128]

3.5 Microhardness profiles of welds

Microhardness values were measured to investigate the effect of Al concentration on the microstructural properties. The values across the weld in transverse direction were measured at the load of 0.3 kg at intervals of 200 microns with dwell time of 20s. The microhardness values gradually decreased from the centerline of the fusion zone towards the base metal. The value was higher in the weld zone for sample 1a which is aluminized as shown in the Fig. 3.11. The value was 35-40 Hv higher for sample 1a despite the weld zone being prepared at the same process parameters (weld current and travel speed). Literature suggests that, as Al concentration increases, the average microhardness increases for 10Cr-Al alloys[142].

Ref.[136] also reported that, Al concentration does affect the grain size. They reported that as the concentration increases ($0.53 \leq Al \leq 9.65$ wt%), the grain size decreases. In our work, similar trend has been observed for the coated steel. The concentration of Al in the weld zone of coated steel was ~ 1-2 wt% and grain size for sample 1a was lower with respect to 1b (uncoated P91). It appears from the microhardness data that the reduced grain size may be the reason of higher microhardness (Hall-pand so onh relation).

Another possibility of an increased hardness could be solid solution strengthening due to Al being dissolved in weld metal. In addition, the higher values of microhardness could also possibly be attributed to the formation of AlN in the weld zone which may increase the hardness for the coated sample. The exact understanding on which hypothesis stands true needs to be further elucidated. The study of other mechanical properties such as tensile and impact strength is separately addressed in subsequent chapter for butt weld joints of coated steels.

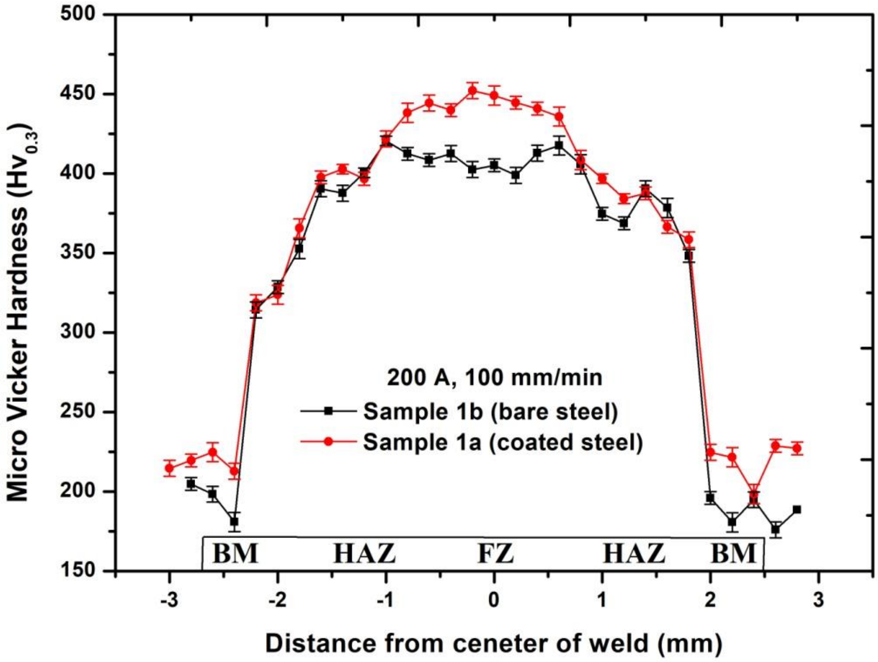

Figure 3.11 Comparison of micro-hardness measurement across the weld for sample 1a and 2a [128]

3.6 Discussion

In this chapter, the effect of aluminide coating on weld bead's size and shape is reported. The results are briefly discussed below.

The coated steel plates revealed a diffusion aluminide coating with a top Al2O3 layer of 2-3 microns followed by an Fe-Al diffusion aluminide layer of 70-90 microns. When such coated plate were subjected to bead-on-plate trials, the top insulating layer of alumina seems to have played a key role. The welded zone was found to be lower in width due to arc constriction during welding. The alumina layer has good insulation properties. Hence, when the arc interacts with the top alumina layer, the electron does not get a free path to travel like in the bare material. Due to this, constriction of arc takes place which increases the current density. Subsequently, the depth of penetration increases and bead width of weld becomes narrower compared to that obtained in the bare 9Cr-1Mo steel bead on plate [128]. Similar effect with an oxide layer known as an insulating effect is explained by Vilarinho et *al.*[129]. The same mechanism is also reported elsewhere where an enhanced depth of penetration was achieved for GRADE 91 steels [131, 143].

The presence of aluminide coating constricts the arc, acts as an insulating layer and restricts the movement of electron when the arc interacts with substrate during welding. Similar effect with an oxide layer known as an insulating effect is explained by villarao [129]. Consequently, the appearance of bead for coated Grade 91 steel was narrower compared to bare Grade 91 due to increased energy density. This also increases the depth of penetration in welds prepared at same current (200A) and travel speed (100 mm/min). Subsequently, the D/W ratio was higher at the same heat input for coated and bare Grade 91.

During coating Al diffuses into the base metal and reacts with the nitrogen at the interface and forms AlN. These precipitates do not get dissolved due to their high melting point (2200 °C) and get transferred in to the weld bead as inclusions during TIG welding process. Similar observations have been reported elsewhere [144]. The Al concentration remains almost constant between ~1-2% across the weld zone despite the higher concentration due to the coating at the base metal side. The concentration of Al affects the grain size of the weld zone and decreases it as compared to the bare Grade 91 steel. In addition, the grain size could also be influenced by the presence of AlN precipitates in weld pool due to grain boundary pinning effect [145-147]. Consequently, the hardness for the coated Grade 91 steel is higher compared to bare Grade 91 steel.

The weld microstructure was further investigated with respect to the presence of different detrimental phase formation such as delta (δ) ferrite. The same is described in detail in chapter 4 of this thesis. Subsequently, the mechanical properties of coated weld metal are also an area of rigorous investigation which has been covered in Chapter 5.

CHAPTER 4

EFFECT OF ALUMINIUM ON DELTA(δ) FERRITE FORMATION

4.1 Introduction

As observed in the previous chapter (chapter 3), the welding process of coated steels can lead to a change of weld microstructure. Various factors such as cooling rate after welding, content of the different substitutional alloy, the primary solidification product leads to nucleation of phases such as delta ferrite (δ), austenite (γ), or a mixture of both in 9 Cr steels [148, 149]. The presence of these delta ferrite (δ) and austenite (γ) phases have been studied using the equilibrium diagram for 9-12% Cr steels by different authors [150-152]. After welding, liquid metal in weld pool solidifies as delta-ferrite. The transformation of delta-ferrite to austenite phase under equilibrium condition starts at around 1480 °C and ends at around 1200 °C [101, 153]. However, this equilibrium transformation is not possible during the weld cooling cycle due to the high cooling rates. Hence, some amount of untransformed delta-ferrite may remain present even at ambient temperatures in the weld metal and up to some extent in the the heat affected zone [125, 154]. This delta (δ) ferrite phase present in weld metal has several detrimental effects on mechanical properties such as toughness, creep, impact and ductility [102, 155-157]. It is therefore important to keep a check on the % delta ferrite present in the weld metal and such delta ferrite content is measured as ferrite factor. This ferrite factor is calculated as a ratio of the chromium equivalent (Cr') to the Nickel equivalent (Ni') which is nothing but the ratio of ferrite stabilizing (or ferrite former) elements to austenite stabilizing (or austenite former) elements [152, 158-161]. Thus, the formation of the delta ferrite phase strongly depends on the composition of the solidifying metal (weld metal in our case). Aluminium is reported to be an element promoting the formation of delta ferrite phase (δ) in weld metals [162].

In the case of the Al-coated or aluminized steels, aluminium content in weld metal is critical and can contaminate the metallurgy of weld joint. It also promotes delta ferrite formation in the weld metal [163, 164]. The presence of Al in the weld metal contaminated from the coated surface can cause the formation of delta ferrite as Al is a ferrite stabilizer [165]. Bertin et *al.* [104, 105] noticed that after the arc-welding of Aluminium coated steel, a phase consisting of delta ferrite formed in the welded joint which yielded inferior the tensile strength. Briand et *al.* [106] reported that a concentration of Aluminium >2% in weld pool results in formation of delta ferrite and a lower hardness in the weld zone. This δ phase is also reported to impair mechanical properties. The presence of delta ferrite increases solidification cracking, impairs fracture toughness due to notch sensitivity of the delta ferrite phase, and reduces the creep ductility at high temperature in 9-12% Cr metals and welds [107]. Corroborating this, Wang et *al.* and Anderko et *al.* reported that the presence of delta ferrite deteriorates the impact properties and raises the ductile to Brittle Transition temperature (DBTT) of the martensitic stainless steel [102, 108].

The formation of delta ferrite is also dependent on the heat input during the welding process. Arivazhagan et *al.* have explained that the emergence of delta ferrite occurs due to high heat input during autogenous GTAW for Reduced Activated Ferritic Martensitic (RAFM) steels[156]. The effect of heat input and cooling rate was also studied by Sam et *al.* [154] wherein delta ferrite phase was reported to form in the weld metal interface of RAFM steels. This was reported to be because of the epitaxial growth from partially melted ferrite grains. The RAFM steels were developed for fusion reactor applications with P91 steel as a surrogate material and thus such a problem of delta ferrite in 9Cr steels is a matter of investigation from fabricability perspective. Pandey et *al*. [111, 166] further observed that this delta ferrite is also formed in weld joint of dissimilar P91-P92 steels, thus posing a threat to the acceptability of the weld joint. Therefore, it is essential to examine the presence of delta ferrite along with the heat input, aluminum concentration in the weld zone as its presence affects the mechanical properties. This investigation enables us to decide on the weldability of aluminized P91 steels with reference to the ferrite factor.

4.2 Effect of Heat Input

As mentioned in the experimental work, the weld speed was varied (100,125,150 mm/min) along with the constant current 200A for both coated and bare P91. The heat input measured for the Aluminized P91 steel was higher (2.12kJ/mm) compared to the bare (un-coated) P91 steel samples (1.44kJ/mm) at same current (200A) and same weld speed (100 mm/min). Both samples (coated and bare) were considered for further investigations as maximum heat input was observed with 100 mm/min welding speed. As explained in chapter 3, the coating which has insulating surface causes the arc constriction for coated steels, thereby increasing the power density and the heat input for the coated steel is higher [128]. To investigate the effect of heat input, the microstructure and phase analysis of the weld joint was carried out using scanning electron microscopy (SEM) and X-ray diffraction respectively. The results were further corroborated using vicker’s microhardness tests. X-ray diffraction was done at cross-sections of welds. Fig. 4.01 shows diffractographs of weld zone where 1a) indicates peaks for weld metal of bare P91 steel while 1b) is for coated weld sample.

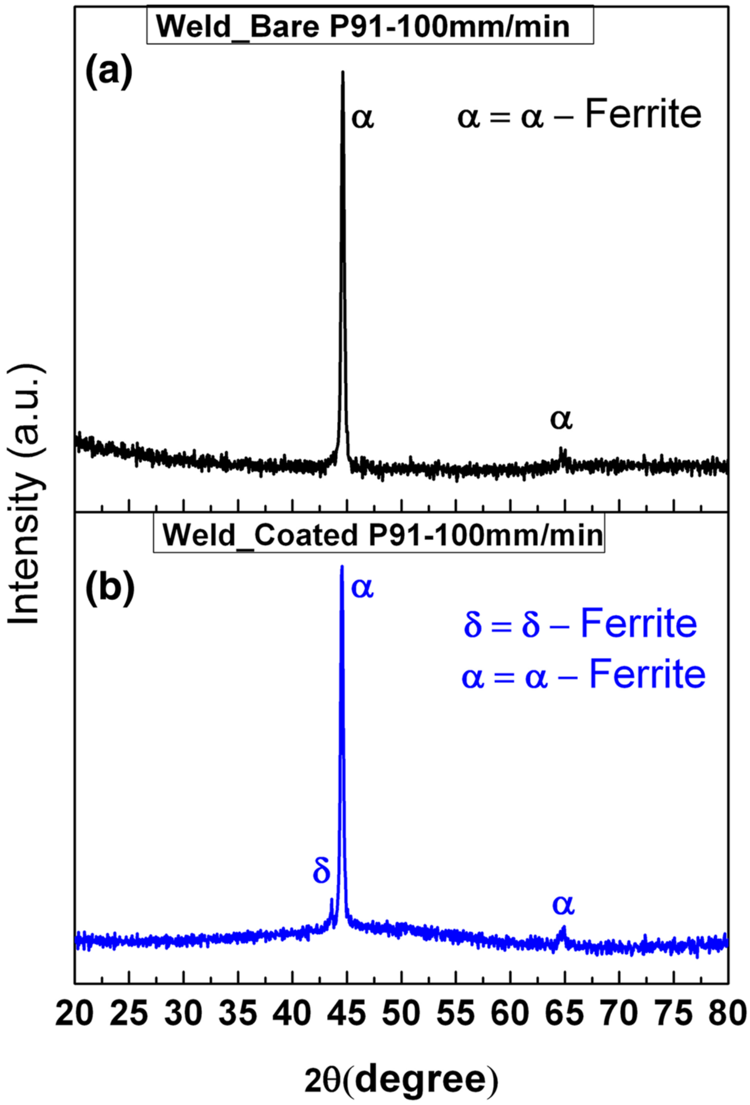

Figure 4.01 X-ray diffraction plot of weld metal prepared at 100 mm/min [167]

In Fig. 4.01a) peaks at $2\theta = 45.07°$, $65.64°$ corresponds to the plane (110) and (200) of α-Ferrite phase as per the ICDD card no. 01-076-6587. In comparison to this, the weld of coated steel indicated the presence of delta ferrite as indentified by reflection of

(110) peak at 2θ = 43.6285° based on ICDD card no. 01-089-4186. The low intensity of peak indicates low concentration of delta ferrite.

The theoretical assessment of the presence of delta ferrite can be done by monitoring the temperature using thermocouples. The thermal mapping of weld zone during welding indicated peak temperature at a location 10mm away from the centerline of the weld during the welding process. It was approximately 1120 °C for the coated steel, while it is 670 °C for bare P91 steel. The time vs temperature plot has been shown in Fig. 4.02. As explained earlier, under the equilibrium conditions, the formation of delta ferrite starts at approximately 1480 ºC and ends at around 1200 ºC [153, 154].

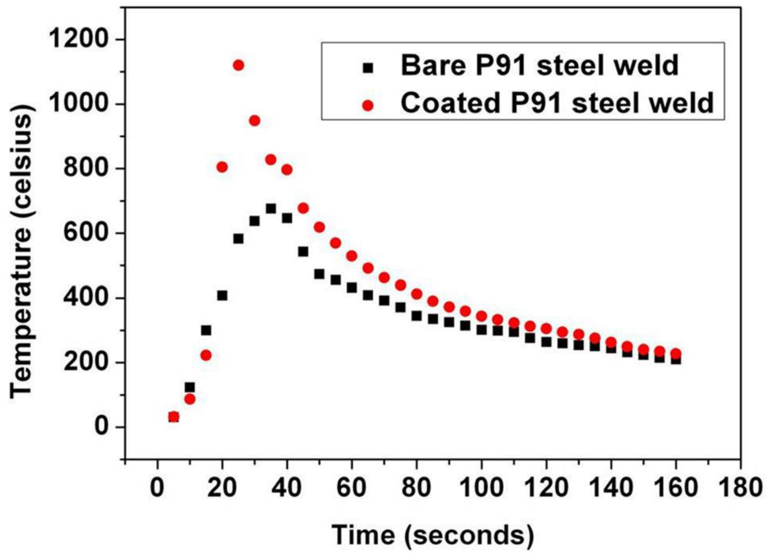

Figure 4.02 Time vs temperature comparison for coated and bare P91 [167]

However, this equilibrium transformation is not possible during the weld cooling cycle. The higher cooling rate in the weld zone causes more delta ferrite formation [107], and as the delta ferrite will not get adequate time to transform to austenite so it will remain within the weld zone at ambient temperature. Fig. 4.02 indicates that the cooling rate was higher for the coated P91 steel. Hence, the results from XRD and time vs temperature plot indicate possibility of delta ferrite. The formation of δ-ferrite in the weld zone can also be predicted by several empirical formulae.

4.3 Delta (δ) ferrite prediction in welds

It is well known that the δ – ferrite formation depends on various parameters such as elemental composition (of weld), temperature and time profiles, cooling rates. Based on this, the δ – ferrite prediction has been analyzed by different authors [107, 114, 154-156, 168], and they reported empirical formulas such as Schaffler, Schneider, Kaltenhauser and New house as given below.

i. Schaeffler formula [107, 168]:

$$Cr + 1.5Si + Mo + 5V + 0.5Nb + 0.75W - Ni - 0.5Mn - 30C - 30N - 0.3Cu - Co \quad (1.2)$$

ii. Schneider formula [107, 168]:

$$Cr + 2Si + 1.5Mo + 5V + 1.75Nb + 0.75W - Ni - 0.5Mn - 30C - 25N - 0.3Cu \quad (1.3)$$

iii. Newhouse formula [169]:

$$Cr + 6Si + 4Mo + 11V + 5Nb + 1.5W - 2Mn - 4Ni - 40C - 30N - 2Co - Cu \quad (1.4)$$

iv. Kaltenhauser formula [170] :

$$Cr + 6Si + 4Mo + 8Ti + 2Al + 4Nb - 2Mn - 4Ni - 40(N + C) \quad (1.5)$$

These formulae describe the difference between the weighted effects for the ferrite and austenite forming elements, i.e., the chromium and nickel equivalent values [107, 154, 168]. Each equation was formulated based on the effect of various alloying elements on the stability of δ-ferrite phase based on which the formation of delta ferrite could be predicted. However, it is important to choose which type of equation would best fit to predict δ-ferrite accurately, as the elements considered in the equation should include the critical elements in the substrates. Sam et *al.* [154] had considered New house formula in their study, as their investigation was related to δ-ferrite in Reduced Activated Ferritic Martensitic (RAFM) steels where elements such as W, Nb and V were major alloying elements. Arivazhagan et *al.* [155, 156] utilized the Schneider equation. They modified it, as the Ta element was not taken into the account though it is a ferrite stabilizer and was a principal alloying element in their case. Pandey et *al.* [112, 157] used the Schneider equation and explained the effect of delta ferrite on impact toughness for the dissimilar weld joints of 9Cr steels. Since our investigation was focused on the effect of coating on the delta ferrite formation, the effect of Al in the weld pool was needed to be considered. Our assessment on prediction of δ-ferrite thus needs an equation considering Al as alloying element in comparison to other equations.

In order to analyze the applicability of all formulae reported above for δ-ferrite prediction, a compositional analysis of the welded joint is required. The elemental analysis of weld metal was conducted using spark emission spectroscopy conducted at the center of the weld for both coated and bare 9Cr-1Mo samples. The elemental composition of coated and bare P91 weld metal is shown in table 4.01. The bare 9Cr-1Mo steel was found to have 0.04 wt% Al in as received condition as shown in table 4.01. However, in weld of coated substrates, the Al concentration was found to increase from 0.04% to 0.19%. Since Al is known as a ferrite stabilizer element, it is important to analyze whether this change in Al content of weld metal leads to a change in δ-ferrite content [165]. From different equations shown above, the Kaltenhauser formula includes composition of Al whereas other equations do not consider Al%. Hence Kaltenhauser formula was more relevant here as it increases the weighted effect of Aluminium on δ-ferrite formation as reported for 9Cr steels [107, 114, 168].

The Kaltenhauser equation 1.4 describes the difference between chromium equivalent and is Nickel equivalent. The difference between Cr_{eq} and Ni_{eq} values is known as ferrite factor. The calculated ferrite factor and delta ferrite prediction from Kaltenhauser in comparison with other empirical formulae has been shown in Table 4.02. Work reported in Refs. [154-156] indicate that if the ferrite factor (Cr_{eq} - Ni_{eq}) is above 10, then there is a possibility of delta ferrite formation in weld pool.

Table 4.01 Elemental composition of weld metal for coated weld and un-coated (bare) welds using spark emission spectroscopy

Elements	C	Cr	Mo	Si	V	Mn	Al	Nb	Ti	N	Ni	Cu	Fe
Coated weld (Wt%)	0.14	8.70	0.95	0.22	0.21	0.40	0.19	0.07	0.04	0.06	0.31	0.05	Balance
Un-coated weld (Wt%)	0.21	8.59	0.98	0.20	0.21	0.41	0.03	0.07	0.04	0.04	0.30	0.07	Balance
Standard Deviation(±)	0.006	0.081	0.001	0.018	0.001	0.010	0.001	0.008	0.001	0.006	0.017	0.013	0.005

Table 4.00.2 Ferrite factor prediction for 9Cr-1Mo steel in various conditions from various formulae.

		Schaeffler	**Schneider**	**Kaltenhauser**	**Newhouse**
As received	Ferrite Factor (Cr_{eq}- Ni_{eq})	5.92	7.67	6.88	6.95
	Delta-ferrite prediction	No	No	No	No
Coated Weld	Ferrite Factor (Cr_{eq}- Ni_{eq})	5.92	5.64	12.75	9.75
	Delta-ferrite prediction	No	No	**Yes**	No
Un-coated weld	Ferrite Factor (Cr_{eq}- Ni_{eq})	3.29	5.80	4.36	7.38
	Delta-ferrite prediction	No	No	No	No

4.4 Microstructure of delta ferrite

The results from various empirical formulas indicate that the delta ferrite is expected within the weld metal of coated steels due to Al contamination. Hence, it was important to analyze the microstructure of P91 weld joint using microscopy techniques to validate the prediction of delta ferrite phase by Kaltenhauser equation. The microscopy was conducted in as received condition and then compared with the microstructures of weld metal for coated and uncoated welds. The P91 material considered for the experimental work was supplied in normalized and tempered condition. The normalizing treatment was done at 1050 °C for 0.5 hour and tempering was done at ~780 °C with holding time of 1hour followed by cooling in air. Fig. 4.03 illustrates the tempered martensite microstructure of P91 steel in as-received condition after both the heat treatments. The microstructure of weld metal for un-coated steel is shown in Fig. 4.04. Weld metal comprised of fully martensitic laths and prior austenite grain boundaries and was found to be free from delta ferrite as predicted from empirical formulae in table 3.

Fig. 4.05 shows microstructure (optical as well as the SEM image) of weld metal of coated steel produced through autogenous TIG welding process at 2.12 kJ/mm heat input (weld current-200A, weld speed-100 mm/min). The morphology of weld metal indicates the presence of delta ferrite. To confirm the same, a higher magnification image by electron microscopy (Fig. 4.05(b)) was taken at a region marked as circle in Fig. 4.05 a). The delta ferrite is free from carbides as reported by Arivazhagan et *al.* [156]. SE image (Fig. 4.05 (b)) shows a delta ferrite region where carbides are completely absent. Further, the delta ferrite observed here showed a polygonal shape. Delta ferrite in polygonal shape and island of delta ferrite in a matrix of tempered martensite has been reported in refs. [107, 168]. A similar kind of polygonal shape of delta ferrite was observed and shown in Fig. 4.06 a) while 4.06 b) where the island of delta ferrite in the martensite matrix structure have been clearly identified. The delta ferrite regions were more at grain boundaries while as the interior of grain showed less delta ferrite phase. This may be due to more energy available at the grain boundary than the grain interior region and hence the variation in quantity of delta ferrite [156]. The quantification of delta ferrite content was done by analysing the volume fraction of delta ferrite in microstructure of weld zone using image J software. The amount of delta ferrite in the weld zone was found to be ~5.09%. This supports the prediction of delta ferrite (ferrite factor) through Kaltenhauser formulae as indicated in table 4.02 [167].

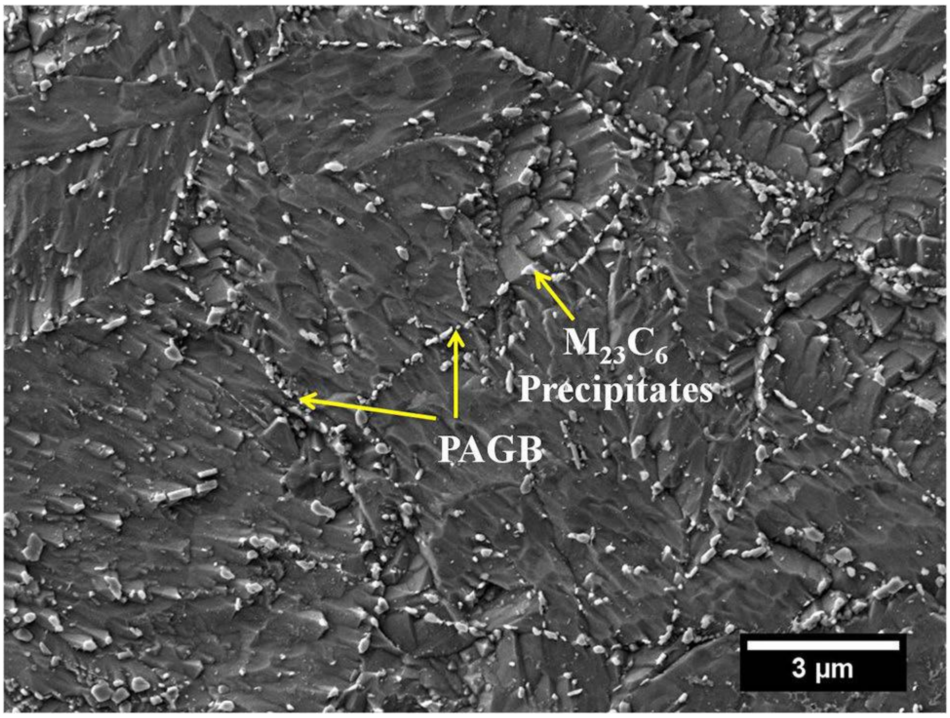

Figure 4.03 SE image of P91 steel's microstructure in as-received condition [167]

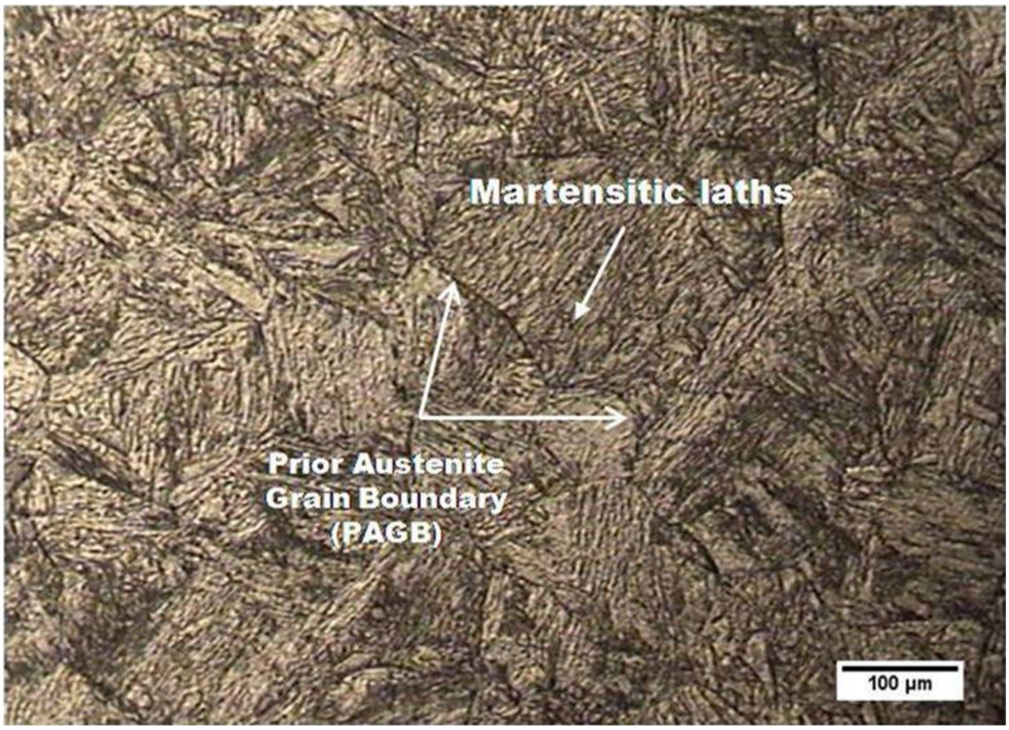

Figure 4.04 Weld metal's microstructure of bare P91 steel prepared at 100 mm/min weld speed and 200 A current [167]

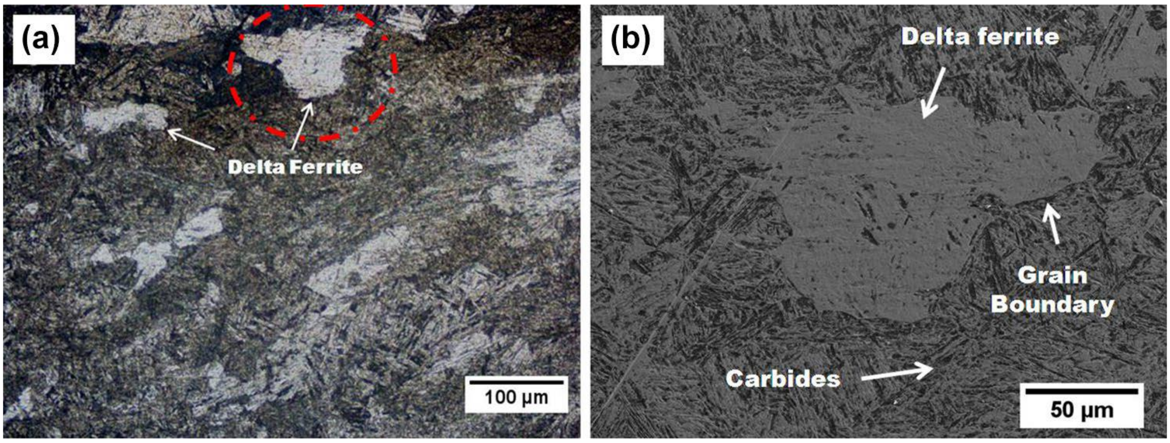

Figure 4.05 Weld metal's microstructure Weld metal's microstructure of coated P91 prepared at 100 mm/min weld speed and 200 A current. The encircled part in (a) (optical image) is highlighted as (b) (SE image) [167]

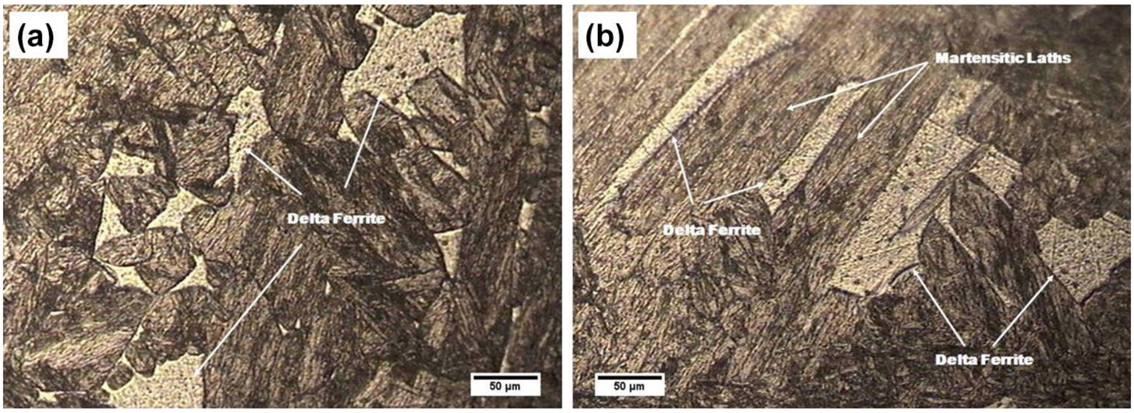

Figure 4.06 a) Polygonal delta ferrite (b) island of delta ferrite in matrix of tempered martensite observed at prepared at 100 mm/min weld speed and 200 A current [167]

4.5 Microhardness

As it is known that different phases in a given microstructure can be differentiated by their microhardness. Hence, Vicker's microhardness tests were performed to confirm the delta ferrite observed in microstructure of coated P91 steel welds (see Fig. 4.05 and 4.06). Delta ferrite is a softer phase while the tempered martensite is a hard phase and hence can be easily identified using microhardness tests. The vicker's microhardness measurements were done at the load of 0.05 kg at a dwell time of 20 seconds at different delta ferrite locations. As explained earlier, the delta ferrite phase is free from carbides and hence in the absence of carbides and precipitates the hardness value would be lower compared to martensite. Further, the ferrite phase is softer than the tempered martensite. In this context, Sam et *al*. [154] has reported that the delta ferrite would be leaner in carbon during the subsequent transformation of delta ferrite to austenite and austenite to martensite and thus the hardness of delta ferrite at same load would be lower. Sam et *al*. reported the microhardness values of delta ferrite were ~195±5 $HV_{0.05}$ in welded zone of Reduced

Activated Ferritic Martensitic (RAFM) steels[154]. Pandey et *al.* [157] has also measured the microhardness in delta ferrite region and reported similar values such as 190±10 $HV_{0.05}$ and 198±10 $HV_{0.05}$. Similar hardness values of delta ferrite were observed in this work. The SEM image which includes microhardness indentation in martensite region and delta ferrite in weld zone of coated steel is shown in Fig. 4.07. The phase which consists of carbides i.e. martensite was found to have a microhardness of 396 ±5 $HV_{0.05}$. Delta ferrite being comparatively softer revealed a microhardness of 192 ±5 $HV_{0.05}$.

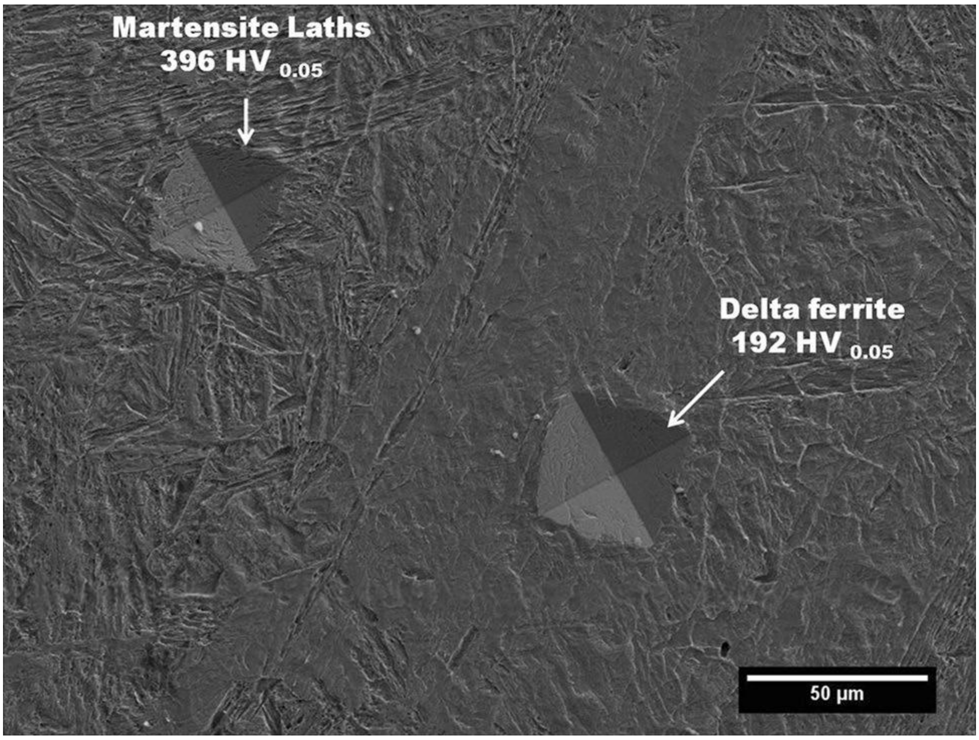

Figure 4.07 SE image indicating micro-Vicker hardness indentations at 0.05 kg load and values for phases in the weld zone prepared at 100 mm/min weld speed and 200 A current [167]

4.6 Discussion

The elemental composition of weld metal could be instrumental in predicting the delta ferrite formation. The weld metal prepared at 100 mm/min and 200A weld current for aluminized coated steel has been found to have delta-ferrite. Further, variations in volume fraction and morphology of the delta ferrite are observed within the fusion zone. The conclusions for this investigation are mentioned below.

Al concentration in the weld zone due to contamination from aluminide coating may cause the formation of delta ferrite as Al acts as a ferrite former. An average Al content if exceeds ~0.13 wt% would lead to possibility of delta ferrite formation. In this work, the spectroscopy results of weld metal revealed ~0.19 wt% Al.

The volume fraction of delta ferrite quantified by microscopy was validated using a theoretical prediction of delta ferrite by Kaltenhauser equation. The Kaltenhauser's equation was found to be more accurate to predict the delta ferrite as it is considers %Al contribution in formation of delta ferrite, which other formulae do not consider. In addition,

One of the possible reasons for the formation of delta ferrite could be high heat input. Alumina coating at the surface constricts the arc and due to that heat input was higher for coated steels, resulting in higher temperature in weld. The volume fraction observed of delta ferrite was ~5.09% at 2.12 kJ/mm (100 mm/min weld speed, 200A current) for coated steels. The X-ray diffraction analysis also confirmed the presence of delta ferrite phase.

The delta ferrite appearance was in polygonal shape and was distinguished at prior austenitic grain boundaries. Isolated islands of delta ferrite in a martensite matrix were also noticed. In addition, the delta ferrite phase was free from carbides as confirmed from microscopy and subsequently, the hardness was low (~192 $HV_{0.05}$) compared to martensite which has 396 $HV_{0.05}$. The low hardness of 192 HV corroborates the presence of delta ferrite.

This investigation can be further continued to examine the effect of pre-heating on cooling rate during welding and, subsequently on the formation of delta ferrite. Since delta ferrite poses different mechanical properties than the bulk microstructure comprising of lath martensite, the effect of delta ferrite volume fraction on tensile and impact properties of weld joint is required. Thus, delta ferrite formation in the weld metal is crucial and Aluminium is a critical element impacting the concentration of delta ferrite in the weld. Based on this study, it is important that the Al content of weld be reduced so as to bring down the delta ferrite content to acceptable levels.

CHAPTER 5

ASSESSMENT OF MECHANICAL PROPERTIES OF BUTT WELD JOINT IN COATED P91 STEELS

As observed in the previous chapters, the Al contamination of weld pool was observed leading to microstructural changes and increase in the δ-Fe content. Such changes would lead to a detrimental effect on the properties of resultant weld joint. Since such coated steels would be required to undergo fabrication and welding process in end application, it was important to evolve a methodology of welding by which such weld contamination and degradation is avoided. Therefore, a study on the assessment of mechanical properties of weld joint of aluminized coated steels was attempted under this research work.

Though literature on weldability of aluminized steels is scarcely reported, work related to weld contamination by Al gives an indication of the extent of possible degradation of the weld properties. Corroborating our observations in the previous chapter, published literature indicates that the presence of Al in weld metal deteriorates the tensile strength and microhardness of coated steels [171-173]. Such Al in weld joint could lead to rupture of joint as compared to base metal after arc welding of coated steels[105].The Al from the aluminide coating would dissolve in the weld metal and an Al concentration of ~ 1-2 % in the weld metal was sufficient to promote the formation of δ-Fe [167]. This δ-Fe formation is known to impair the mechanical properties such as impact strength, tensile strength and microhardness [102, 154, 157, 168]. Hence, it is clear from the reported literature that Al contamination of weld is detrimental for the weld quality and should be avoided to the extent possible. Our experimental results from previous chapters also corroborate the above observation. In order to address these issues, it is essential to minimize the Al concentration in weld metal of coated steels. The edge preparation (V-groove chamfering) as per ASME standards has been attempted to reduce the Al concentration in the weld metal.

5.1 Conventional TIG welding process with Single V-grove butt joint

The most common weld joint is the butt weld joint, where both the parts lie in the same plane and join at their edges. If the material or part has a thickness greater than 3mm, the edges of the part or material are subject to machined, i.e., joint preparation or edge preparation for butt joint [174, 175].

The butt joint has mainly two types of edge preparation, which are single V grove and double V groove. The single V groove (Fig. 5.01 (a)) is in use to when the thickness of the part is between ¼" to ¾". The double V grove (Fig. 5.01 (b)) is for use on plates thicker than ¾ inch. Most of the industrial welding jobs comprise of thicknesses lower than ¾ inch and hence the single V groove edge preparation is the most widely followed practice. Such an edge preparation in our case (i.e. chamfering of the edges) would lead to removal of coating (to some extent) thereby minimizing the Al contamination of the resultant weld zone.

(a) **(b)**

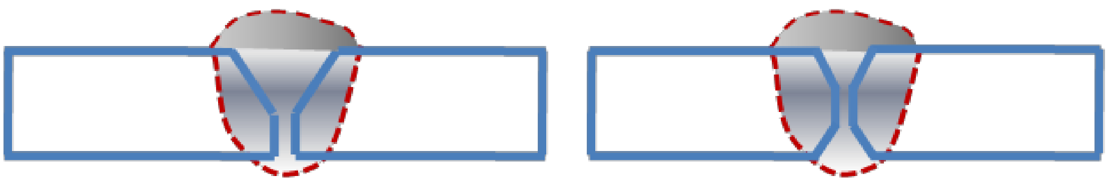

Figure 5.01 (a) Single V-grove (b) Double V-grove

The P91 steel (coated and un-coated) plates used for the welding process under this study had dimensions of 150mm x 100mm x 5mm. Hence, single V-groove edge preparation was employed as coated, and uncoated steel plates had a thickness of 5mm. This V-groove was prepared in accordance with ASME Section IX, QW-402 specifications. The V-groove design is shown in Fig. 2.07 (chapter-2).This V-groove edge preparation as per ASME standards was reported in recently published literature for the weld joints of P91 steels [111, 113, 124]. As per the permitted standard, AWSER 90S-B9 filler wire was used for this conventional welding process. The welding parameters including pre-heating temperature, weld current, travel speed, voltage and average heat input for root pass and subsequent GTAW passes are listed in table 2.04 (chapter-2). The control of residual stresses in welding for both samples (coated and without coated) was important. Standard welding procedures (WPS) such as adequate clamping and tack weld were adopted prior to welding so as to control the distortion and residual stresses based on reported literature [176].

The resultant weld joints (both, coated and uncoated)were then subjected to radiography tests as per ASME Section V article 2 in as welded condition to ensure the weld is defect free. This was done to ensure that the comparison of welded joints in coated and uncoated steels was at par and deprived of any variables attributed to physical defects. The weld joint for coated steel, and uncoated steel were observed defect free as per the acceptance standard ASME section IX QW 191.2.2. As per the ASME standard, the post weld heat treatment is required to be conducted so as to restore the toughness [125, 177]. Therefore, the welded plates were then subjected to post weld heat treatment (PWHT). The PWHT was carried at 760°C ± 5°C for 2h.

Similar PWHT has been reported for 9Cr-1Mo steel weld joints by different authors [111, 113, 124] and hence was considered for the present study.

5.2 XRD analysis of weld metal

Fig. 5.02 a) describes the X-ray diffraction patterns in the as-received condition of 9Cr-1Mo steel, which consists of significant substrate peaks of Fe. The Fig. 1a) showcased the peaks at $2\theta = 44.67°$, $65.02°$ and $82.33°$ corresponding to the plane (110), (200) and (211) as per the ICDD (International Center for Diffraction Data) card # 01-076-6587.The aluminized process which includes normalizing and plasma tempering heat treatment results in the formation of α-Al_2O_3, FeAl phases in the coating as reported by Jamanapara et *al.*[178, 179] and Zala et *al.*[128, 180]. The same has been confirmed with XRD and showcased in Fig. 1b).

The bead-on-plate trials revealed that the delta ferrite formation in the weld metal region was due to arc constriction caused by alumina film and higher heat input (~2.12 kJ/mm) for coated steel [19]. Therefore, it is essential to control the heat input during welding to avoid delta ferrite formation. Owing to this, V-groove edge preparation was adopted to mitigate the effect of coating on heat input. Equation 1 is shown below to evaluate the heat input, which is cited by different authors [118, 181].

Eq. .1.5 Heat input for TIG welding process [118, 181].

$$\text{Heat input (kJ/mm)} = \frac{0.9 \times V \times I \times 60}{1000 \times S} \qquad (1.5)$$

Where the efficiency of the arc is considered 0.9, V=arc voltage, I=arc current S=welding speed (in mm/sec). In this study, the weld joints have been made with ~1.1-1.4 kJ/mm for both, coated and uncoated steel substrates. This heat input is comparatively less to the reported heat-input (2.12 kJ/mm), which forms the delta ferrite formation. The XRD study of weld microstructure for coated and un-coated weld confirms the ferrite-martensite phase (Fig. 5.02 (c) and (d)) with three major peaks of (110), (200) and (211) which are identical to the substrate. No peak of δ-Fe was observed. XRD results indicate that the weld microstructure is free from delta ferrite as the heat input was controlled through V-groove design.

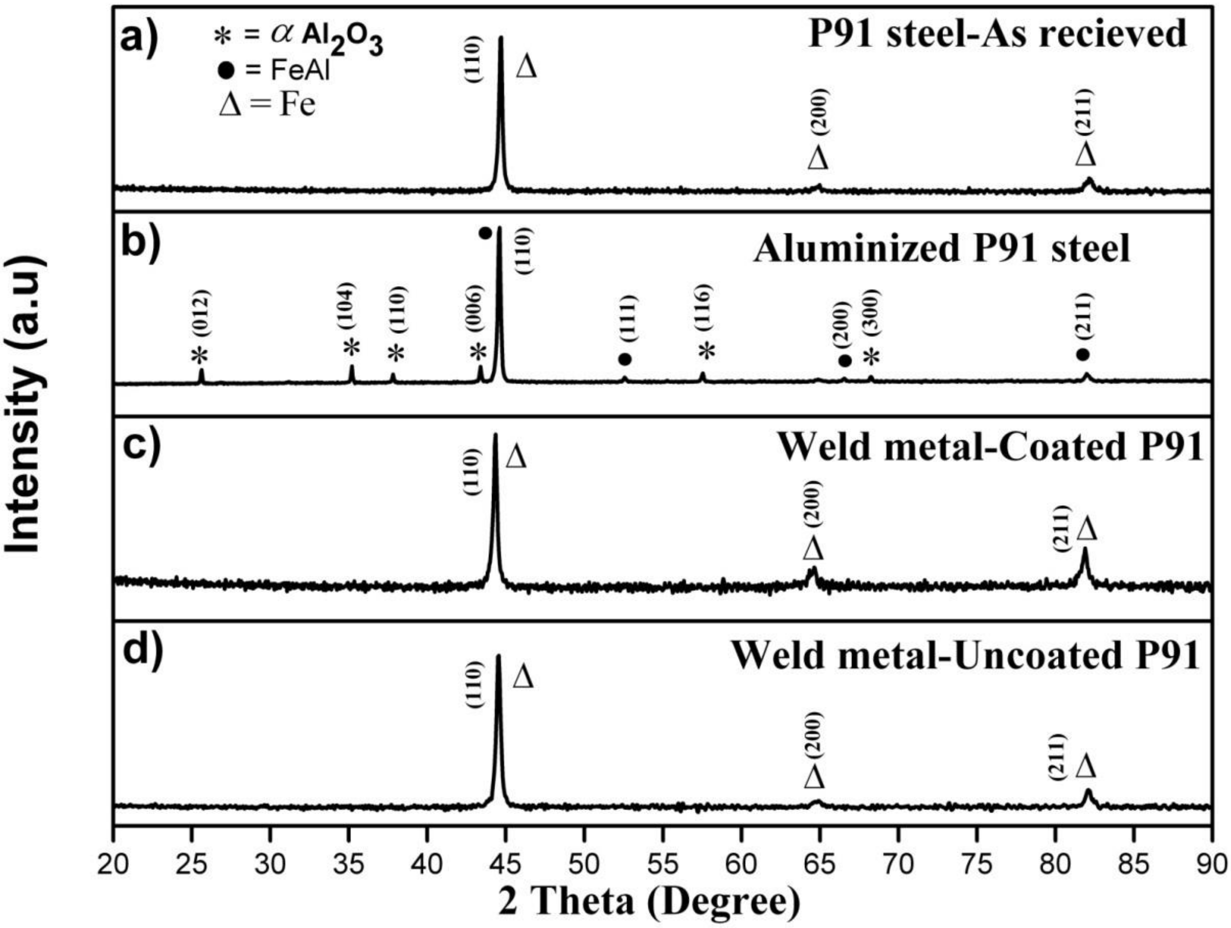

Figure 5.02 XRD spectra of a) P91 Steel- as received b) Aluminized P91 steel c) weld metal of coated P91 steel d) un-coated P91 steel.

5.3 Microstructure

To understand the effect of coated layer on the weld microstructure, different regions of weld metal cross-section were investigated. Kong et *al*. investigated the effect of Al-10% Si coating layer and its concentration in weld metal for ferritic stainless steel [99]. He reported that the concentration of Al and Si were higher at the edges of weld metal compared to the fusion zone. Various areas are highlighted as a square box in macro structure of coated steel (Fig. 5.03(i)) were carefully studied to examine the microstructure.

The Al_2O_3 at the top does not dissolve during the conventional GTAW welding as it has a higher melting point (2200 °C). Lumps of Al_2O_3 were observed at the weld fusion line in irregular shape (see Fig. 5.03 (a)) and while the highlighted circle marked in Fig. 5.03 (a) is further examined at higher resolution in Fig. 5.03 (b). Al_2O_3particles were observed within the grain along with martensitic laths and were distributed randomly near the weld fusion line. Similarly, for the square box 2 marked in Fig. 5.03 (i) revealed randomly distributed Al_2O_3 particles in Fig. 5.03 (c). These particles have been analyzed using elemental mapping through EDS equipped with SEM. The concentration of various elements such as Fe,Al and O is shown in Fig. 5.03 (d),(e) and (f) respectively. This also indicates the formation of Al_2O_3 near the fusion line which may affect the mechanical properties.

The Al_2O_3 at the top does not dissolve during the conventional GTAW welding as it has a higher melting point (2200 °C). Lumps of Al_2O_3 were observed at the weld fusion line in irregular shape (see Fig. 5.03 (a)) and while the highlighted circle marked in Fig. 5.03 (a) is further examined at higher resolution in Fig. 5.03 (b). Al_2O_3particles were observed within the grain along with martensitic laths and were distributed randomly near the weld fusion line. Similarly, for the square box 2 marked in Fig. 5.03 (i) revealed randomly distributed Al_2O_3 particles in Fig. 5.03 (c). These particles have been analyzed using elemental mapping through EDS equipped with SEM. The concentration of various elements such as Fe,Al and O is shown in Fig. 5.03 (d),(e) and (f) respectively. This also indicates the formation of Al_2O_3 near the fusion line which may affect the mechanical properties.

SEM analysis of center of weld metal (Fig. 5.04 (i)) illustrates the typical 9Cr-1Mo steel microstructure, which has $M_{23}C_6$ precipitates at prior austenite grain boundaries (PAGB). The $M_{23}C_6$ precipitates shown in Fig. 5.04 (a) and (b) were confirmed with spot analysis through EDS. The microstructure observations do not show any evidence of delta ferrite phase for both coated and uncoated weld metal. This observation supports our XRD results. Thus, by incorporating V-groove edge preparation as a part of welding protocol, we can mitigate the issue of delta ferrite formation in welds of aluminized 9Cr-1Mo steel [128, 167]. This is because the V-groove preparation will remove some part of the coating and the Al contamination of weld would be minimal. Consequently, the deteriorating effect of delta ferrite on mechanical properties can be prevented.

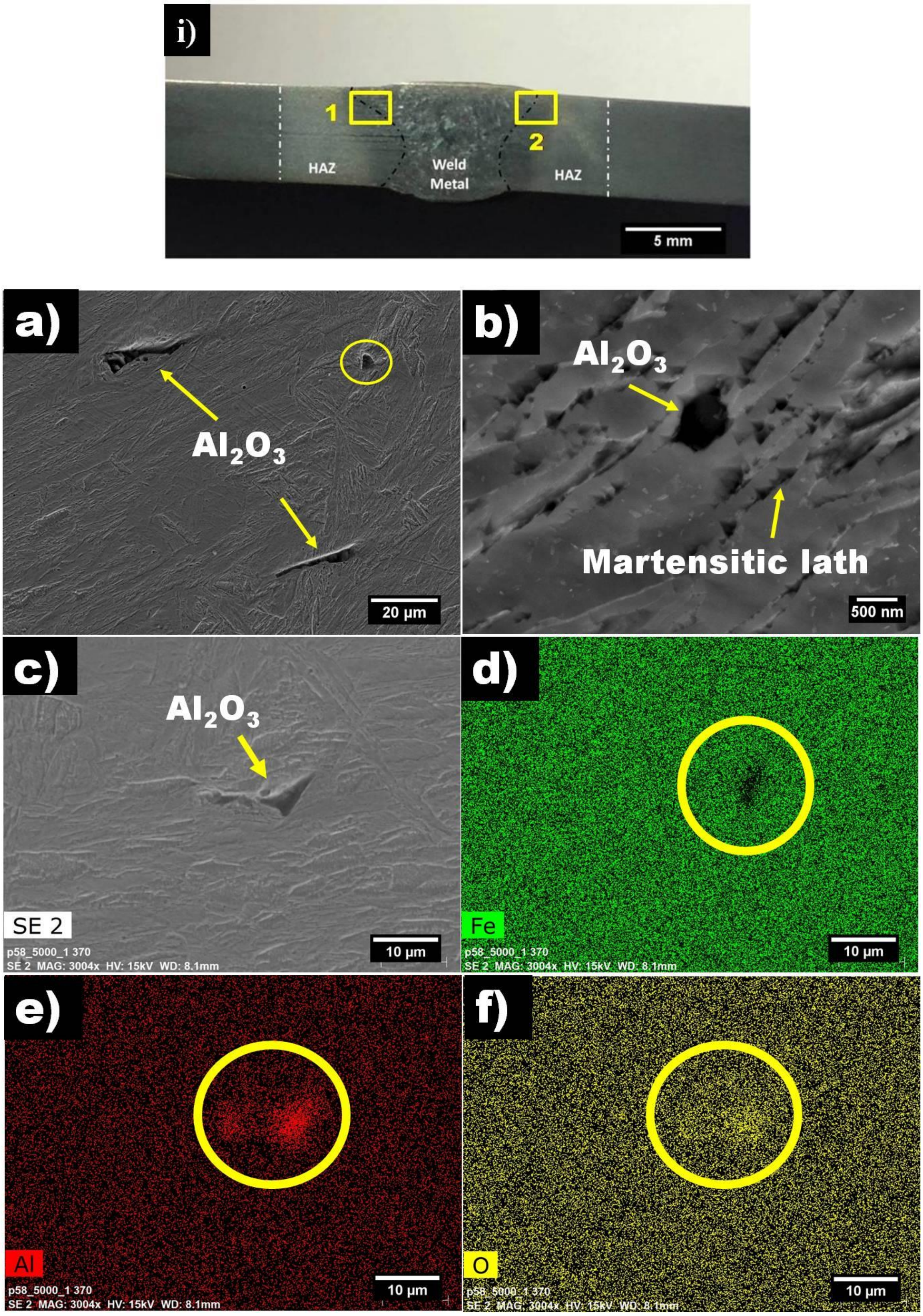

Figure 5.03 SEM images with the color mapping of weld microstructure for coated steel a) lumps of Al_2O_3 b) Al_2O_3 particle at higher magnification highlighted in figure a). c) Al_2O_3 particle d) Color map of element Fe. e) element Al. f) element O

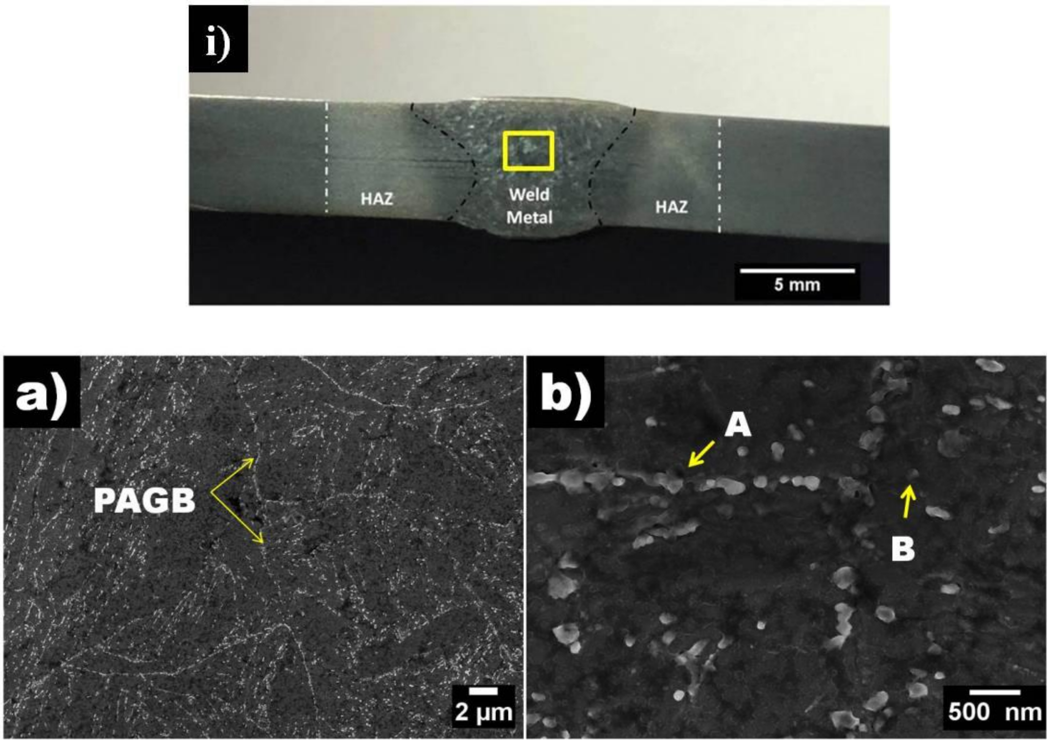

Figure 5.04 Microstructure analysis of the weld metal in the center for aluminized coated 9Cr-1Mo steel a) weld metal with Prior Austenite Grain Boundary (PAGB) b) $M_{23}C_6$ precipitate indicated as A and MX precipitates indicated as B

5.4 Mechanical properties and fractography studies

The mechanical properties of weld joints for coated and uncoated 9Cr-1Mo steel were investigated for tensile strength and impact toughness and compared with a substrate in as received condition. The specimen were extracted transversely from the centre of the weld joint for tensile and impact testing. All the tensile tests were carried out in accordance with ASTM E8M-04 standard and all impact tests were conducted in accordance with ASTM E-23 standard. The dimensions of the tensile test specimen with a schematic are shown in the Fig. 2.10.The tests were conducted for three times for each condition and average values have been considered for analysis. The photographs of fractured tensile test specimens are shown in Fig. 5.05. The photograph indicates that the fracture took place from the base metal in the case of coated and uncoated weld joints (Fig. 5.05 (b) and (c)). Hence, the strength of weld metal is higher compared to the base metal.

Many authors [182-184] have reported that the presence of oxides can lead to the formation of cracking. Here, the Al_2O_3 oxide particles were observed at the weld fusion line in coated steel and confirmed through SEM-EDS studies. However, the oxide particles did not significantly deteriorate the tensile strength. The tensile strength of weld joints for coated and uncoated steel was in-line with the substrate. The details of tensile properties are mention in table 5.01. The strength of the coated weld joint is marginally inferior compared to un-coated weld.

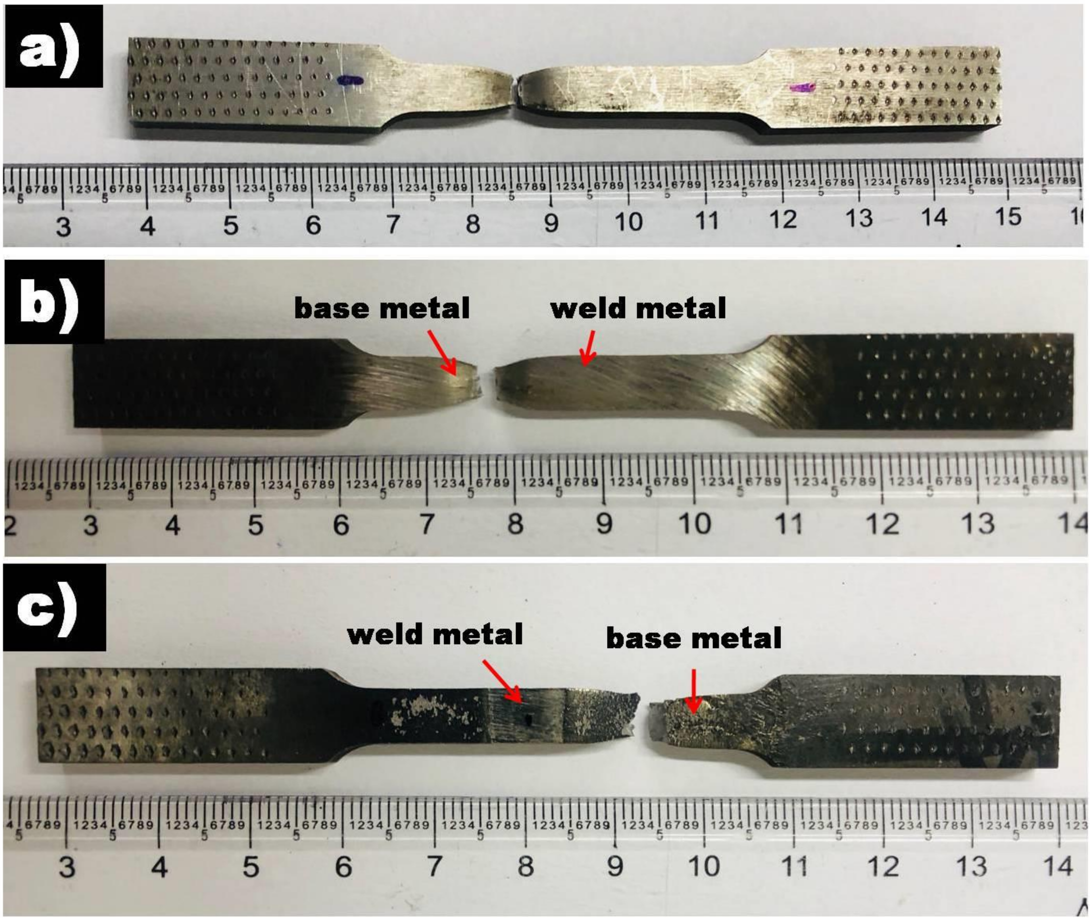

Figure 5.05 Macro images of tensile test specimens after fracture a) As-received condition b) un-coated weld c) coated weld

One of the possible reasons for this marginal decrease would be the precipitate coarsening during PWHT [185]. Zang et a*l.* reported that the coarsening of $M_{23}C_6$ affects the tensile strength compared to the as weld condition [185]. In this work, the coated layer has alumina which acts as an insulating material during the PWHT of weld joints. The FeAl coating is reported to have lower thermal conductivity (0.17 W/cm-K) than the P91 steel substrate (Fe – 0.8W/cm-K) [186] which means that the heat transfer (to cool down) will take more time than the uncoated substrates. The FeAl coating has a ~50 to 70 µm thickness on a plate of a dimensions of 150mm and 100 mm thickness. In addition, the alumina layer of at the top of the plate has 0.12 W/cm-K thermal conductivity, which is also lower compared to the P91 steel plate. Consequently, $M_{23}C_6$ precipitates would get more time for coarsening in case of coated steel as the conduction would be less [186] compared to the uncoated steel. The average sizes of precipitates were observed ~75-80 nm for the weld metal of coated steel and ~50-55 nm for the uncoated steels. However, further detailed studies on the effect of PWHT on precipitates coarsening and mechanical properties are required and same is going on by authors for better understanding. Fig. 5.06 represents the engineering stress-strain curve for coated weld joint, un-coated weld and bare 9Cr-1Mo steel in as-received condition.

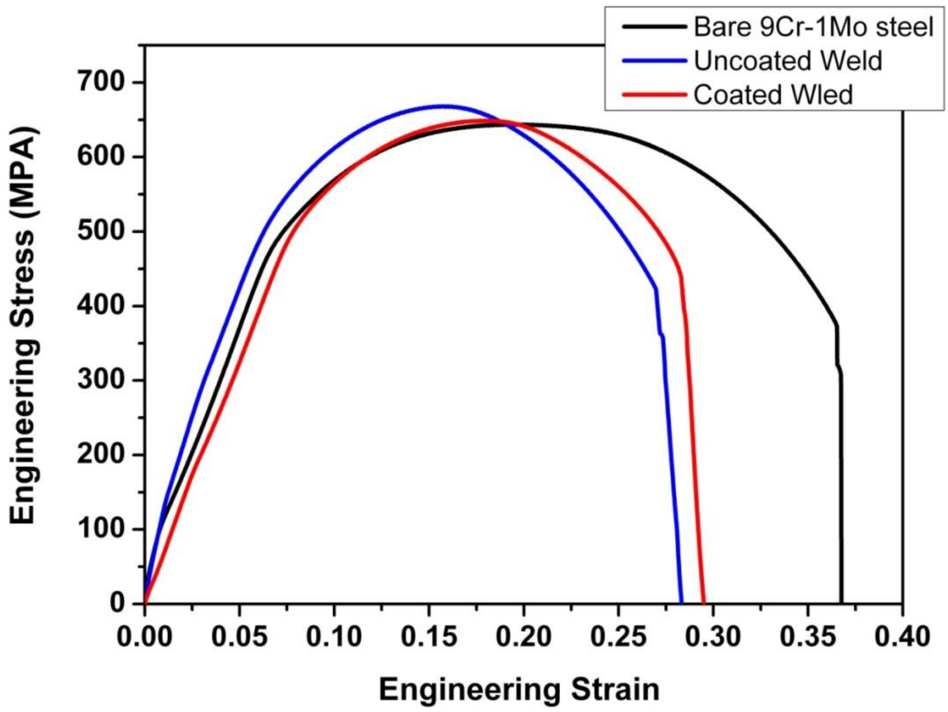

Figure 5.06 Stress-strain curve for weld joint of coated, un-coated and bare 9Cr-1Mo steel

The curve indicates the ductility is slightly higher for as-received 9Cr-1Mo steel compared to the weld metal of coated steel and uncoated steel. The fractured surfaces were analyzed through SEM. Fig. 5.07 a) showcases the fractured surface of 9Cr-1Mo steel in as received condition. It includes micro dimples indicated as ‘1’ in yellow color and quasi cleavages marked as ‘2’, which is clear evidence of ductile failure. Quasi cleavage is fracture mode which combines the characteristics of cleavage and dimple fracture [187]. Fig. 5.07 b) represents the fractured surface of uncoated weld metal which has dimples resulted from a coalescence of micro-voids and cleavage facets. Similarly, Fig. 5.07 c) and d) are fractured surfaces for coated weld metal. The fractured surface indicates that the fracture is an inter-granular ductile failure as in Fig. 5.07 d), precipitates are observed at the centre of the grain. Those precipitates are confirmed with back–scattered SEM image and energy dispersive spectroscopy. Similar fracture modes have been reported for the tensile fracture of 9Cr-1Mo steel [114, 188, 189]. SEM observation of fractography indicates that the fracture is inter-granular type suggesting ductile nature of the substrate. The oxide particles i.e. Al_2O_3do not have any significant effect on fracture mechanism as they were randomly distributed near the weld line. However, this hypothesis would need further elucidation and detailed investigation.

Table 5.01 Tensile property of as-received base metal, uncoated and coated weld joints.

Sample Type	UTS (MPa)	% Elongation	Fracture Zone
As received P91 steel	643±18	22.23	Base metal
Un-coated weld P91 steel	667±14	16.66	Base metal
Coated weld P91 steel	648±16	18.58	Base metal

The desired impact toughness for 9Cr-1Mo steel is 45 J for prototype fast breeder reactor applications [125, 190-192]. Charpy V-notch toughness tests were carried out as per ASTM E-23 standard. The schematic of impact samples is shown in Fig. 2.10 and the results are illustrated in Fig. 5.08. At room temperature, the value of toughness was 74 J for 9Cr-1Mo steel in as-received condition (without any weld joint). Since the weld metal undergoes severe metallurgical changes, both during welding and during PWHT, the resultant properties of the weld metal are likely to be inferior to the parent metal. In this work, the impact tests of uncoated weld samples indicated 55 J and those of coated weld indicated 52J energy. This are inferior, compared to the as-received 9Cr-1Mo steel (parent metal) but satisfies the 45 J criteria required to be met for fusion blanket applications in fusion devices. Likewise, this criteria is also valid for other welding joints involving P91 grade steels.

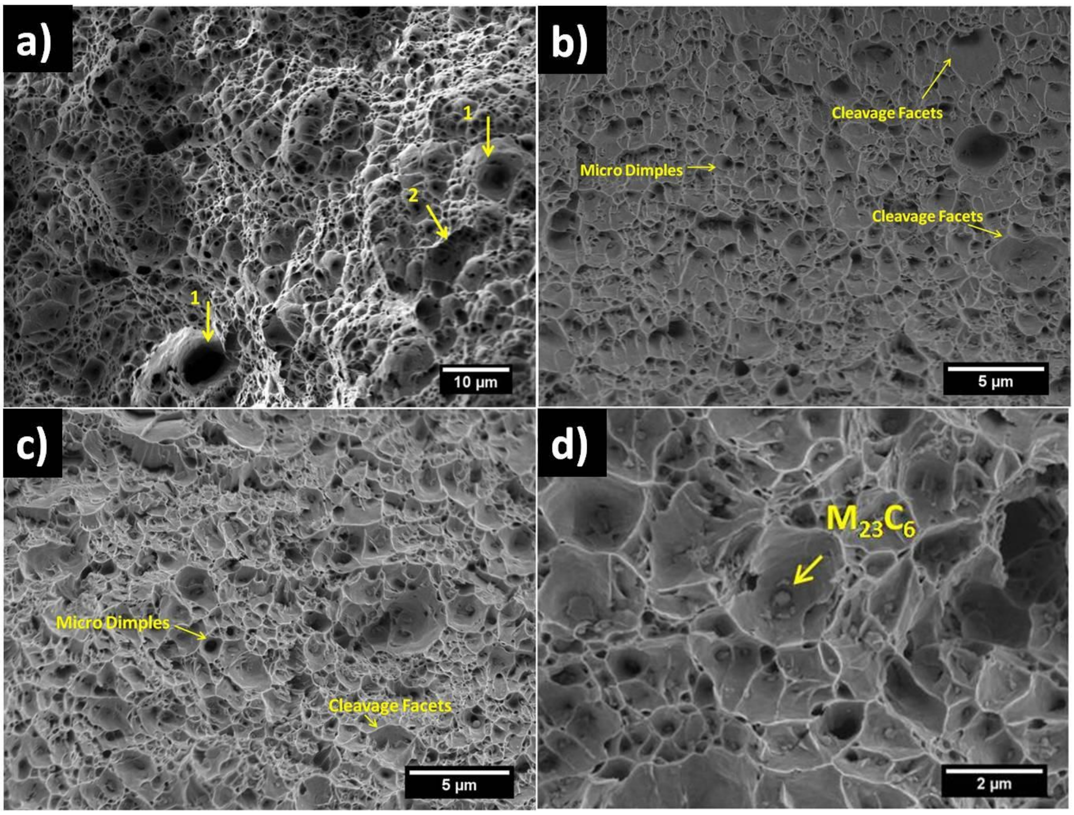

Figure 5.07 SEM image of a fractured surface of a) As received 9Cr-1Mo steel b) uncoated weld metal c) coated-weld metal d) $M_{23}C_6$ precipitates within a grain of the fractured surface.

Table 5.02 An average values of impact toughness for as-received base metal, uncoated weld and coated weld at room temperature, 0°C, -25°C

Sample Type	Average Impact Toughness (J)		
	Room Temp	0°C	-25°C
As received (bare) P91 steel	74	42	29
Un-coated weld P91 steel	55	38	28
Coated weld P91 steel	52	28	26

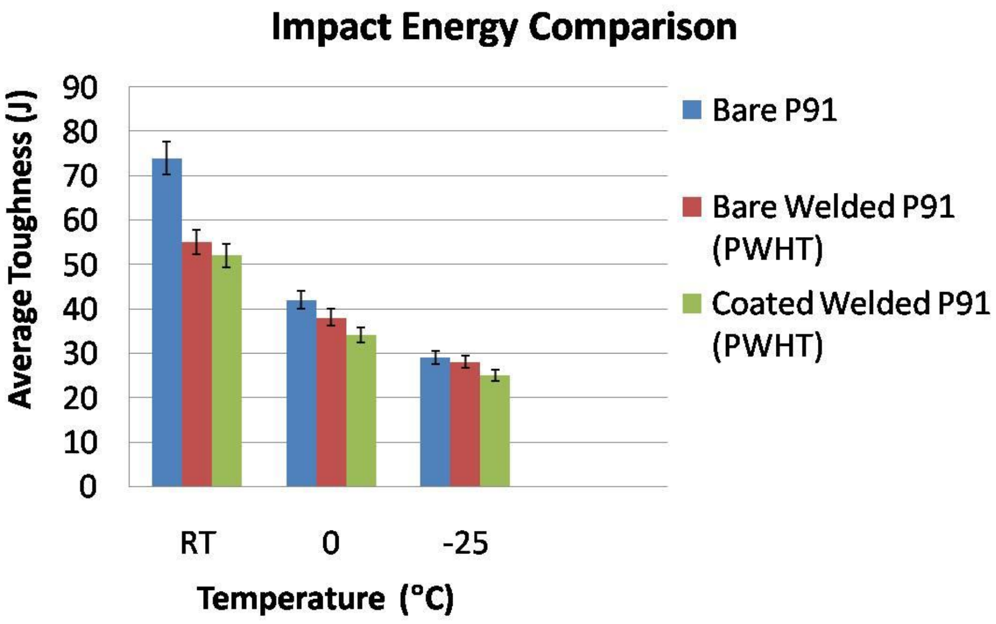

Figure 5.08 Impact toughness at 0 °C, -25 °C and room temperature

In addition, the samples are sub-size specimens which support the fact that the value would be higher in case of a sample with 10 mm thickness. Further, the tests carried out at 0°C and -25°C shows that the impact strength is in-line with 9Cr-1Mo steel in as-received condition. Vora et *al.*; reported that the carbide precipitates in the weld zone cause the crack initiation for 9Cr steels [120]. Hence, the carbide precipitates would play a dominant role in causing the various fracture modes compared to the oxide inclusions. The fracture surfaces after impact tests were also analyzed with SEM. Fig. 5.09 (a) and (b) showcase the fracture surfaces for both coated and uncoated weld respectively. Trans-granular brittle mode combined with ductile failure has been observed for both coated and uncoated steel which supports the reported fractrography by Chatterjee et *al*. [193]. The effect of precipitates on mechanical properties for coated weld metal would require detail study with respect to its size and distribution as the cooling during the PWHT would be critical.

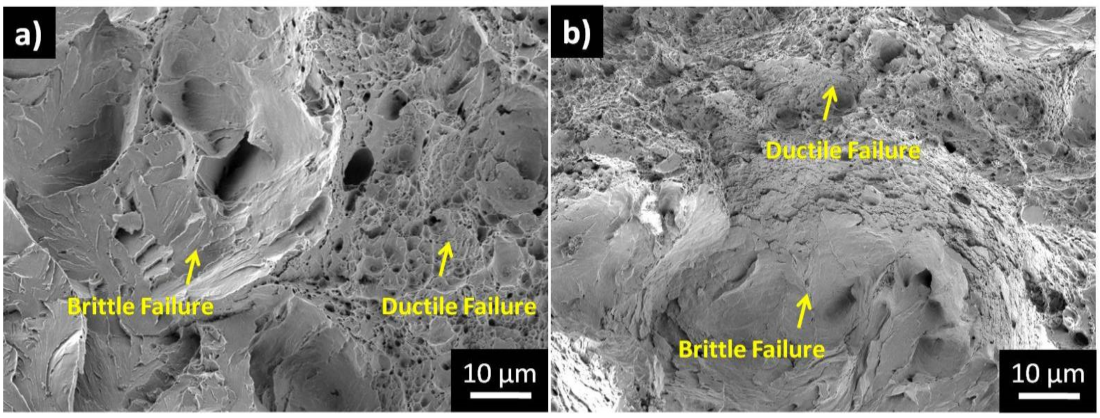

Figure 5.09 SEM images of fractured surfaces after impact tests at Room temperature a) un-coated weld metal b) coated-weld metal

5.5 Discussion

The effect of coating on mechanical properties for butt weld joint with a V-groove has been studied. The microstructure and mechanical properties, such as tensile and impact toughness, have been examined and correlated. Based on this study, the following conclusions were made.

The edge preparation (V-groove) eliminates the coated layer at the top, and the likelihood of delta ferrite formation can be prevented. XRD results confirmed that the weld metal microstructure was free from the delta ferrite phase. The diffractrograph revealed major peaks of αFe phase with (110) plane for both uncoated and coated weld, which is similar to the 9Cr-1Mo steel in as received state.

The Al_2O_3 particles were observed in irregular shape and more concentrated near the weld fusion line of coated steel. These particles/inclusions could be avoided by proper removal of oxides from the surface. The weld metal microstructure exhibits prior austenite grain boundary (PAGB) with $M_{23}C_6$ precipitates and MX type precipitates within matrix. The $M_{23}C_6$ precipitates were coarser in size in coated substrates than in the uncoated ones. It appears that the decreased thermal conductivity of the coated substrates could be the possible reason behind this.

Tensile tests were carried out to elucidate the effect of Al_2O_3 inclusions on tensile strength. The UTS observed for weld metal of coated steel was 648±16MPa, which is in line with the 9Cr-1Mo steel in as received condition (643±18MPa) and weld metal (667±14MPa) of un-coated steel. The fracture took place from the base metal in both the weld joints. Fractured surface indicates transgranular ductile fracture which is acceptable as per standards. It appeared that the oxide inclusions i.e. Al_2O_3 do not have any significant effect on tensile properties.

The weld joint of coated and uncoated steel were subjected to the impact tests at 0°C, -25°C and room temperature. The toughness values for coated steel, un-coated steel were 55J and 52J, respectively, which are inferior compared to the base metal (74 J) in ac-received condition owing to the size of precipitates in the weld metal. However, the impact values of weld joints are acceptable since the required impact toughness is 45 J for prototype fast breeder reactor applications.

References

[1] R.L. Klueh, D.R. Harries; *High-chromium ferritic and martensitic steels for nuclear applications*, **ASTM International, (2001)**.

[2] R.L. Klueh, K. Ehrlich, F. Abe; *Ferritic/martensitic steels: promises and problems*, **Journal of nuclear materials,** 191 **(1992)** 116-124.

[3] W.B. Jones, C. Hills, D. Polonis; *Microstructural evolution of modified 9Cr-1Mo steel*, **Metallurgical Transactions A**, 22 **(1991)** 1049-1058.

[4] R.L. Klueh; *Chromium-molybdenum steels for fusion reactor first walls—a review*, **Nuclear Engineering and Design**, 72 **(1982)** 329-344.

[5] R. Kozlowski; *Power generation in the 21st century, Ultra efficient, low emission plant*, No. IAE--54/A **(1999).**

[6] R. Klueh, D. Gelles, T. Lechtenberg; *Development of ferritic steels for reduced activation, the US program, in, Oak Ridge National Lab, TN (USA)*; **Hanford Engineering Development Lab**, **(1986)**.

[7] R. Klueh, D. Alexander, E. Kenik; *Development of low-chromium, chromium-tungsten steels for fusion*, **Journal of Nuclear Materials**, 227 **(1995)** 11-23.

[8] R. Klueh, J. Vitek; *Elevated-temperature tensile properties of irradiated 214 Cr-1 Mo steel*, **Journal of nuclear materials**, 126 **(1984)** 9-17.

[9] S. Swaminathan, C. Mallika, N.G. Krishna, C. Thinaharan, T. Jayakumar, U. Mudali; *Evolution of surface chemistry and morphology of oxide scale formed during initial stage oxidation of modified 9Cr–1Mo steel*, **Corrosion science**, 79 **(2014)** 59-68.

[10] A. Uehira, S. Ukai, T. Mizuno, T. Asaga, E. Yoshida; *Tensile properties of llCr-0.5 Mo-2W, V, Nb stainless steel in LMFBR environment*, **Journal of nuclear science and technology**, 37 **(2000)** 780-786.

[11] K. Anderko; *Zur eignung warmfester vergütungsstähle mit 9 bis 12% chrom für komponenten im kern schneller reaktoren—ein überblick*, **Journal of Nuclear Materials**, 95 **(1980)** 31-43.

[12] J. Davis, D. Michel; *Proceedings of the topical conference on ferritic alloys for use in nuclear energy technologies*, **(1984)**.

[13] J. Seran; *Effects of radiation on materials*, 14th Int. Symp., Philadelphia, **ASTM**, **(1990)**.

[14] A. Mirandola, A. Stoppato, A. Benato; *Steam Power Generation*, **Handbook of Clean Energy Systems**, **(2015)** 1-18.

[15] G.W. Meetham, M.H. Van de Voorde; *Materials for high temperature engineering applications*, **Springer Science & Business Media**, **(2000)**.

[16] C. Cabet, F. Dalle, E. Gaganidze, J. Henry, H. Tanigawa; *Ferritic-martensitic steels for fission and fusion applications*, **Journal of Nuclear Materials**, 523 **(2019)**: 510-537.

[17] J. Francis, W. Mazur, H. Bhadeshia; *Review type IV cracking in ferritic power plant steels*, **Materials Science and Technology** 22 **(2006)** 1387-1395.

[18] A. Fry, S. Osgerby, M. Wright; *Oxidation of alloys in steam environments-a review*, **(2002)**.

[19] S. Chetal, P. Chellapandi, P. Puthiyavinayagam, S. Raghupathy, V. Balasubramaniyan, P. Selvaraj, P. Mohanakrishnan, B. Raj; *Current status of fast reactors and future plans in India*, **Energy Procedia**, 7 **(2011)** 64-73.

[20] F. Carre, P. Yvon, P. Anzieu, N. Chauvin, J Malo; *Update of the French R&D strategy on gas-cooled reactors*, **Nuclear engineering and design**, 240 **(2010)** 2401-2408.

[21] J.Z. Briggs, T. Parker; *The super 12% Cr steels*, Climax Molybdenum Co., **(1965)**.

[22] A. Greeff, C. Louw, H Swart; *The oxidation of industrial FeCrMo steel*, **Corrosion Science**, 42 **(2000)** 1725-1740.

[23] A. Khanna, P. Rodriguez, J. Gnanamoorthy; *Oxidation kinetics, breakaway oxidation, and inversion phenomenon in 9Cr-1Mo steels*, **Oxidation of metals** 26 **(1986)** 171-200.

[24] C. Ostwald, H. Grabke; *Initial oxidation and chromium diffusion. I. Effects of surface working on 9–20% Cr steels*, **Corrosion Science** 46 **(2004)** 1113-1127.

[25] S. Newcomb, W.M. Stobbs, E. Metcalfe, Mathematical, P. Sciences; *A microstructural study of the oxidation of Fe-Ni-Cr alloys I. protective oxide growth*, Philosophical Transactions of the Royal Society of London. Series A, **Mathematical and Physical Sciences**, 319 **(1986)** 191-218.

[26] J. Żurek, E. Wessel, L. Niewolak, F. Schmitz, T. U. Kern, L. Singheiser, W. Quadakkers; *Anomalous temperature dependence of oxidation kinetics during steam oxidation of ferritic steels in the temperature range 550–650 C,* **Corrosion science**, 46 **(2004)** 2301-2317.
[27] P. Mayer, A. Manolescu; *The role of structural and compositional factors in corrosion of ferritic steels in steam*, **High-temperature corrosion**, **(1983)** 368-379.
[28] J. Vossen, P. Gawenda, K. Rahts, M. Röhrig, M. Schorr, M. Schütze; *Limits of the oxidation resistance of several heat-resistant steels under isothermal and cyclic oxidation as well as under creep in air at 650 C,* **Materials at High Temperatures**, 14 **(1997)** 387-401.
[29] D. Schmidt, M. Galetz, M. Schütze; *Ferritic–martensitic steels: Improvement of the oxidation behavior in steam environments via diffusion coatings,* **Surface and coatings technology**, 237 **(2013)** 23-29.
[30] I.G. Wright, R. Dooley; *A review of the oxidation behaviour of structural alloys in steam*, **International Materials Reviews**, 55 **(2010)** 129-167.
[31] H.J. Grabke, E.M. Müller‐Lorenz, B. Eltester, M. Lucas, D. Monceau; *Resistance of 9‐20% Cr‐steels against metal dusting*, **Steel research**, 68 **(1997)** 179-185.
[32] H. Grabke, Corrosion; *Metal dusting*, **Materials and Corrosion**, 54 **(2003)** 736-746.
[33] M. Maier, J. Norton, P. Frampton; *Metal dusting of 9–20% Cr steels in increased pressure environments at 560° C,* **Materials and Corrosion**, 49 **(1998)** 330-335.
[34] C. Schroer, O. Wedemeyer, J. Novotny, A. Skrypnik, J. Konys; *Performance of 9% Cr steels in flowing lead-bismuth eutectic at 450 and 550 C, and 10− 6 mass% dissolved oxygen*, **Nuclear Engineering and Design**, 280 **(2014)** 661-672.
[35] G. Müller, A. Heinzel, J. Konys, G. Schumacher, A. Weisenburger, F. Zimmermann, V. Engelko, A. Rusanov, V. Markov; *Results of steel corrosion tests in flowing liquid Pb/Bi at 420–600 C after 2000 h*, **Journal of Nuclear Materials**, 301 **(2002)** 40-46.
[36] J. Zhang, N. Li; *Review of the studies on fundamental issues in LBE corrosion*, **Journal of Nuclear Materials**, 373 **(2008)** 351-377.

[37] J. Zhang; *A review of steel corrosion by liquid lead and lead–bismuth*, **Corrosion Science**, 51 **(2009)** 1207-1227.
[38] J. Zhang N. Li, Y. Chen, A. Rusanov; *Corrosion behaviors of US steels in flowing lead–bismuth eutectic (LBE)*, **Journal of Nuclear Materials**, 336 **(2005)** 1-10.
[39] S. Dépinoy; *Evolution microstructurale d'un acier 2.25 Cr-1Mo au cours de l'austénitisation et du revenu: croissance des grains austénitiques, séquence de précipitation des carbures et effets sur les propriétés mécaniques*, in, Paris, **ENMP**, **(2015)**.
[40] P. Ennis, W. Quadakkers; *High chromium martensitic steels-microstructure, properties and potential for further development*, **VGB Powertech-International Edition**, 81 **(2001)** 87-90.
[41] C. Rosado, M. Schütze; *Protective behaviour of newly developed coatings against metal dusting*, **Materials and Corrosion**, 54 **(2003)** 831-853.
[42] A. Zrodnikov, G. Toshinsky, O. Komlev, Y.G. Dragunov, V. Stepanov, N. Klimov, V. Generalov, I. Kopytov, V. Krushelnitsky; *Innovative nuclear technology based on modular multi-purpose lead–bismuth cooled fast reactors*, **Progress in Nuclear Energy**, 50 **(2008)** 170-178.
[43] E. De Les Valls, L. Sedano, L. Batet, I. Ricapito, A. Aiello, O. Gastaldi, F. Gabrie; *Lead–lithium eutectic material database for nuclear fusion technology*, **Journal of Nuclear Materials**, 376 **(2008)** 353-357.
[44] V. Coen; *Lithium-lead eutectic as breeding material in fusion reactors*, **Journal of nuclear materials**, 133 **(1985)** 46-51.
[45] S. Kumar, N. Krishnamurthy; *Corrosion of Fe9Cr1Mo steel in stagnant liquid lead–lithium eutectic*, **Fusion Engineering and Design**, 87 **(2012)** 509-514.
[46] S. Malang, R. Mattas; *Comparison of lithium and the eutectic lead-lithium alloy, two candidate liquid metal breeder materials for self-cooled blankets*, **Fusion Engineering and Design**, 27 **(1995)** 399-406.
[47] D. Rapisarda, I. Fernandez, I. Palermo, M. Gonzalez, C. Moreno, A. Ibarra, E. de les Valls; *Conceptual design of the EU-DEMO dual coolant lithium lead equatorial module*, **IEEE Transactions on Plasma Science**, 44 **(2016)** 1603-1612.

[48] S. Smolentsev, N.B. Morley, M.A. Abdou, S. Malang; *Dual-coolant lead–lithium (DCLL) blanket status and R&D needs*, **Fusion Engineering and Design**, 100 **(2015)** 44-54.

[49] S. Konishi, M. Enoeda, M. Nakamichi, T. Hoshino, A. Ying, S. Sharafat, S. Smolentsev; *Functional materials for breeding blankets—status and developments*, **Nuclear Fusion**, 57 **(2017)** 092014.

[50] C. Courtessole, S. Smolentsev, T. Sketchley, M. Abdou; *MHD PbLi experiments in MaPLE loop at UCLA*, **Fusion Engineering and Design**, 109 **(2016)** 1016-1021.

[51] I. Ricapito, A. Ciampichetti, R. Lässer, Y. Poitevin, M. Utili; *Tritium extraction from liquid Pb-16Li: a critical review of candidate technologies for ITER and DEMO applications*, **Fusion Science and Technology**, 60 **(2011)** 1159-1162.

[52] R.G. Ballinger, J. Lim; *An overview of corrosion issues for the design and operation of high-temperature lead-and lead-bismuth-cooled reactor systems*, **Nuclear Technology**, 147 **(2004)** 418-435.

[53] P. Tortorelli, O.J. Chopra; *Corrosion and compatibility considerations of liquid metals for fusion reactor applications*, **Journal of Nuclear Materials**, 103 **(1981)** 621-632.

[54] E. Platacis, A. Ziks, A. Poznjak, F. Muktepavela, A. Shisko, S. Sarada, P. Chakraborty, K. Sanjay, M. Vrushank, R. Fotedar; *Investigation of the Li-Pb flow corrosion attack on the surface of P91 steel in the presence of magnetic field*, **Magnetohydrodynamics**, 48 **(2012)** 343-350.

[55] P. Chakraborty, V. Kain, P.K. Pradhan, R.K. Fotedar, N. Krishnamurthy; *Corrosion of modified 9Cr–1Mo steel and Indian RAFMS in static Pb–17Li at 773 K*, **Journal of Fusion Energy**, 34 **(2015)** 293-297.

[56] J. Knaster, P. Favuzza; *Assessment of corrosion phenomena in liquid lithium at T< 873 K. A Li (d, n) neutron source as case study*, **Fusion Engineering and Design**,118 **(2017)** 135-141.

[57] G. Benamati, C. Fazio, I. Ricapito; *Mechanical and corrosion behaviour of EUROFER 97 steel exposed to Pb–17Li*, **Journal of Nuclear Materials**, 307 **(2002)** 1391-1395.

[58] S.E. Wulf, W. Krauss, J. Konys; *Long-term corrosion behavior of Al-based coatings in flowing Pb–15.7 Li, produced by electrochemical ECX process,* **Nuclear Materials and Energy**, 16 **(2018)** 158-162.

[59] J. Konys, W. Krauss, Z. Zhu, Q. Huang; *Comparison of corrosion behavior of EUROFER and CLAM steels in flowing Pb–15.7 Li*, **Journal of Nuclear Materials**, 455 **(2014)** 491-495.

[60] H. Glasbrenner, J. Konys, Z. Voß; *Corrosion behaviour of low activation steels in flowing Pb–17Li*, **Journal of Nuclear Materials**, 281 **(2000)** 225-230.

[61] J. Konys, W. Krauss, Z. Voss, O. Wedemeyer; *Corrosion behavior of EUROFER steel in flowing eutectic Pb–17Li alloy*, **Journal of Nuclear Materials**, 329 **(2004)** 1379-1383.

[62] J. Konys, W. Krauss, J. Novotny, H. Steiner, Z. Voss, O. Wedemeyer; *Compatibility behavior of EUROFER steel in flowing Pb–17Li*, **Journal of Nuclear Materials**, 386 **(2009)** 678-681.

[63] J. Konys, W. Krauss, H. Steiner, J. Novotny, A. Skrypnik; *Flow rate dependent corrosion behavior of Eurofer steel in Pb–15.7 Li*, **Journal of Nuclear Materials**, 417 **(2011)** 1191-1194.

[64] J. Konys, W. Krauss, N. Holstein; *Development of advanced Al coating processes for future application as anti-corrosion and T-permeation barriers*, **Fusion Engineering and Design**, 85 **(2010)** 2141-2145.

[65] D. Smith, J.-H. Park, I. Lyublinski, V. Evtikhin, A. Perujo, H. Glassbrenner, T. Terai, S. Zinkle; *Progress in coating development for fusion systems*, **Fusion Engineering and Design**, 61 **(2002)** 629-641.

[66] F. Yang, X. Xiang, G. Lu, G. Zhang, T. Tang, Y. Shi, X. Wang; *Tritium permeation characterization of Al2O3/FeAl coatings as tritium permeation barriers on 321 type stainless steel containers*, **Journal of Nuclear Materials**, 478 **(2016)** 144-148.

[67] R.A. Causey, R.A. Karnesky, C. Marchi; *Tritium barriers and tritium diffusion in fusion reactors*, **(2012)**.

[68] T. Wang, J. Pu, C. Bo, L. Jian; *Sol–gel prepared Al2O3 coatings for the application as tritium permeation barrier*, **Fusion Engineering and Design**, 85 **(2010)** 1068-1072.

[69] G. Benamati, C. Chabrol, A. Perujo, E. Rigal, H. Glasbrenner; *Development of tritium permeation barriers on Al base in Europe*, **Journal of Nuclear Materials**, 271 **(1999)** 391-395.

[70] H. Liu, J. Tao, J. Xu, Z. Chen, Q. Gao; *Corrosion and tribological behaviors of chromium oxide coatings prepared by the glow-discharge plasma technique*, **Surface and Coatings Technology**, 204 **(2009)** 28-36.

[71] L. Naiming, X. Faqin, W. Xiangqing, T. Wei; *Influence of process parameters on thickness and wear resistance of rare earth modified chromium coatings on P110 steel synthesized by pack cementation*, **Journal of Rare Earths**, 29 **(2011)** 396-400.

[72] M. Nakamichi, H. Kawamura; *Characterization of Y2O3 coating under neutron irradiation*, **Journal of nuclear materials**, 258 **(1998)** 1873-1877.

[73] Z. Yao, A. Suzuki, D. Levchuk, T. Chikada, T. Tanaka, T. Muroga, T. Terai, *Hydrogen permeation through steel coated with erbium oxide by sol–gel method*, **Journal of Nuclear Materials**, 386 **(2009)** 700-702.

[74] T. Chikada, S. Naitoh, A. Suzuki, T. Terai, T. Tanaka, T. Muroga, *Deuterium permeation through erbium oxide coatings on RAFM steels by a dip-coating technique*, **Journal of Nuclear Materials**, 442 **(2013)** 533-537.

[75] D. Levchuk, H. Bolt, M. Döbeli, S. Eggenberger, B. Widrig, J. Ramm; *Al–Cr–O thin films as an efficient hydrogen barrier*, **Surface and Coatings Technology**, 202 **(2008)** 5043-5047.

[76] Y. Hatano, K. Zhang, K. Hashizume; *Fabrication of ZrO2 coatings on ferritic steel by wet-chemical methods as a tritium permeation barrier*, **Physica Scripta**, **(2011)** 014044.

[77] S. Majumdar, B. Paul, P. Chakraborty, J. Kishor, V. Kain, G. Dey; *Formation of Al2O3/FeAl coatings on a 9Cr-1Mo steel, and corrosion evaluation in flowing Pb-17Li loop*, **Journal of Nuclear Materials**, 486 **(2017)** 60-65.

[78] B. Paul, K. Raju, M. Vadsola, T. Murthy, J. Kishor, P. Arora, P. Chakraborty, K. Singh, S. Majumdar, V. Kain; *Investigations on wear and liquid metal corrosion behavior of aluminized IN-RAFMS*, **Fusion Engineering and Design**, 128 **(2018)** 204-214.

[79] J. Kaur, K. Singh, B. Paul, M. Gonal; *Microstructure, Analysis, Development of Coating on the Surface of Reduced Activation Ferritic Martensitic Steel (RAFMS)*

Substrate Using Hot Dip Aluminization and Heat Treatment, **Metallography, Microstructure, and Analysis**, 8 **(2019)** 118-122.

[80] J. Huang, H. Xie, L.M. Luo, X. Zan, D.G. Liu, Y. Wu; *Preparation and properties of FeAl/Al2O3 composite tritium permeation barrier coating on surface of 316L stainless steel*, **Surface and Coatings Technology**, 383 **(2020)** 125-128.

[81] S. Majumdar, A. Borgohain, V. Kain, *Interaction between liquid lead-bismuth eutectic and aluminized Inconel 625 superalloy at 600 and 850° C*, **Journal of Nuclear Materials**, 518 **(2019)** 54-61.

[82] X. Xiang, X. Wang, G. Zhang, T. Tang, X. Lai, *Preparation technique and alloying effect of aluminide coatings as tritium permeation barriers: a review*, **International Journal of Hydrogen Energy**, 40 **(2015)** 3697-3707.

[83] C. Shan, A. Wu, Y. Li, Z. Zhao, Q. Chen, Q. Huang, S. Shi, *The behaviour of diffusion and permeation of tritium through 316L stainless steel with coating of TiC and TiN+ TiC*, **Journal of Nuclear Materials**, 191 **(1992)** 221-225.

[84] D. Devia, E. Restrepo-Parra, P. Arango; *Comparative study of titanium carbide and nitride coatings grown by cathodic vacuum arc technique*, **Applied Surface Science**, 258 **(2011)** 1164-1174.

[85] E. Denisov, I. Gabis, T. Kompaniets, A. Kurdyumov, A. Yukhimchuk, *Hydrogen interaction with TiN films, in:* ***Hydrogen and helium recycling at plasma facing materials***, **(2002)**, pp. 157-162.

[86] V. Popov, E. Denisov; *Inhibition of hydrogen permeability by TiN: evaluation of kinetic parameters*, in: **Hydrogen Materials Science and Chemistry of Carbon Nanomaterials**, **(2007)**, pp. 671-680.

[87] X. Xiang, X. Wang, G. Zhang, T. Tang, X. Lai; *Preparation technique and alloying effect of aluminide coatings as tritium permeation barriers: a review*, **International Journal of Hydrogen Energy**, 40 **(2015)** 3697-3707.

[88] K.G. Field, M.N. Gussev, R. Howard, Y. Yamamoto, R. Howard, S. Briggs; *First annual progress report on radiation tolerance of controlled fusion welds in high temperature oxidation resistant FeCrAl alloys*, **ORNL/TM-2015/770**, **(2015)**.

[89] S. David, J. Horton, C. McKamey, T. Zacharia, R. Reed; *Welding of iron aluminides*, **Welding Journal**, 68 **(1989)** 372-381.

[90] N. Aleshin, S. Gerasimov, L. Yajiang, M. Haijun, Y.A. Puchkov, B. Yakushin; *Microstructure and composition of welds of Fe 3 Al intermetallic with austenitic corrosion-resistant steels*, **Metal Science and Heat Treatment**, 52 **(2011)** 437-441.

[91] N. Stoloff, A. Castagna, J. Scott, D. Duquette; *Environmental embrittlement of Fe 3 Al alloys under monotonic and cyclic loading*, **International Journal of Fatigue**, 6 **(1995)** 448-449.

[92] H. Neumann, J. Moravec, J. Bradac; *TIG welding process effect on the iron aluminide Fe3Al, Metal*, 5 **(2010)** 18-20.

[93] C. Liu, E. Lee, C. McKamey; *An environmental effect as the major cause for room-temperature embrittlement in FeAl*, **Scripta Metallurgica**, 23 **(1989)** 875-880.

[94] C. Liu, C. McKamey, E. Lee, *Environmental effects on room-temperature ductility and fracture in Fe3Al*, **Scripta Metallurgica**, 24 **(1990)** 385-389.

[95] J. Regina; *Weldability of Fe-Al-Cr Overlay Coatings for CorrosionProtection in Oxidizing/Sulfidizing Environments*, in, Oak Ridge National Lab.(ORNL), Oak Ridge, TN (United States), **(2003)**.

[96] S. David, T. Zacharia; *Weldability of Fe~ 3Al-Type Aluminide*, **WELDING JOURNAL-NEW YORK**, 72 **(1993)** 201-s.

[97] J. Regina, J. Dupont, A. Marder; *The effect of chromium on the weldability and microstructure of Fe-Cr-Al weld cladding*, **WELDING JOURNAL-NEW YORK**, 86 **(2007)** 170.

[98] T.J. Park, J.P. Kong, S.H. Uhm, I.S. Woo, J.S. Lee, C.Y. Kang; *Effect of Al–Si coating layer on the penetration and microstructures of ferritic stainless steel, 409L GTA welds*, **Journal of Materials Processing Technology**, 211 **(2011)** 415-423.

[99] J.P. Kong, T.J. Park, J.K. Kim, S.H. Uhm, I.S. Woo, J.S. Lee, B.G. Park, C.Y. Kang; *Characterization of laser welds in Al–10 wt.% Si coated ferritic stainless steel*, **Materials & Design**, 32 **(2011)** 917-925.

[100] J. Onoro; *Martensite microstructure of 9–12% Cr steels weld metals*, **Journal of Materials Processing Technology**, 180 **(2006)** 137-142.

[101] S. Sam, C. Das, V. Ramasubbu, S. Albert, A. Bhaduri, T. Jayakumar, E.R. Kumar; *Delta ferrite in the weld metal of reduced activation ferritic martensitic steel*, **Journal of Nuclear Materials**, 455 **(2014)** 343-348.

[102] K. Anderko, L. Schäfer, E. Materna-Morris; *Effect of the δ-ferrite phase on the impact properties of martensitic chromium steels*, **Journal of nuclear materials**, 179 **(1991)** 492-495.
[103] F. Abe, T. Noda, H. Araki, S. Nakazawa; *Alloy composition selection for improving strength and toughness of reduced activation 9Cr-W steels,* **Journal of nuclear materials**, 179 **(1991)** 663-666.
[104] P. Bertin, O. Dubet, S. Gadrey, F. Richard; *Method For Arc-Welding Aluminum-Coated Metal Parts Using An Inert Gas Containing Nitrogen*, in, **Google Patents**, **(2011)**.
[105] P. Bertin, O. Dubet, S. Gadrey, F. Richard; *Method For Arc-Welding Aluminum-Coated Metal Parts Using Oxidizing Gas*, in, **Google Patents**, **(2011)**.
[106] F. Briand, O. Dubet; *Hybrid Arc/Laser-Welding Method For Aluminized Steel Part Using A Gas Including Nitrogen And/Or Oxygen*, in, **Google Patents**, **(2011)**.
[107] J. Onoro; *Martensite microstructure of 9–12% Cr steels weld metals,* **Journal of Materials Processing Technology**, 180 **(2006)** 137-142.
[108] P. Wang, S. Lu, N. Xiao, D. Li, Y. Li, *Effect of delta ferrite on impact properties of low carbon 13Cr–4Ni martensitic stainless steel*, **Materials Science and Engineering: A**, 527 **(2010)** 3210-3216.
[109] J.D. Kim, J.-H. Lee, K.-C. Kim; *Welding Characteristics of Aluminized Steel Sheet by Nd: YAG Laser (I)-Effects of AI Coating Weight on Weld Strength*, **Journal of Welding and Joining**, 25 **(2007)** 65-71.
[110] N. Jamnapara, S. Mukherjee, *A Process for Plasma Oxidation of a Substrate and an Apparatus therefor*, in: **Google Patents** IN, **(2011)**.
[111] C. Pandey, M.M. Mahapatra, P. Kumar, N. Saini; *Comparative study of autogenous tungsten inert gas welding and tungsten arc welding with filler wire for dissimilar P91 and P92 steel weld joint*, **Materials Science and Engineering: A**, 712 **(2018)** 720-737.
[112] C. Pandey, M. Mahapatra, P. Kumar, N. Saini, *Autogenous TIG and GTA with filler welding of dissimilar P91 and P92 steels*, **Materials Science and Engineering: A** 712 **(2018)** 720-737.

[113] C. Pandey, A. Giri, M. Mahapatra, P. Kumar; *Characterization of microstructure of HAZs in as-welded and service condition of P91 pipe weldments*, **Metals and Materials International**, 23 **(2017)** 148-162.

[114] C. Pandey, A. Giri, M. Mahapatra; *Evolution of phases in P91 steel in various heat treatment conditions and their effect on microstructure stability and mechanical properties,* **Materials Science and Engineering: A**, 664 **(2016)** 58-74.

[115] K.H. Dhandha, V.J. Badheka; *Effect of activating fluxes on weld bead morphology of P91 steel bead-on-plate welds by flux assisted tungsten inert gas welding process*, **Journal of Manufacturing Processes**, 17 **(2015)** 48-57.

[116] S.G. Nayee, V.J. Badheka; *Effect of oxide-based fluxes on mechanical and metallurgical properties of Dissimilar Activating Flux Assisted-Tungsten Inert Gas Welds,* **Journal of Manufacturing Processes** 16 **(2014)** 137-143.

[117] J.J. Vora, V.J. Badheka; *Experimental investigation on mechanism and weld morphology of activated TIG welded bead-on-plate weldments of reduced activation ferritic/martensitic steel using oxide fluxes,* **Journal of Manufacturing Processes**, 20 **(2015)** 224-233.

[118] K.H. Dhandha, V.J. Badheka; *Effect of activating fluxes on weld bead morphology of P91 steel bead-on-plate welds by flux assisted tungsten inert gas welding process*, **Journal of Manufacturing Processes**, 17 **(2015)** 48-57.

[119] K.-H. Tseng, C.-Y. Hsu; *Performance of activated TIG process in austenitic stainless steel welds,* **Journal of Materials Processing Technology**, 211 **(2011)** 503-512.

[120] J.J. Vora, V.J. Badheka; *Experimental investigation on microstructure and mechanical properties of activated TIG welded reduced activation ferritic/martensitic steel joints,* **Journal of Manufacturing Processes**, 25 **(2017)** 85-93.

[121] J.J. Vora, V.J. Badheka; *Experimental investigation on effects of carrier solvent and oxide fluxes in activated TIG welding of reduced activation ferritic/martensitic steel*, **International Journal of Advances in Mechanical & Automobile Engineering,** 3 **(2016)** 75-79.

[122] Z. Sun, D. Pan; *Welding of titanium alloys with activating flux*, **Science and technology of welding and joining**, 9 **(2004)** 337-344.

[123] J.J. Vora, V.J. Badheka; *Improved penetration with the use of oxide fluxes in activated TIG welding of low activation ferritic/martensitic steel*, **Transactions of the Indian Institute of Metals**, 69 **(2016)** 1755-1764.

[124] C. Pandey, M. Mahapatra, P. Kumar, N. Saini; *Effect of normalization and tempering on microstructure and mechanical properties of V-groove and narrow-groove P91 pipe weldments*, **Materials Science and Engineering: A**, 685 **(2017)** 39-49.

[125] B. Arivazhagan, R. Prabhu, S. Albert, M. Kamaraj, S. Sundaresan; *Microstructure and mechanical properties of 9Cr-1Mo steel weld fusion zones as a function of weld metal composition*, **Journal of materials engineering and performance**, 18 **(2009)** 999.

[126] N. Saini, C. Pandey, M.M. Mahapatra, H. Narang, R. Mulik, P. Kumar; *A comparative study of ductile-brittle transition behavior and fractography of P91 and P92 steel*, **Engineering Failure Analysis**, 81 **(2017)** 245-253.

[127] J.D. Kim, J.H. Lee, K.W. Kim; *Joining, Welding Characteristics of Aluminized Steel Sheet by Nd: YAG Laser (I)-Effects of AI Coating Weight on Weld Strength*, **Journal of Welding and Joining**, 25 **(2007)** 65-71.

[128] A. Zala, N. Jamnapara, V. Badheka, S. Sam, M. Ranjan; *Effect of aluminide coatings on penetration and microstructure of TIG welded 9Cr-1Mo steel for fusion blanket applications*, **Fusion Engineering and Design**, 144 **(2019)** 172-179.

[129] L.O. Vilarinho, S. Raghunathan, B. Lucas; *OBSERVATION OF INSULATION MECHANISM DURING FBTIG*, **(2009)**.

[130] S. Jayakrishnan, P. Chakravarthy; *Flux bounded tungsten inert gas welding for enhanced weld performance—A review*, **Journal of Manufacturing Processes**, 28 **(2017)** 116-130.

[131] A.K. Singh, V. Dey, R. Rai, *A study to enhance the depth of penetration in grade P91 steel plate using alumina as flux in FBTIG welding*, **Arabian Journal for Science and Engineering**, 42 **(2017)** 4959-4970.

[132] O. Greyjevo, A. Metodo; *Optimization of weld bead geometry in TIG welding process using grey relation analysis and Taguchi method*, **Materiali in tehnologije**, 43 **(2009)** 143-149.

[133] A. Agüero, R. Muelas, A. Pastor, S. Osgerby; *Long exposure steam oxidation testing and mechanical properties of slurry aluminide coatings for steam turbine components*, **Surface and Coatings Technology**, 200 **(2005)** 1219-1224.

[134] E. Huttunen-Saarivirta, M. Honkanen, S.A. Tsipas, H. Omar, D. Tsipas, *Microstructure and elevated-temperature erosion-oxidation behaviour of aluminized 9Cr-1Mo Steel*, **Applied Surface Science**, 259 **(2012)** 674-684.

[135] J. Kalivodova, D. Baxter, M. Schütze, V. Rohr; *Corrosion behaviour of boiler steels, coatings and welds in flue gas environments*, **Materials and corrosion**, 59 **(2008)** 367-373.

[136] J. Hong, H. Choi, S. Lee, J.K. Kim, Y. mo Koo; *Effect of Al content on magnetic properties of Fe-Al Non-oriented electrical steel*, **Journal of Magnetism and Magnetic Materials**, 439 **(2017)** 343-348.

[137] J. Burke, D. Turnbull; *Progress in Metal Physics vol. 3,* **London: Pergamon Press**, **(1952).**

[138] D. Ghosh; *Effects of Grain Size and Nitrogen Content on Tensile Flow Properties of 316LN Stainless Steel at 300 K and 823 K*, in: **Metallurgical Engineering and Materials Science**, INDIAN INSTITUTE OF TECHNOLOGY BOMBAY, Bombay, **(2016)**, pp. 66.

[139] H. Pous-Romero, I. Lonardelli, D. Cogswell, H. Bhadeshia; *Austenite grain growth in a nuclear pressure vessel steel*, **Materials Science and Engineering: A**, 567 **(2013)** 72-79.

[140] Y. Oda, Y. Tanaka, A. Chino, K. Yamada; *The effects of sulfur on magnetic properties of non-oriented electrical steel sheets*, **Journal of Magnetism and Magnetic Materials**, 254 **(2003)** 361-363.

[141] H. Fu, M.-X. Zhang, D. Qiu, P. Kelly, J. Taylor; *Grain refinement by AlN particles in Mg–Al based alloys*, **Journal of Alloys and Compounds**, 478 **(2009)** 809-812.

[142] J. Ejenstam, M. Thuvander, P. Olsson, F. Rave, P. Szakalos; *Microstructural stability of Fe–Cr–Al alloys at 450–550° C*, **Journal of Nuclear Materials**, 457 **(2015)** 291-297.

[143] S. Jayakrishnan, P. Chakravarthy; *Flux bounded tungsten inert gas welding for enhanced weld performance—A review,* **Journal of Manufacturing Processes** 28 **(2017)** 116-130.

[144] J. Kalivodova, D. Baxter, M. Schütze, V. Rohr, corrosion, *Corrosion behaviour of boiler steels, coatings and welds in flue gas environments*, **Materials and corrosion**, 59 **(2008)** 367-373.

[145] H. Pous-Romero, I. Lonardelli, D. Cogswell, H. Bhadeshia; *Austenite grain growth in a nuclear pressure vessel steel*, **Materials Science and Engineering: A**, 567 (2013) 72-79.

[146] Y. Oda, Y. Tanaka, A. Chino, K. Yamada; *The effects of sulfur on magnetic properties of non-oriented electrical steel sheets*, **Journal of magnetism and magnetic materials**, 254 **(2003)** 361-363.

[147] H. Fu, M.-X. Zhang, D. Qiu, P. Kelly, J. Taylor; *Grain refinement by AlN particles in Mg–Al based alloys*, **Journal of Alloys and Compounds**, 478 **(2009)** 809-812.

[148] H. Fredriksson; *The mechanism of the peritectic reaction in iron-base alloys*, **Metal Science**, 10 **(1976)** 77-86.

[149] H. Fredriksson, J. Stjerndahl; *Solidification of iron-base alloys*, **Metal science**, 16 **(1982)** 575-586.

[150] P. Palani, N. Murugan; *Prediction of delta ferrite content and effect of welding process parameters in claddings by FCAW*, **Materials and Manufacturing Processes**, 21 **(2006)** 431-438.

[151] P. Marshall; *Austenitic stainless steels: microstructure and mechanical properties*, **Springer Science & Business Media**, **(1984)**.

[152] J. Onoro; *Martensite microstructure of 9–12% Cr steels weld metals*, **Journal of Materials Processing Technology**, 180 **(2006)** 137-142.

[153] M. Li, F. Sun, D. Li, P.E. O'Donoghue, S.B. Leen, N. O'Dowd; *The effect of ferrite phases on the micromechanical response and crack initiation in the intercritical heat‐affected zone of a welded 9Cr martensitic steel*, **Fatigue & Fracture of Engineering Materials & Structures**, 41 **(2018)** 1245-1259.

[154] S. Sam, C. Das, V. Ramasubbu, S. Albert, A. Bhaduri, T. Jayakumar, E.R. Kumar; *Delta ferrite in the weld metal of reduced activation ferritic martensitic steel*, **Journal of Nuclear Materials**, 455 **(2014)** 343-348.
[155] B. Arivazhagan, M. Vasudevan; *A comparative study on the effect of GTAW processes on the microstructure and mechanical properties of P91 steel weld joints*, **Journal of Manufacturing Processes**, 16 **(2014)** 305-311.
[156] B. Arivazhagan, G. Srinivasan, S. Albert, A. Bhaduri; *A study on influence of heat input variation on microstructure of reduced activation ferritic martensitic steel weld metal produced by GTAW process*, **Fusion Engineering and Design**, 86 **(2011)** 192-197.
[157] C. Pandey, M.M. Mahapatra, P. Kumar, N. Saini, J.G. Thakre, R. Vidyarthy, H. Narang; *A brief study on δ-ferrite evolution in dissimilar P91 and P92 steel weld joint and their effect on mechanical properties*, **Archives of Civil and Mechanical Engineering**, 18 **(2018)** 713-722.
[158] D. Olson; *Prediction of austenitic weld metal microstructure and properties*, **Welding journal**, 64 **(1985)** 281s-295s.
[159] N. Saini, R.S. Mulik, M.M. Mahapatra, R. Kannan, N.K. Sharma, L. Li; *Dissolution of δ-ferrite and its effect on mechanical properties of P92 steel welds*, **Materials Science and Engineering: A** 12 **(2020)** 139370.
[160] M. Alizadeh-Sh, S. Marashi, M. Pouranvari; *Microstructure–properties relationships in martensitic stainless steel resistance spot welds*, **Science and Technology of Welding and Joining** 19 **(2014)** 595-602.
[161] P. Mayr, T. Palmer, J. Elmer, E. Specht, S. Allen; *Formation of delta ferrite in 9 Wt pct Cr steel investigated by in-situ X-ray diffraction using synchrotron radiation*, **Metallurgical and Materials Transactions A** 41 **(2010)** 2462-2465.
[162] A. Kluken, Ø. Grong, G. Rørvik; *Solidification microstructures and phase transformations in Al-Ti-Si-Mn deoxidized steel weld metals*, **Metallurgical and Materials Transactions A**, 21 **(1990)** 2047-2058.
[163] W. Vanovsek, C. Bernhard, M. Fiedler, G. Posch; *Influence of aluminum content on the characterization of microstructure and inclusions in high-strength steel welds*, **Welding in the World** 57 **(2013)** 73-83.

[164] F. Hull; *Delta ferrite and martnesite formation in stainless steels*, **Welding journal** 52 **(1973)** 193.

[165] A. Mein, G. Fourlaris, D. Crowther, P. Evans; *The influence of aluminium on the ferrite formation and microstructural development in hot rolled dual-phase steel*, **Materials Characterization**, 64 **(2012)** 69-78.

[166] C. Pandey, M.M. Mahapatra, P. Kumar, N. Saini; *Dissimilar joining of CFEF steels using autogenous tungsten-inert gas welding and gas tungsten arc welding and their effect on δ-ferrite evolution and mechanical properties*, **Journal of Manufacturing Processes**, 31 **(2018)** 247-259.

[167] A. Zala, N. Jamnapara, V. Badheka, C. Sasmal, S. Sam, M. Ranjan; *Delta (δ) Ferrite Formation in the Welds of Aluminized 9Cr-1Mo Steels, Metallography, Microstructure, and Analysis*, 8 **(2019)** 256-262.

[168] J. Onoro; *Weld metal microstructure analysis of 9–12% Cr steels*, **International journal of pressure vessels and piping**, 83 **(2006)** 540-545.

[169] P. Patriarca, S. Harkness, J. Duke, L. Cooper; *US advanced materials development program for steam generators*, **Nuclear Technology** 28 **(1976)** 516-536.

[170] R. Kaltenhauser; *Improving the engineering properties of ferritic stainless steels*, **Metals Eng Quart** 11 **(1971)** 41-47.

[171] F. Briand, O. Dubet; *Hybrid Arc/Laser-Welding Method For Aluminized Steel Part Using A Gas Including Nitrogen And/Or Oxygen*, in, **Google Patents**, **(2013)**.

[172] F. Briand, O. Dubet; *Hybrid arc/laser-welding method for aluminized steel parts using gammagenic elements and a gas containing less than 10% of nitrogen or oxygen*, in, **Google Patents**, **(2016)**.

[173] P. Bertin, O. Dubet, S. Gadrey, F. Richard; *Method For Arc-Welding Aluminum-Coated Metal Parts Using An Inert Gas Containing Nitrogen*, in, **Google Patents**, **(2013)**.

[174] D. Howse; *Developments in A-TIG welding*, **Exploiting Advances in Arc Welding Technology** **(1998)** 3-9.

[175] R. Talbert; *Steelworker*, Vol.1, **The Center**, **(1997)**.

[176] P. Biswas, D.A. Kumar, N. Mandal, M. Mahapatra; *A study on the effect of welding sequence in fabrication of large stiffened plate panels*, **Journal of Marine Science and Application** 10 **(2011)** 429-436.

[177] C. Wang, R. Klueh, B. Chin; *The weldability of low activation Cr-W steels*, **Journal of nuclear materials**, 191 **(1992)** 831-835.

[178] N. Jamnapara, S. Mukherjee, A. Khanna; *Phase transformation of alumina coating by plasma assisted tempering of aluminized P91 steels*, **Journal of Nuclear Materials**, 464 **(2015)** 73-79.

[179] N. Jamnapara, V. Nayak, D. Avtani, N. Chauhan, D. Panda, S. Gupta, K. Kalaria, N. Vaghela, S. Mukherjee, A. Khanna; *Al2O3 films grown by glow discharge plasma aluminising*, **Surface Engineering**, 30 **(2014)** 467-474.

[180] A. Zala, N. Jamnapara, C. Sasmal, P. Chaudhuri, M. Ranjan, I*nvestigation of alumina film formed over aluminized RAFM steel by plasma assisted heat treatment*, **Fusion Engineering and Design**, 146 (2019) 2002-2006.

[181] B. Arivazhagan, M. Vasudevan; *A study of microstructure and mechanical properties of grade 91 steel A-TIG weld joint*, **Journal of materials engineering and performance**, 22 **(2013)** 3708-3716.

[182] T. Parekh, P. Patel, C. Sasmal, N. Jamnapara; *Effect of plasma processed Ti-Al coating on oxidation and tensile behavior of Ti6Al4V*, **Surface and Coatings Technology** 394, **(2020)** 125704.

[183] F. Stott, G. Wood; *Internal oxidation*, **Material Technology** 4 **(1988)** 1072-1078.

[184] A. Strang, E. Lang, *Effect of coatings on the mechanical properties of superalloys*, **High Temperature Alloys for Gas Turbines (1982)** 469-506.

[185] S. Zhang, T. Melfi, B. Narayanan; *Effects of precipitates on mechanical properties of P91 submerged arc welds*, **Science and Technology of Welding and Joining**, 21 **(2016)** 147-156.

[186] B. Reddy, S. Deevi, *Thermophysical properties of FeAl (Fe-40 at.% Al)*, **Intermetallics**, 8 **(2000)** 1369-1376.

[187] C. Beachem, R. Pelloux; *Electron fractography—a tool for the study of micromechanisms of fracturing processes*, **Fracture toughness testing and its applications**, ASTM International, **(1965)**.

[188] J. Blach, L. Falat, P. Ševc; *Fracture characteristics of thermally exposed 9Cr–1Mo steel after tensile and impact testing at room temperature*, **Engineering Failure Analysis**, 16 **(2009)** 1397-1403.

[189] C. Pandey, A. Giri, M. Mahapatra; *Effect of normalizing temperature on microstructural stability and mechanical properties of creep strength enhanced ferritic P91 steel*, **Materials Science and Engineering: A**, 657 **(2016)** 173-184.

[190] M. Sireesha, S. Sundaresan, S.K. Albert; *Microstructure and mechanical properties of weld fusion zones in modified 9Cr-1Mo steel*, **Journal of materials engineering and performance**, 10 **(2001)** 320-330.

[191] C. Pandey, M. Mahapatra; *Effect of heat treatment on microstructure and hot impact toughness of various zones of P91 welded pipes*, **Journal of Materials Engineering and Performance**, 25 **(2016)** 2195-2210.

[192] C. Pandey, N. Saini, M.M. Mahapatra, P. Kumar; *Study of the fracture surface morphology of impact and tensile tested cast and forged (C&F) Grade 91 steel at room temperature for different heat treatment regimes*, **Engineering Failure Analysis**, 71 **(2017)** 131-147.

[193] A. Chatterjee, D. Chakrabarti, A. Moitra, R. Mitra, A. Bhaduri; *Effect of normalization temperatures on ductile–brittle transition temperature of a modified 9Cr–1Mo steel*, **Materials Science and Engineering: A**, 618 **(2014)** 219-231.

[194] J. Wallace; *Grain Refinement of Steels*, **Journal of materials & minerals**, 15 **(1963)** 372-376.

Thesis Highlights

Name of the Student: Zala Arunsinh Bakulsinh
Name of the CI/OCC: Institute for Plasma Research, Gandhinagar
Enrolment No.: ENGG06201504007
Thesis Title: Investigations on weldability of aluminide coated 9Cr steel
Discipline: Engineering Sciences **Sub-Area of Discipline: Metallurgy and Material Science**
Date of viva voce: 4th February, 2021

Aluminide coating on 9Cr-1Mo steels is widely reported for enhancing service life conditions in numerous applications such as petrochemical plant, turbine-driven systems and especially for test blanket module of fusion reactors. One of the critical issues associated with such aluminide coatings (α-Al_2O_3 + FeAl) is the fabrication sequence.

In this study, effects of aluminide coatings have been investigated by autogenous TIG welding through bead-on-plate trials. The weld microstructures were investigated using X-ray diffraction (XRD), scanning electron microscopy with energy dispersive x-rays (SEM-EDX) and microhardness tests. It was observed that the presence of alumina (Al_2O_3) on the top of coated samples resulted in an improved depth of penetration (DOP) due to arc constriction. The schematic of arc constriction is shown in Fig. 1.

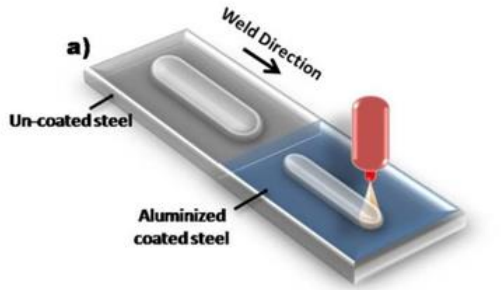

Figure 1 Schematic of arc constriction for the Aluminide coated 9Cr-1Mo steel

The concentration of Al in the weld zone contaminated the weld metal and it supports the δ-ferrite formation which would deteriorate mechanical properties. Results with bead-on-plate trials show that the δ-ferrite (Fig. 2 (a),(b)). had an average volume fraction of ~5.09% in the weld metal with an average 192–198$HV_{0.05}$ microhardness. This is approximately half of the reported microhardness martensitic laths (396–410$HV_{0.05}$).

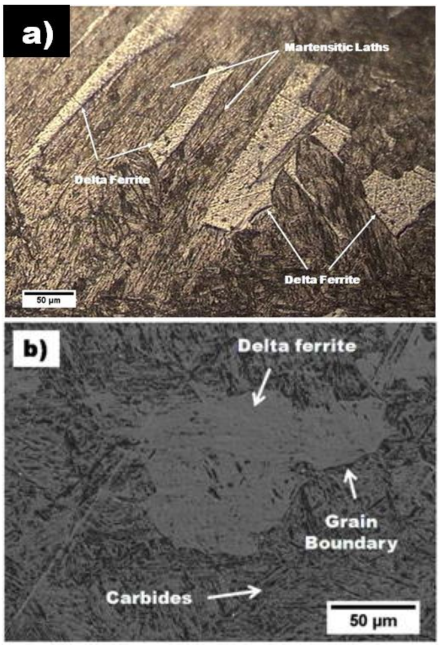

Figure 2. a) optical microstructure of delta ferrite b) SEM image of delta ferrite grain

To restrict the delta ferrite formation within the permissible limit, conventional TIG welding process had been attempted with V-groove design in accordance to ASME standards. The microscopic studies indicated the presence of alumina inclusion at the weld fusion line. Despite such inclusions, the observed tensile strength of the weld joint for coated steel is 648 MPa±16MPa which is in line with weld joint of un-coated steel (667±14 MPa) and substrate (643 MPa±18MPa). The impact toughness tests were carried out at 0°C,-25°C and room temperature indicate that there is no drastic effect of coating on weld joint and the observed toughness values are acceptable as per the reported data (45J). The present investigation would be helpful to understand the effect of aluminized coating on weldability for 9Cr-1Mo steels. Subsequently, the welding parameters deduced from this study can be utilized for the welding of aluminized 9Cr-1Mo steels for power plant, chemical processing industries and nuclear applications.